Monitoring and forecasting drought through the assimilation of satellite water observations

Siyuan Tian

A thesis submitted for the degree of Doctor of Philosophy of
The Australian National University

Research School of Earth Sciences, ANU
February 2019

Declaration

I, Siyuan Tian, declare that this thesis is my original research performed during the academic program towards the degree of Doctor of Philosophy of The Australian National University.

This thesis does not incorporate any material either previously submitted for a degree or diploma at any university, previously published or written by another person, except where due reference is made in the text.

Acknowledgments

First and foremost I want to thank my supervisor Paul Tregoning for providing me this opportunity to do this project and his invaluable support during the last four years. It has been an great honor to have Albert van Dijk, Luigi Renzullo, Jeffery Walker and Simon McClusky as my associate supervisors. This work would never be accomplished without the constant support from all my supervisors. I appreciate the time they spared, the ideas they shared, and the guidance they provided to make my Ph.D experience productivity and stimulating. The joy and enthusiasm they have for their research were contagious and motivational for me and provided me the excellent examples of successful scientists.

I have appreciated many fruitful discussions with Michael Roderick on the plant-water relations. I would also like to thank Valentijn Pauwels for helping me better understand data assimilation methods. Moreover, I would like to thank Natthachet Tangdamrongsub from University of Newcastle and Bailing Li from NASA Goddard Space Flight Center for sharing their great work on GRACE assimilation and inviting me to collaborate on their publications. Discussions and collaborations with them were valuable and enjoyable experiences for me.

I am really lucky to be a group member in both the Geodesy group in RSES and Water and Landscape Dynamics group in FSES. Everyone from the groups has contributed immensely to my life and study. I express my gratitude to Herb McQueen for helping me not only on the computing issues but also any problem in my life. I would like to thank Sébastien Allgeyer for his patient help on my coding problems. Without him, I would never be able to run the assimilations successfully with the super computer. Thanks to Achraf Koulali for always helping me with various questions on various problems. I also would like to thank Julian Byrne for providing assistance on using the computing resources provided by Terrawulf.

I would like to thank Bianca Kallenberg, Salim Masoumi, Umma Zannat, Veronika Emetc and Siru Zheng, as well as all the staff and students at RSES and FSES for making such friendly and enjoyable working environments. Their friendship and support has led to a pleasant experience.

Finally, I would like to thank my family and friends for all their unconditional love and encouragement. Thank you for cheering me up through the tough times and supporting me in all my pursuits.

Abstract

Drought poses the greatest threat to freshwater availability and food security, affecting larger areas for longer periods than any other natural hazards. In many regions, droughts increase in frequency and severity due to climate change. As a slow developing natural disaster, better estimates of water availability can be valuable for forecasting droughts and their impacts on ecosystem, agriculture and food security. With accurate knowledge of root-zone soil water and groundwater dynamics, effective planning of water resources and agriculture can be made months in advance. However, the simulated root-zone soil moisture and groundwater are often highly uncertain due to the unpredictable nature of soil water and groundwater dynamics caused by human activities such as water extraction and irrigation. Ground-based and remotely sensed measurements of water content are often limited in both spatial coverage and temporal resolution. Therefore, quantifying the change of water availability and its impacts on vegetation conditions at large scales remains largely unexplored.

In my study, contrasting satellite observations of water presence over different vertical domains were assimilated into a global water balance model, providing unprecedented accuracy of soil moisture profile and groundwater storage estimates. The water availability at different depths observed from soil moisture (SMOS) and space gravity (GRACE) missions provides an opportunity to separate total water storage vertically into different layers through data assimilation. However, combining these two data sets is challenging due to the disparity in temporal and spatial resolution at both vertical and horizontal scales. SMOS provides global high spatial and temporal resolution (i.e. $40km^2$, 3-day) near-surface (0-5cm) soil moisture estimates from microwave brightness temperature observations. In contrast, the GRACE mission provides accurate measurements of the entire vertically integrated terrestrial water storage column, but it is characterized by low spatial and temporal resolutions

(i.e. $300km \times 300km$, monthly). An ensemble Kalman smoother based global data assimilation system was developed to resolve the discrepancy between model and observations in space and time.

The use of data assimilation integrates these two measurements to effectively constrain model simulations and to accurately characterize the vertical distribution of water storage. Compared with model estimates without the assimilation or single-variant assimilation, joint assimilation typically led to more accurate soil moisture profile and groundwater estimates with improved consistency with in situ measurements. The improved water storage estimates integrated over different depths were used to determine the vegetation-accessible storage in association with vegetation growth and surface greenness. Accessible storage reflects a combination of vertical root distribution and soil properties, and its spatial distribution correlates with aridity and vegetation type. Skillful forecasts of vegetation conditions are achievable several months in advance for most of the world's drylands, which offers exciting new prospects for the improvement of drought early warning systems to help reduce human suffering and economical and environmental damage.

Contents

List of Figures

List of Tables

Chapter 1

Introduction

1.1 Climate, water and vegetation

1.1.1 Drought monitoring and forecasting

Among all natural disasters, drought poses the greatest threat to freshwater and food security, affecting people over larger areas and for longer periods. Droughts of the 21th century are exacerbated by the change in climate and the increase in water demands. The increasing frequency, severity and duration of droughts lead to a rise in drought-driven tree mortality and ecosystem transformations (Crausbay et al., 2017). The warming climate and water deficiencies may cause a widespread shift from tree-dominated to shrub and grass-dominated landscapes (Jiang et al., 2013). Therefore, there is a compelling need to improve the understanding of vegetation dynamics under climate change and water stress.

Drought, by definition, is a condition of insufficient usable water sources (i.e. soil moisture, groundwater, snowpack, streamflow and reservoir storage) caused by precipitation deficit over a time period (McKee et al., 1993). The drought onset time varies greatly from months to years for agricultural droughts (soil moisture) and hydrological droughts (groundwater, streamflow and reservoir). An ideal drought monitoring or forecast system should express

the water deficit as a function of water source and appropriate time scale. The most prominent drought indices used for assessing drought severity are precipitation-based, such as rainfall deciles (Gibbs, 1967) and standardized precipitation index (SPI) (McKee et al., 1993). However, these precipitation-based drought indices are primarily for monitoring meteorological drought without consideration of temperature anomalies, soil effects, land use and crop growth. The PDSI (Palmer Drought Severity Index) (Palmer, 1968) incorporates antecedent precipitation, moisture supply and moisture demand with a two-layer lumped parameter model without considering the spatial variability of land cover and soil properties. The GRACE Groundwater Drought Index (GGDI) based on satellite-observed water storage budgets can capture the groundwater drought in U.S. Central Valley, as a results of both human activities and natural changes, but is not sensitive to soil moisture variability at various depths (Thomas et al., 2017). Thus, each index has its strengths and weaknesses in monitoring different types of droughts.

Soil moisture is a key component in the water cycle and an important regulator of plant productivity. The characterization of the spatial variability of soil moisture is highly desirable for monitoring both agricultural and hydrological droughts. The temporal availability and vertical distribution of soil moisture indicates the agricultural potential and available water storage (Keyantash and Dracup, 2002; Sheffield et al., 2004). Drying soil causes reduced vegetation productivity and increased fire risk, in turn accelerating the depletion in groundwater and reservoirs by the increase in human demand for water. Severe die-off of overstory plants was found expressed in NDVI (normalized difference vegetation index) after 15 months of depleted soil water content across southwestern North American woodlands (Breshears et al., 2005). Sheffield et al. (2004) used the drought index combining soil moisture at different layers to monitor different types of droughts on a monthly time scale at a high resolution across the Unite States. The lack of long-term and large-scale soil moisture profile measurements restricts soil moisture modelling based

drought monitoring and forecasting (Sheffield and Wood, 2008a; Narasimhan and Srinivasan, 2005; Sheffield et al., 2004). Thus, accurate observation-based knowledge of the spatial and vertical distribution of water availability can be valuable for drought monitoring and forecasting.

Current drought forecasting services emphasize the provision of seasonal climate forecasts based on atmospheric forecast models (Pozzi et al., 2013). However, their skill is limited due to the rapidly decreasing predictability of the climate system beyond the first few weeks. Soil water availability and vegetation conditions reflect recent and antecedent precipitation with a longer memory of prevailing climate that can span weeks to months. The soil moisture at 2-3 m depth can have originated even from past rainy seasons (Schulze et al., 1996). Thus, better estimation of water availability and vegetation conditions can be valuable for drought preparation and agricultural planning.

1.1.2 Vegetation response to water availability

Since satellite-observed spectral reflectance from the NOAA AVHRR (Advanced Very High Resolution Radiometer) sensor became available, the Normalized Difference Vegetation Index (NDVI) has been widely used to characterize the spatial and temporal variability of healthy and dense vegetation (Kogan, 1995). NDVI is calculated based on the simple phenomenon that green and healthy vegetation absorbs more visible light (VIR) for use in photosynthesis and strongly reflects near-infrared light (NIR) (Equation 1.1). Stressed vegetation with increased reflectance in visible light and decreased reflectance in near-infrared light has lower values of NDVI. Healthy and dense vegetation has larger NDVI with a maximum value close to 1. NDVI is the primary tool for monitoring vegetation dynamics on a regional and continental scale (Anyamba and Tucker, 2005), and it is used more often in investigating ecological responses to climate and environmental change (Liu and Kogan, 1996; Ichii et al., 2002; Ji and Peters, 2003; Pettorelli et al., 2005; Gu et al., 2007; Badeck et al., 2004).

$$NDVI = (NIR - VIR_{red})/(NIR + VIR_{red}) \tag{1.1}$$

NDVI is responsive to chlorophyll variations but is vulnerable to additive noise effects and canopy background variation (Huete, 1988). The enhanced vegetation index (EVI), which utilizes a blue band in addition to the red and NIR bands is more responsive to the variations in canopy structure (Huete et al., 2002). NDVI shows larger dynamic range in semiarid regions than EVI, but a smaller range over humid forest (Huete et al., 2002). Moreover, NDVI was found to be more sensitive to crop change during green up and senescence, while the EVI was found more sensitive at the peak of growing season (Wardlow et al., 2007). Both NDVI and EVI demonstrated good capability in monitoring vegetation dynamics spatially and temporally and are complementary for different climate regions and vegetation types.

Soil water availability is a critical factor that governs the spatial and temporal dynamics of ecosystem processes in water limited regions (Singh et al., 1998). Vegetation conditions are strongly controlled by the pulsing and unpredictable nature of soil moisture dynamics in association with the alterations of indeterminacy and magnitude of rainfall events (Porporato et al., 2004). For instance, soil water availability may be different for frequent small pulses versus one large pulse, depending on whether these pulses occur in a dry or wet period (Ni et al., 2002). Apart from the precipitation, soil type, land cover and surface topography predominately determine the vegetation response to soil moisture fluctuations (Gu et al., 2008). For example, loamy soils susceptible to evaporative loss would have less water available for plant use than sandy soils in dry regions (Singh et al., 1998). On the other hand, the density of plants, the stage of plant growth and the rate of evapotranspiration also constrain the amount of water retained in the soil column (Cassel and Nielsen, 1986). The temporal and spatial variation in water availability and vegetation response are not linearly related and have threshold behaviors (Snyder and Tartowski, 2006). The quantification of vegetation responses to soil wa-

ter availability is critical to effectively improve the forecasting skill of climate impacts on ecosystem structure and function.

The majority of the studies on drought stress on plants are limited to regional scales. Gu et al. (2008) found that plants were most responsive to intermediate soil moisture change with 2 weeks time lags in grassland sites using soil moisture data from Oklahoma Mesonet Network. Chen et al. (2014) found that vegetation greenness typically lags soil moisture at less than 10 cm depth by one month over mainland Australia. Similarly, stronger correlation between NDVI and soil moisture was found to lag by up to 8 weeks in the U.S. Corn Belt, implying that soil moisture may be a useful predictor for vegetation condition estimates (Adegoke and Carleton, 2002).

1.1.3 Monitoring water availability

Effective management of water and food security requires reliable predictions of water availability and distributions. Various approaches have been developed to monitor and predict key components of the water cycle from distributed hydrological modelling, ground-based monitoring networks, to airborne and spaceborne remote sensing techniques. However, advancing real-time early warning of droughts and floods through forecasting changing water and vegetation conditions remains challenging regionally and globally.

Hydrological models simulate water content regularly in time and space through the simulation of hydrological processes. The accuracy of model estimation is largely dependent on the model physics, parameterization and the quality of forcing data sets. Global models often perform more poorly than catchment models, owing to the coarse resolution of global meteorological forcing, the lack of model calibration, and the complex and different dynamics of hydrological process over different regions. The simplification of model physics is often a trade-off between accuracy and computational cost.

Ground-based monitoring networks are point-scale measurements with limited number of samples and uneven distribution. Extrapolating isolated

measurements of soil moisture or groundwater level to represent the water distribution at basin scale is often difficult both spatially and vertically due to the variations of topography, land cover types and soil properties (Wang et al., 2007). Therefore, the ground-based measurements are often used for field experiments and model validation and calibration.

Remote sensing techniques mitigate the absence of observations over large areas and remote locations and provide opportunities for instantaneous measurements of water cycle components such as precipitation, surface water, snow, soil moisture, and total water storage. For instance, GPM (Global Precipitation Measurement) provides global rainfall and snowfall retrievals every 3 hours from 2014 (Hou et al., 2014). Water stored in the uppermost few centimetres of soil is a key to the water and energy exchanges between the surface and the atmosphere (Kerr et al., 2010). Both passive microwave radiometry and active microwave radar have been widely used for mapping soil moisture with the brightness temperature measurements. The primary limitations of microwave techniques are the radiometric sensitivity to surface heterogeneity, surface roughness, topography, surface water and RFI (Radio Frequency Interference). Total water storage as the main cause of time-variable gravity change, was derived from the GRACE (Gravity Recovery And Climate Experiment) mission from 2002 to 2017 (Tapley et al., 2004). The strong seasonally varying signals of water storage derived from GRACE measurements have been widely used for monitoring the availability of freshwater, especially groundwater (Yeh et al., 2006; Syed et al., 2008; Rodell et al., 2009; van Dijk et al., 2011; Rodell et al., 2018). GRACE Follow-On a successor to the GRACE mission, started tracking Earth's water movement in 2018. Although, these satellite observations of water content are spatial comprehensive, the temporal and spatial resolution are non-continuous and highly constrained by the instruments and mission design. The combination of model simulations and satellite observations tends to become the most effective and popular tool for monitoring water availability recently.

1.1.4 Hydrological data assimilation

Data assimilation was pioneered by meteorologists and has been widely used to improve weather forecast and ocean dynamics prediction for decades (Walker and Houser, 2005). Significant advancements in data assimilation in hydrology applications have been made with the increasing satellite observations of water cycle such as remotely sensed precipitation, streamflow, surface soil moisture, snow, and total water storage (Walker and Houser, 2001a; Rodell and Houser, 2004; Zaitchik et al., 2008; Clark et al., 2008; Liu et al., 2011; Li et al., 2013). The concept of data assimilation is to optimally merge the information from uncertain observations and uncertain model simulations (Reichle et al., 2002). The criteria used in the estimation process to determine the influence of dynamics and data onto the state estimate are therefore crucial for solving this problem (Robinson and Lermusiaux, 2000).

Data assimilation algorithms are developed from simple rule-based direct insertion, to advanced smoothing and sequential methods, to sophisticated variational methods (Liu et al., 2012a). The sequential method is a near-real time model updating method that only uses the present available observations. It is more computation efficient and suitable for forecasting applications. The variational method allows the model to run backwards and use both present and future observations. It is highly suited for reanalysis problems but more complex to implement. Among various approaches, the ensemble Kalman filter (Evensen, 2003) is the most widely used data assimilation approach for its convenience in error covariances estimation for a non-linear model with propagated ensemble states.

A lot of previous work confirmed that the assimilation of surface soil moisture observations impacts deeper-layer soil moisture predictions and could lead to improved estimates of evaporative fluxes, drainage and runoff (Walker and Houser, 2001a; Li et al., 2012; Liu et al., 2011). Walker and Houser (2001a) implemented a one-dimensional Kalman filter to assimilate near-surface soil moisture observations into a catchment-based land surface model. The results

illustrated that the accuracy of soil moisture profile estimates as well as runoff and evapotranspiration were improved. Renzullo et al. (2014) demonstrated that the assimilation of AMSR-E and ASCAT-derived surface soil moisture into the AWRA-L model yielded similar performance for the top-layer, however ASCAT data improved root-zone soil moisture estimation for more sites. Li et al. (2012) tested the conventional and mass conservation updating scheme and showed that both schemes reduced the bias in the shallow root zone and the mass conservation scheme provided better estimates in the deeper profile. Xu et al. (2015) and Lievens et al. (2015) assimilated SMOS soil moisture retrievals over the Great Lakes basin and Murray Darling basin. Moreover, Chakrabarti et al. (2014) assimilated SMOS soil moisture for quantifying drought impacts on crop yield and found higher improvement during agricultural drought. An ensemble Kalman smoother was used to assimilate monthly GRACE TWS into the Catchment Land Surface Model (CLSM) for the Mississippi river basin and western and central Europe for improved groundwater estimation (Zaitchik et al., 2008; Li et al., 2012). Forman et al. (2012) assimilated GRACE data into a snow-dominated basin, with an ensemble Kalman smoother and a similar method as used by Zaitchik et al. (2008). They evaluated the results with snow water equivalent and runoff. Eicker et al. (2014) used an ensemble Kalman filter to assimilate GRACE into the WaterGAP model to update model states and parameters together. Houborg et al. (2012) and Li et al. (2012) used GRACE data assimilation system results in drought monitoring using improved groundwater storage estimates. van Dijk et al. (2014b) developed a data assimilation scheme that used GRACE data, satellite water level data and 'off-line' estimations from several hydrological models in a global water cycle reanalysis. These various studies showed that data assimilation holds considerable potential for improving water content estimation, in turn resulting in better initial conditions for forecasting the impacts of water deficit on ecosystems.

1.2 Motivation

Accurate knowledge of water availability is critical for forecasting the impacts of drought on ecosystems, especially in semi-arid and arid regions. Operational systems for drought early warning or water availability monitoring are still lacking in many parts of the world, in particular in less developed countries with inadequate monitoring networks and limited facilities. There is a compelling need for quantifying vegetation response to variations in water availability for better management of water resources, agricultural planning and natural hazard preparedness.

In this research, to accurately estimate water storage in individual compartments, I developed a global data assimilation framework that optimally integrates the dynamics of surface soil moisture and total water storage jointly. The main objective of this study is to improve the prediction of water availability and vegetation response with accurate estimates of current water storage availability at different depths. Informing the water availability and potential impacts on vegetation vigor months in advance can be of great value to ensure water and food security and reduce environmental and economical loss.

1.3 Thesis structure

Chapter 2 provides a brief overview of the model and data sets used in this study, including the water balance model, satellite-observed total water storage and near-surface soil moisture data.

Chapter 3 to 5 are organized based on three published papers. Consequently, there may be some repetition in these chapters with the description of dataset and materials in **Chapter 2**.

Chapter 3 introduces the data assimilation method developed for this study to jointly integrate GRACE and SMOS data in a water balance model. The results were evaluated extensively with in-situ measurements of soil moisture, groundwater, streamflow and evaporation over Australia. This chapter is based on the material published in

Tian, S., Tregoning, P., Renzullo, L. J., van Dijk, A. I., Walker, J. P., Pauwels, V. R., & Allgeyer, S. (2017). Improved water balance component estimates through joint assimilation of GRACE water storage and SMOS soil moisture retrievals. Water Resources Research, 53(3), 1820-1840.

Chapter 4 is a study of the global joint assimilation on improving the estimation of root-zone soil moisture and vegetation response. Further modifications of the method in the global study are described here. This study focuses on the investigation of the benefits of improving soil water availability to anticipating vegetation response. This chapter is based on the material published in

Tian, S., Renzullo, L. J., van Dijk, A. I., Tregoning, P., Walker, J. P. (2019). Global joint assimilation of GRACE and SMOS for improved estimation of root-zone soil moisture and vegetation response. Hydrology and Earth System Sciences, 23(2), 1067–1081

Chapter 5 introduces a forecasting framework using the improved water storage estimates from the global data assimilation in **Chapter 4**. This chapter

highlights the benefits of using accurate water availability information in forecasting drought impacts on vegetation. This chapter is based on the material published in

Tian, S., van Dijk, A. I., Tregoning, P.,& Renzullo, L. J. (2019) Forecasting dryland vegetation condition months in advance through satellite data assimilation. Nature Communications, 10(1), 469

Chapter 6 concludes the key findings of this study with both benefits and limitations, followed by the suggestions for the future work.
Appendix A includes the supplementary material of the case study in **Chapter 3**.

Chapter 2

Water balance model and satellite water observations

The first part of this chapter briefly introduces the World-Wide-Water (W3) model used in this study for water balance estimation. To further improve the water storage estimation, W3 model simulations were constrained by two types of water content retrievals reflecting water content at different depths. Retrievals of total water storage change from GRACE and near-surface soil moisture from SMOS are described in the second part of this chapter include details of the satellite missions and products.

2.1 Ecohydrological model

2.1.1 Model overview

The ecohydrological model used in this study is the World-Wide-Water (W3) model, based on the landscape hydrology component model of the Australian Water Resource Assessment (AWRA-L) system (van Dijk et al., 2013c) (available at http://www.wenfo.org/wald/). It is a grid-distributed biophysical model that provides relevant information about the history and present state of the water balance in agreement with both ground gauging and satellite observa-

tions (Van Dijk and Renzullo, 2011). The model has been used in a wide range of applications, including operational water resources assessment service by the Bureau of Meteorology Australia (http://www.bom.gov.au/water/landscape/), drought and flood monitoring (van Dijk et al., 2013b; Guerschman et al., 2011), and agricultural studies (Bryan et al., 2015). Both W3 and AWRA-L has been extensively evaluated with in-situ and satellite observations and other models, and it has been demonstrated to reproduce soil moisture, streamflow, total water storage, and vegetation greenness with accuracy commensurate to or better than other models (Van Dijk et al., 2011; Van Dijk and Renzullo, 2011; van Dijk et al., 2013c).

2.1.2 Model structure

The W3 model can be described as a hybrid between a simplified grid-based land surface model and a lumped catchment model applied to individual grid cells (van Dijk et al., 2013c). Each grid cell contains an mix land cover classes (Hydrological Response Units; HRUs) and is conceptualized as a catchment that does not laterally exchange water with neighboring cells. The minimum meteorological input data are daily gridded precipitation, incoming short-wave radiation, minimum and maximum temperature. These inputs define the resolution of the model output. Precipitation is assumed to be the only water input into the system. The precipitation enters the grid cell through the vegetation and soil moisture stores and exits the grid cell through evapotranspiration, run-off or groundwater discharge. Each grid cell contains two HRUs, namely, deep-rooted vegetation (trees) and shallow-rooted vegetation (grass). Different vegetation has different degrees of access to soil water. Soil and vegetation water and energy fluxes are simulated at sub-grid level by assigning parameters separately for each HRU. The unsaturated soil water is partitioned into three layers: top-layer (0-10 cm), shallow-layer (10-100 cm) and deep layer (1-10 m). The groundwater and river water dynamics are simulated at grid cell level (van Dijk, 2010a).

2.2 GRACE terrestrial water storage

Terrestrial water storage (TWS) consists of all forms of water stored above and beneath the Earth's surface, including soil water, groundwater, snow, ice, vegetation water and surface water in rivers, lakes, and reservoirs. TWS is a controlling component in the water cycle and regulates water, energy and biogeochemical fluxes (Famiglietti, 2004). Accurate measurements of TWS have significant implications for water resource management (Syed et al., 2008). The lack of direct measurements of TWS at large scale was not resolved until the launch of Gravity Recovery and Climate Experiment (GRACE) satellites (Tapley et al., 2004). The GRACE mission has revolutionized space-borne remote sensing, providing remarkable prospects for tracking water movement over the globe.

2.2.1 Mission overview

The GRACE mission was launched in 2002 to map the global gravity field with a spatial resolution of hundreds of kilometres. The GRACE Follow-On (GRACE FO) mission is continuing GRACE's legacy from May 2018 onwards. The GRACE mission consisted of two identical satellites flying in a near-polar obit about 220 km apart and 450 km above the Earth. Mass anomalies cause a change in the gravity field of the Earth, which affects the flight of the satellites and causes changes in the distance between them. The changes in distance between these two satellites, caused by the changing Earth gravity field, is measured via a sensitive K-band microwave ranging system with a measurement precision of 10 μm (Tapley et al., 2004). Each satellite carries a Global Positioning System (GPS) receiver, laser retro-reflector, star sensors and accelerometers on board (Bruinsma et al., 2010). The distance between the two satellites increases when the first satellite approaches a stronger gravity anomaly and speeds up. The first satellite lingers over the anomaly region due to the deceleration caused by it. Concurrently, the following satellite will

catch up to the first satellite, which decreases the distance. Similar changes in distance occur for weaker gravity anomalies.The time varying Earth's gravity map is derived from the continuously changing intersatellite range-rate coupled with the absolute positions measurements from GPS instruments on board.

The total water storage estimates from GRACE are anomalies with respect to a static reference gravity field. The time varying quantity of the gravity field is small but contains important geophysical information, reflecting the interaction between the atmosphere, terrestrial water, oceans and the solid Earth. Since the gravity effects of the solid Earth, oceans, and atmosphere are reduced in the data processing, the GRACE-detected time varying gravity field mainly reflects the changes in terrestrial water storage on seasonal and shorter time scales (Jiang et al., 2014). GRACE-observed terrestrial water storage anomalies at large scale provide a complement to traditional ground-based hydrological measurements, which tend to be restricted to the scales of individual catchments (Wahr et al., 1998). GRACE TWS estimates are integrated water storage changes throughout the whole water column including the soil water, groundwater, surface water, snow and ice. Due to the highly accurate, global and homogenous nature, GRACE data have been utilized efficiently to study terrestrial water storage change, sea-level changes, ice-sheet mass balance, ocean circulation as well as droughts and floods (Chen et al., 2009; Hu et al., 2006; Jiang et al., 2014; Ramillien et al., 2008; Rodell and Famiglietti, 2002; Rodell et al., 2018).

2.2.2 Products

The raw data collected from satellites known as Level-1A are not available to public. These data go through extensive and irreversible processing and are converted to the Level-1B data. The Level-1B data including the inter-satellite range, range-rate and range-acceleration. are used to produce the monthly gravity field estimates in form of spherical harmonic coefficients as Level-2 products. The Level-1B and Level-2 products are released by Physical

Oceanography Distributed Active Archive Center (PO.DAAC) and Information System and Data Center (ISDC). GRACE Level-3 products, with time series of surface mass anomalies after suitable correction and filtering, are available from different international centres, such as the Jet Propulsion Laboratory (JPL), the Centre of Space Research at the University of Texas (CSR), the GFZ (GeoForschungsZentrum) German Research Centre for Geosciences and French Groupe de Recherche de Géodésie Spatiale (GRGS).

By implementing different inversion methods, it is possible to derive the estimates of the Earth's temporal gravity field at time intervals of 1-,10- or 30-day (Bruinsma et al., 2010; Kurtenbach et al., 2009; Tapley et al., 2004). The majority of these solutions solve the gravity field with spherical harmonic basis functions. Figure 2-1a shows the total water storage anomalies estimates based on JPL RL05 spherical harmonics. However, empirical smoothing has to be applied to mitigate the typical north-south stripes for unconstrained spherical harmonics solutions from GRACE (Swenson and Wahr, 2006). True geophysical signal of interest along with the stripes can be removed with the smoother or destriping algorithms in the post-processing. In addition to spherical harmonics solutions, the mass concentration (mascon) solutions have been used for gravity estimation. JPL RL05M product uses surface spherical cap mascons to estimate mass change directly from intersatellite range-rate measurement from GRACE (Watkins et al., 2015). The primary advantage of the mascon solutions is that no post-filtering or scaling is required for users. It also shows improved spatial resolution and accuracy over areas where the signal magnitude is small (Watkins et al., 2015). Mascon solution (Figure 2-1b) shows similar spatial patterns of water storage anomalies with spheric harmonics solution but stronger magnitude of water loss and gain than spherical harmonic solution in many places, such as the Amazon, India and Mexico. The mascon solution also shows the water storage anomalies at the actual resolution of GRACE without spatial filtering. Therefore, the JPL RL05M 3 degree monthly mascon solutions (available at the GRCTellus: grace.jpl.nasa.gov)

were used in this study. In order to better assess or improve hydrological models, the uncertainties in GRACE TWS estimates need to be quantified and used appropriately.

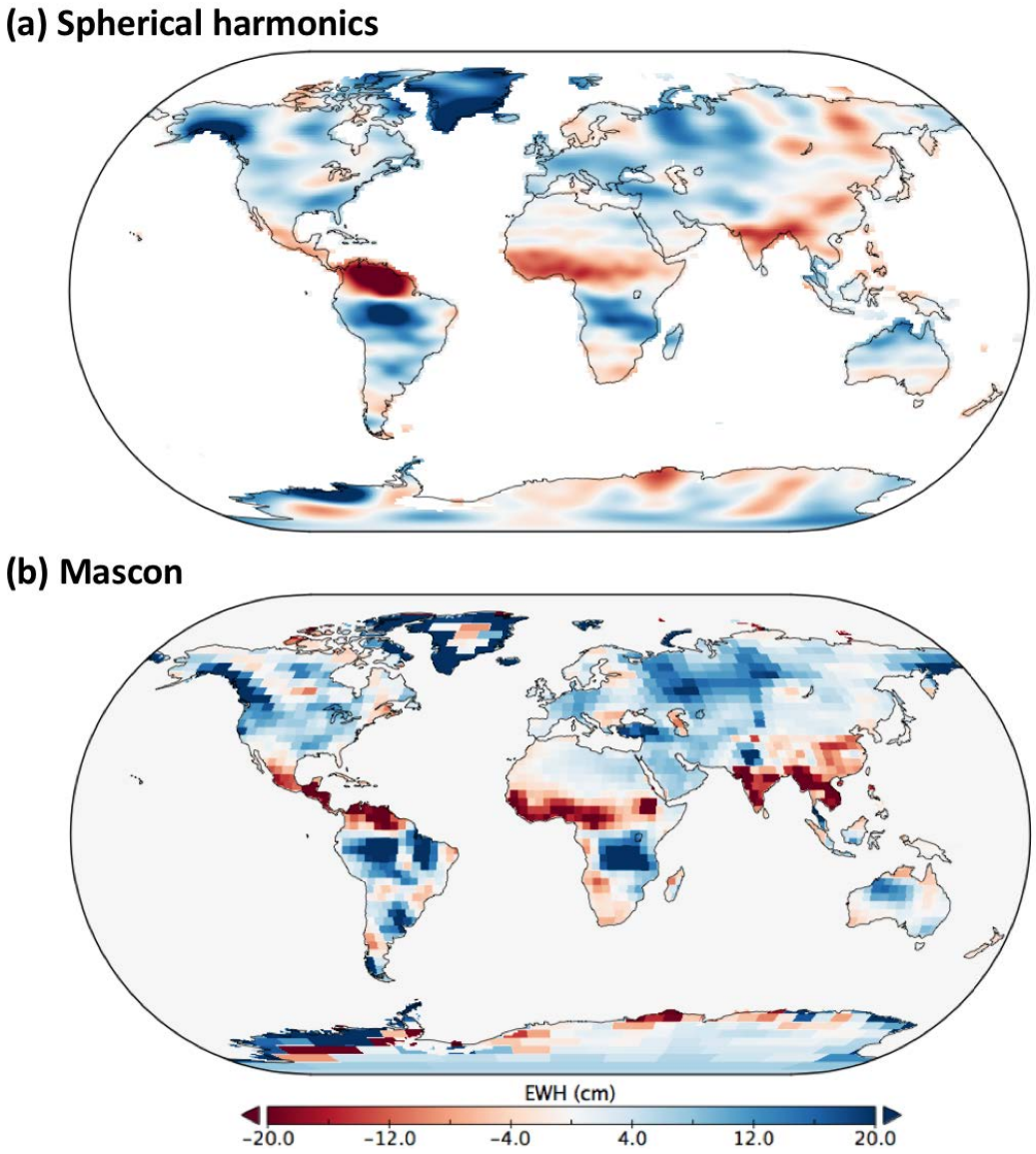

Figure 2-1: GRACE total water storage anomalies in EWH (equivalent water height) in March 2003 from JPL spherical harmonics solutions and mascon solutions.

2.3 SMOS surface soil moisture

Surface soil moisture is an important reservoir of water that can be evaporated into the atmosphere and also a tracer of precipitation (Kerr et al., 2010). In contrast to indirect approaches like optical sensing, microwave systems are capable of measuring the dielectric constant of soil in all weather and are often less affected by the atmosphere, clouds or vegetation. There are three types of microwave systems: radar, scatterometer and radiometry. Synthetic aperture radars (SARs) offer high spatial resolution but rather low temporal sampling and are affected by speckle and scattering at the surface (Kerr et al., 2010). Scatterometers compromise between spatial and temporal resolution with a coarser spatial resolution but a more frequent revisit. The surface roughness and vegetation effects of the scatterometer data is still significant but provide relatively accurate measurements over arid and semiarid regions (Gruhier et al., 2010). Compared to active systems, passive microwaves are less influenced by surface roughness and vegetation.

Numerous studies have demonstrated the potential of low-frequency passive microwaves for retrieving surface soil moisture using ground or airborne radiometers (Schmugge and Jackson, 1994; Chanzy et al., 1997). However, it requires a large antenna diameter to achieve high spatial resolution which is really technically challenging. The use of space-borne L-band radiometers was not possible until the development of interferometry, which can measure the phase difference of incident radiation (Kerr et al., 2001). SMOS (Soil Moisture and Ocean Salinity) is the first mission dedicated to global mapping of the surface soil moisture and ocean sanity together using a low frequency L-band (1.4 GHz) radiometer.

2.3.1 Mission overview

Carrying the first polar-orbiting, space-borne, 2D interferometric radiometer, the SMOS mission has observed soil moisture over the land and salinity

over the oceans from space since 2009. It is a relatively new measuring technique for a space-borne radiometer and adopts an interferometric method. The MIRAS (Microwave Imaging Radiometer using Aperture Synthesis) instrument provides brightness temperature measurements over incidence angles from 0° up to 55° at both horizontal and vertical polarization, with a spatial resolution of 30-50 km and a repeat cycle of 2-3 days (Pinori et al., 2008). SMOS is a sun-synchronous satellite and it passes over the equator twice a day, at 6:00 am local solar time in the ascending pass and 6:00 pm in the descending pass. SMOS provides global near-surface soil moisture map with an accuracy about 0.04 m^3/m^3 and vegetation water content with an accuracy of 0.5 kgm^{-2} (Kerr et al., 2001). The penetration depth of the L-band radiometer is about 5 cm, but can be exgrated to increase (decrease) with very low (high) soil water content.

2.3.2 Products

SMOS data is generated and delivered by ESA up to Level-2 products. The Level-3 and Level-4 data are processed by national centres in France and Spain. This study used the CATDS (Centre Aval de Traitement des Données SMOS) soil moisture Level-3 products including daily ascending and descending multi-orbit soil moisture retrieval products and time aggregated products for 3-day, 10-day and monthly (Jacquette et al., 2010). The CATDS Level-3 products are processed based on the Level 1B products with Fourier components of the brightness temperature (Kerr et al., 2013). To provide a more user friendly, regular global grid, it uses the Equal-Area Scalable Earth (EASE) grid instead of ISEA to provide the reprocessed global maps of surface soil moisture with a spatial resolution of approximately 25 km × 25 km. Figure 2-2 shows the spatial coverage of the daily soil moisture retrieval with both ascending and descending orbits.

The nominal accuracy goal of SMOS retrieved soil moisture is 0.04 m^3/m^3. Jackson et al. (2012) and Leroux et al. (2014) compared SMOS data and other

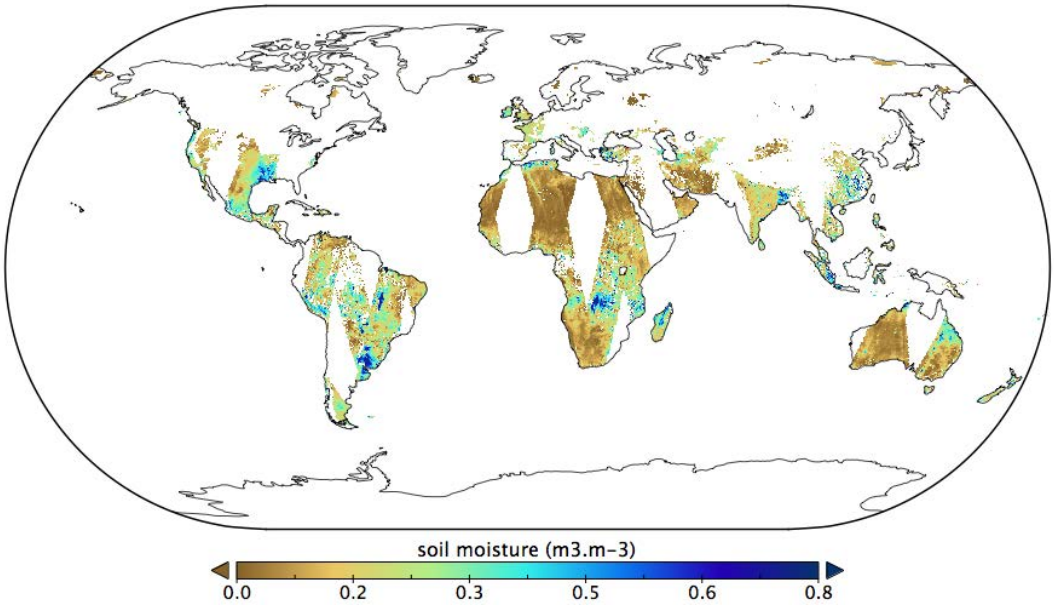

Figure 2-2: Example of CATDS Level-3 daily soil moisture retrievals (20th Feb 2010)

satellite data against four watersheds in the U.S. They demonstrated that SMOS reaches the accuracy target with a RMSE of 0.043 m^3/m^3 (ascending) and 0.047 m^3/m^3 (descending). Leroux et al. (2013) evaluated SMOS error globally via the triple collocation method and pointed out that SMOS works best over North America, Middle East, central Asia and Australia, which are RFI (Radio Frequency Interference) free regions. The RFI contamination is caused by the unauthorized emission within the protected passive band coming from active sources, and unwanted emissions from active services operating in adjacent bands (Oliva et al., 2012).The SMOS error is relatively high over Europe, Asia and North America where the proportion of forest is high. The accuracy of SMOS is also influenced by water bodies, salted water, wetlands, barren or urban area. Since it is sensitive to canopy cover, surface roughness and surface texture, proper parameterization of forest models and soil texture in retrievals is required in the retrieval algorithms but not always achievable (Jackson et al., 2012).

Chapter 3

Joint assimilation of GRACE and SMOS water content retrievals

Due to the difficulty of multi-scale and multi-variant assimilation, the focus of hydrological data assimilation is mainly on improving one state variable with one or multiple observations. In this study, satellite-observed total water storage change and surface soil moisture were assimilated jointly into a water balance model. It was the first time that the contrasting water content retrievals with different spatial and temporal resolution were integrated with model simulations to better redistribute water storage horizontally and vertically. The joint assimilation provides new insights for monitoring subsurface water storage availability, especially root-zone soil water and groundwater without direct measurements. The joint assimilation framework together with the results over Australia are introduced in this chapter. This chapter is based on the material published in Water Resource Research:

Tian, S., Tregoning, P., Renzullo, L. J., van Dijk, A. I., Walker, J. P., Pauwels, V. R., & Allgeyer, S. (2017). Improved water balance component estimates through joint assimilation of GRACE water storage and SMOS soil moisture retrievals. Water Resources Research, 53(3), 1820-1840.

abstract

The accuracy of global water balance estimates is limited by the lack of observations at large scale, and the uncertainties of model simulations. Global retrievals of terrestrial water storage (TWS) change and soil moisture (SM) from satellites provide an opportunity to improve model estimates through data assimilation. However, combining these two data sets is challenging due to the disparity in temporal and spatial resolution at both vertical and horizontal scale. For the first time, TWS observations from the Gravity Recovery and Climate Experiment (GRACE) and near-surface SM observations from the Soil Moisture and Ocean Salinity (SMOS) were jointly assimilated into a water balance model using the Ensemble Kalman Smoother from January 2010 to December 2013 for the Australian continent. The performance of joint assimilation was assessed against open-loop model simulations and the assimilation of either GRACE TWS anomalies or SMOS SM alone. The SMOS-only assimilation improved SM estimates but reduced the accuracy of groundwater and TWS estimates. The GRACE-only assimilation improved groundwater estimates but did not always produce accurate estimates of SM. The joint assimilation typically led to more accurate water storage profile estimates with improved surface SM, root-zone SM, and groundwater estimates against *in-situ* observations. The assimilation successfully downscaled GRACE-derived integrated water storage horizontally and vertically into individual water stores at the same spatial scale as the model and SMOS, and partitioned monthly-averaged TWS into daily estimates. These results demonstrate that satellite TWS and SM measurements can be jointly assimilated to produce improved water balance component estimates.

3.1 Introduction

The ability to accurately estimate terrestrial water storage (TWS) and its components (e.g. soil moisture, groundwater, surface water, snow and ice)

is critical for hydrological studies and water resource assessment and management. Constraining water balance estimates with satellite observations over large areas offers better potential for assessing water availability, especially in areas with sparse ground observations. Data assimilation is an effective approach to optimally combine information from both model predictions and observations. Measurements of water cycle components have been integrated into hydrological models in a number of studies, including measurements of precipitation (e.g. Joyce et al. (2004); Huffman et al. (2007)), soil moisture (e.g. Walker and Houser (2001a); Reichle and Koster (2005); Draper et al. (2009); Renzullo et al. (2014); Dumedah et al. (2015)), TWS (e.g.Zaitchik et al. (2008); Li et al. (2012); van Dijk et al. (2014a); Eicker et al. (2014); Tangdamrongsub et al. (2015)) and snow (e.g. Sun et al. (2004); Rodell and Houser (2004); Andreadis and Lettenmaier (2006)). In many cases, assimilation improved the model estimates.

As a key component in the water cycle, soil moisture (SM) controls the water and energy exchange between the atmosphere and land surface. However, the estimation of soil moisture distribution within the profile at large scales remains challenging due to the lack of root-zone SM observations. The assimilation of near-surface SM observations has been shown to improve near-surface as well as root-zone soil water balance estimates and, in some cases, also produced improved estimates of evaporation, runoff or deep drainage (Walker et al., 2001; Reichle and Koster, 2005; Brocca et al., 2010; Renzullo et al., 2014; Draper et al., 2011). A number of recent studies (Dumedah et al., 2015; Lievens et al., 2015; Martens et al., 2015) assimilated SM retrievals from the SMOS (Soil Moisture and Ocean Salinity) satellite mission (Kerr et al., 2001) into land surface models. SMOS is the first polar-orbiting, space-born, 2D interferometric L-band radiometer, fully dedicated to the retrieval of surface SM and ocean salinity. Martens et al. (2015) found that SMOS SM retrievals sourced from the Level 3 CATDS (Centre Aval de Traitement des Données SMOS) product (Jacquette et al., 2010) have high quality over Australia. The

same SMOS SM retrievals were used in this study. Since SM moisture profile estimates can be improved by the assimilation of surface SM observations, it might be expected that total water storage estimated will also be improved. However, so far this hypothesis has not been tested.

The absence of integrated TWS measurements as an overall water balance constraint was resolved with the launch of the GRACE (Gravity Recovery and Climate Experiment) mission in 2002. It provides a complement to traditional ground-based hydrological measurements which are restricted to the scales of sites or individual catchments. The observed mass changes are the combined result of changes in surface water, soil water, groundwater, vegetation water, snow and ice (Tapley et al., 2004). Therefore, ancillary data sets or model-based methods are needed to partition GRACE-observed mass change into changes in the individual water components.

GRACE-observed TWS is most commonly provided as an integrated monthly-averaged water storage change, known as the TWS anomaly (TWSA). An issue that requires much consideration is how to downscale, in a temporal sense, the monthly GRACE TWSA estimates to the high temporal frequency of the hydrologic model. Zaitchik et al. (2008) assimilated monthly GRACE TWS estimates into the Catchment Land Surface Model (CLSM) using an ensemble Kalman smoother (EnKS)-like approach and distributed the increments evenly over each day of the month. Li et al. (2012) and Forman et al. (2012) applied a similar method as in Zaitchik et al. (2008) and showed the benefits of assimilation in drought monitoring and snow water equivalent estimation. Furthermore, the drought indicators based on assimilated GRACE data, in particular the groundwater storage drought indicator, showed their great value for drought detection (Houborg et al., 2012). Eicker et al. (2014) and Schumacher et al. (2016) assimilated GRACE data using an ensemble Kalman filter (EnKF) to jointly update model states and parameters at monthly time steps with consideration of spatial covariance. Tangdamrongsub et al. (2015) also implemented an EnKF to assimilate GRACE data into a model consid-

ering hydrological routing and demonstrated that GRACE data assimilation can improve overall model behavior but with little improvement in streamflow estimates. van Dijk et al. (2014a) developed an "off-line" assimilation scheme combining GRACE, satellite water level data and hydrological models for global water cycle reanalysis. All these studies demonstrate the potential of GRACE data assimilation to improve TWS and groundwater estimates. However, the assimilation of TWS does not guarantee accurate estimation of surface SM (Li et al., 2012), and vice versa.

Assimilating multiple observations of the water cycle components should maximize consistency between water balance variables and result in improved water balance estimates. In this study, the feasibility and benefits of jointly assimilating SMOS-derived SM and GRACE-derived TWS estimates into a global water balance model (i.e. the World-Wide Water model, W3; van Dijk et al. (2013a), Section 3.2.1) was investigated. To assess the performance of the joint assimilation, the open-loop model (without assimilation), the assimilation of SMOS data only and the assimilation of GRACE data only, respectively, were conducted as comparison against the joint assimilation results. *In-situ* surface SM, root-zone SM, evapotranspiration (ET), streamflow, and groundwater level observations were used to evaluate the assimilation results (Section 3.3). SMOS observed near-surface SM and GRACE observed TWSA were also used as independent data sets to evaluate either GRACE-only or SMOS-only assimilation experiment. TWSA estimated through SMOS-only data assimilation were evaluated against GRACE TWSA data to examine the influence of SM assimilation on TWSA estimates. Conversely, SMOS observations were used to evaluate surface SM estimates in the GRACE-only assimilation experiment as ancillary independent observations in addition to *in situ* measurements. The deficiencies of the assimilation of either SMOS or GRACE data only, and the comparative benefits of joint assimilation for estimating soil moisture profile, groundwater and fluxes are outlined (Section 3.4).

3.2 Materials and Method

3.2.1 Hydrological modelling

The hydrological model employed in this study is the World-Wide Water (W3) model (van Dijk et al., 2013a) (available at http://www.wenfo.org/wald/). It is a global water balance model based on the landscape hydrology component model of the Australia Water Resource Assessment system (AWRA-L) (van Dijk, 2010a; Van Dijk and Renzullo, 2011). Full technical details about AWRA-L can be found in the model technical documentation (van Dijk, 2010a). The W3 model consists of a grid-based, one-dimensional landscape hydrological model with modules describing surface water and groundwater dynamics and snow. It can be considered as a hybrid between a simplified grid-based land surface model and a "lumped" catchment model of water balance, vegetation ecohydrology and phenology (van Dijk et al., 2013a).

Soil water and energy fluxes are simulated individually for two hydrological response units (HRUs), namely, deep-rooted vegetation and shallow-rooted vegetation. Each of the HRUs occupies a fraction of each grid cell f_{HRU}. The groundwater and surface water (rivers, lakes and reservoirs) dynamics are simulated at grid cell level, effectively representing individual catchments. Lateral water distribution between grid cells is not considered in the vertical water balance estimation. Net radiation is the sum of net short-wave radiation and net long-wave radiation (Brutsaert, 1975). Precipitation is partitioned into interception evaporation and net precipitation. The net precipitation is partitioned into infiltration, infiltration excess surface runoff and saturation excess runoff (van Dijk, 2010a).

W3-simulated TWS is the integration of soil moisture, groundwater, surface water, snow and vegetation water storage. The soil water storage is partitioned into individual stores for three layers: top layer S_0, shallow root layer S_s and deep root layer S_d in equivalent water height. Fluxes for these three unsaturated soil layers comprise infiltration, soil evaporation, drainage and root

water uptake. Layer thickness and porosity are not separately specified to avoid model parameter estimation equifinality issues (Renzullo et al., 2014). Instead, a maximum water holding capacity S_{zFC} (field capacity) is specified for each layer z. Spatial estimates of soil water availability from the Australian Soil Resource Information System (http://www.asris.csiro.au) were used to estimate the equivalent physical thickness of the W3-modelled soil layer. Thickness can be estimated by the proportion of field capacity water storage to the available water content (i.e. the difference between field capacity and wilting point for each soil layer). The resulting thicknesses of the top-layer soil in W3 is 5 to 10 cm. The shallow- and deep-root soil layers have an estimated thickness between 15-25 cm and 3-6 m, respectively.

Groundwater balance terms include ground water storage, S_g, recharge from deep drainage, capillary rise (estimated with a linear diffusion equation), evaporation from groundwater saturated areas, and discharge into streams (estimated with a linear reservoir model) (Peña-Arancibia et al., 2010; van Dijk, 2010b,a). The river water balance comprises surface water storage, S_r, inflows from runoff and discharge, open water evaporation and catchment water yield (van Dijk, 2010a). A simple but widely tested snow model used in HBV96 (Hydrologiska Byrans Vattenbalansavdelning model) was implemented in W3 for snow water balance estimation (Bergström et al., 1995). Finally, it is assumed that 80% of vegetation biomass consists of water.

Global daily gridded 0.5° precipitation, short-wave and long-wave downwards radiation, air temperature, wind speed, surface pressure, humidity and snow rate from the WATCH (Water and Global Change) Forcing Data methodology applied to ERA-Interim (WFDEI) (Weedon et al., 2014) (available at https://wci.earth2observe.eu/), were used as meteorological inputs to the model. A global tree cover fraction map (Hansen et al., 2003) was used to determine the vegetation fraction of each HRU. An albedo climatology was derived from Moderate Resolution Imaging Spectrometer white-sky albedo (Moody et al., 2005) (http://modis-atmos.gsfc.nasa.gov/ALBEDO/). The parameter values

used in this study are based on those from AWRA-L version 0.5 (van Dijk, 2010a).

3.2.2 Satellite observations

3.2.2.1 SMOS soil moisture retrieval

SMOS observations allow retrieval of near-surface SM at global scale with a repeat cycle of 2-3 days (Kerr et al., 2001). The SMOS satellite is in a sun-synchronous orbit that has equatorial overpasses at 6:00 am ascending and 6:00 pm descending. The signal depth of the SMOS L-band observations is typically in the range of 0-5 cm, depending on the degree of soil wetness. Daily global SM retrievals from the Level 3 CATDS (Centre Aval de Traitement des Données SMOS) product (Jacquette et al., 2010) from January 2010 to December 2013 were used. The Level 3 SM retrieval algorithm is based on the ESA level 2 processor (Kerr et al., 2012) but enhanced using a multi-orbit retrieval method. The retrievals are available for both ascending and descending orbits on a regular 25 km EASE (Equal Area Scalable Earth) grid instead of the irregular ISEA (Icosahedral Snyder Equal Area) system (Kerr et al., 2008). The data quality index, which considers the error in the retrieval as well as the accuracy of the brightness temperatures, quantifies the uncertainty in the retrievals.

The daily SM estimates used in the assimilation were derived from ascending passes, since the retrievals from early morning or nighttime brightness temperatures show better agreement with *in situ* measurements (Jackson et al., 2012; Dente et al., 2012; de Jeu, 2003; Draper et al., 2009). To facilitate assimilation into the W3 model, SMOS SM retrievals were upscaled from their original 0.25° resolution to the W3 modeling grid of 0.5° resolution by simple averaging to be consistent with the forcing data.

3.2.2.2 GRACE total water storage estimates

Since 2002, GRACE has measured variations in the regional gravity field to provide unique measurements of monthly mass changes at regional to global scale. Changes in water storage induce mass redistribution and, therefore, can be estimated from GRACE after removing atmospheric, ocean and other time-variable gravity effects. The total water storage (TWS) change estimates used in this study were obtained from the most recent release of the monthly $3^\circ \times 3^\circ$ Jet Propulsion Laboratory (JPL: http://grace.jpl.nasa.gov) mascon solution (JPL-RL05M) (Watkins et al., 2015). The mascon surface mass changes are provided with a spatial sampling of 0.5° resolution due to the boundaries of mascons locating parallels of 0.5° increments. The value of each $0.5^\circ \times 0.5^\circ$ grid inside a corresponding mascon is identical. JPL-RL05M used surface spherical cap mascons to directly estimate mass variation from the inter-satellite range-rate measurements. The regularization used employs a combination of quasi-global geophysical models and altimetry observations to obtain accurate mass flux estimates globally and eliminates the need for empirical destriping filtering. A glacial isostatic adjustment (GIA) correction has been applied based on the model introduced by Wahr and Zhong (2012). Additional scaling factors derived from hydrological modelling (Landerer and Swenson, 2012) for the interpretation of signals at sub-mascon resolution were not applied to the data in this study. Uncertainty in each mascon derived, following Wahr et al. (1998), is provided along with the product. Each monthly TWS estimate represents the surface mass anomaly relative to the baseline average over January 2004 to December 2009. To obtain absolute TWS estimates, the averaged model-simulated TWS over the same period was added to the GRACE TWS estimates in the assimilation. Twelve years of GRACE TWS change estimates from April 2002 to December 2013 were used in this study.

3.2.3 Data assimilation method

In this study, two single-observation assimilation experiments (i.e. the SMOS-only assimilation or GRACE-only assimilation, respectively) were conducted as comparisons to the joint assimilation of SMOS and GRACE observations. SMOS SM retrievals were assimilated into the W3 model using both the EnKF (Ensemble Kalman Filter) and EnKS (Ensemble Kalman Smoother). GRACE TWSA estimates were assimilated into the model using the EnKS with a one month assimilation window considering temporal error correlations between each day. Near-daily SMOS SM and monthly GRACE TWSA retrievals were jointly integrated into the W3 model through the EnKS with a one-month assimilation window to resolve their difference in temporal resolution. Like most data assimilation approaches, our approach explicitly acknowledges that precipitation estimates are uncertain. As a result, water balance is not necessarily maintained, that is, changes in the total water storage in each control volume (i.e., grid cell TWS) may vary from the net sum of fluxes (i.e., the original precipitation estimate, evapotranspiration and streamflow). This is addressed in Section 3.4.4.

3.2.3.1 Ensemble Kalman filter and ensemble Kalman smoother

The EnKF is a Monte-Carlo implementation of the Bayesian state update problem that was first introduced by Evensen (1994) to improve the computational feasibility for high-dimensional systems. It is relatively simple and efficient, and has become one of the most popular approaches for assimilating satellite data (e.g. Reichle et al. (2002); Crow and Wood (2003); Clark et al. (2008); Renzullo et al. (2014); Lievens et al. (2015)). The ensemble of model states is generated by propagating the model forward in time with perturbations, known as forecast states. The forecast state ensemble is used to determine model covariances under the assumption of unbiased (i.e. random only) model error. In the analysis or update step, the forecast states representing the uncertainty in model states are adjusted towards the observations

by the Kalman gain matrix, which is determined by model and observation error covariances.

The EnKS is a sequential smoother using only the ensemble of forward-in-time model states, and bears a strong resemblance to the EnKF (Evensen and Van Leeuwen, 2000). Unlike the EnKF, the EnKS computes the analysis from previous times up to the current time within an assimilation window, and information at assimilation times is propagated backwards in time using the ensemble covariances. A fixed-lag (or assimilation window) is defined in practical implementations to improve computational efficiency (Cohn et al., 1994). The assimilation window is determined based on the assumption that the observations will only impact the states in this time interval. The EnKS also eliminates discontinuities or spikes otherwise obtained with sequential filtering of infrequent observations. The benefits of EnKS over EnKF have been demonstrated in several studies (e.g. Evensen and Van Leeuwen (2000); Dunne and Entekhabi (2006); Dunne et al. (2007)).

Generation of an ensemble with an appropriate spread is a critical step in the ensemble-based assimilation. The ensemble spread should be large enough to allow the observations to influence model estimates (Renzullo et al., 2014). Inappropriate ensembles will impact on model error covariances and place undue emphasis on either the observations or the modeled forecast, thus affecting the correlated states (Turner et al., 2008). The initial conditions of the ensembles were perturbed and optimized by a 10-year ensemble open-loop spin-up from 1992 to 2002 to reach dynamic equilibrium. The meteorological forcing data for the model were perturbed to generate an ensemble of forecast states. Each ensemble member i of the state variable x at current time step (t) can be expressed in a discrete form as

$$x_t^{i-} = f(x_{t-1}^{i+}, u_t^i, \alpha, \omega_t^i) \quad i = 1, ..., M, \tag{3.1}$$

where f represents the hydrologic model and u, α, and ω indicate the forcing

data, model parameters and model error respectively. The superscripts '-' and '+' represent the forecast and analysis state, and M denotes the number of ensemble members. In this study, 100 ensemble members were used to ensure an accurate approximation of the error covariances while maintaining computational efficiency.

A previous assimilation study with the closely related AWRA-L model by Renzullo et al. (2014) found that daily precipitation, incoming shortwave radiation and average air temperature were the most important forcing variables and that the perturbation of these variables ensures adequate ensemble spread. Therefore, radiation and air temperature were perturbed with an additive error, and precipitation was perturbed with a multiplicative error. Gaussian noise of 50 W.m^{-2} was added to the shortwave radiation, while air temperature was perturbed with an additive error of 2K. We assumed a multiplicative error in precipitation (P_g) by taking a univariate random sample between ± 0.6 P_g to avoid negative rainfall for low or zero rainfall values.

The satellite observations available at measurement time t can be gathered in a vector y_t with the uncertainties specified in the random error ϵ such that

$$y_t = \mathcal{H}(x_t^{i-}) + \epsilon_i, \quad \epsilon \sim N(0, R), \tag{3.2}$$

where $\mathcal{H}$ is the observation operator that maps the state vector x to the observation space. In both EnKF and EnKS, the analysis state for each ensemble member can be updated with the forecast state and a weighted difference between the observation and model prediction as:

$$x^{i+} = x^{i-} + P^- H^T (H P^- H^T + R)^{-1} [y - \mathcal{H}(x^{i-}) + \epsilon_i], \quad i = 1, ..., M, \tag{3.3}$$

where the model error covariance P can be computed from the ensemble of forecast states. If the model error covariance P approaches zero, less weight is gained from the observation y. On the contrary, if the observation error tends towards zero, the analysis states are dominated by the observations.

In the EnKF, model forecast error covariance at time t is computed as

$$P_t^- = \frac{1}{M-1}\sum_{i=1}^{M}[x_t^{i-} - \overline{x_t^-}][x_t^{i-} - \overline{x_t^-}]^T, \tag{3.4}$$

where the analysis state is only influenced by the observation and model error covariance at the update time t. However, all the forecast states within a smoothing interval are updated together with a set of available observations in the EnKS. Therefore, the temporal correlations within the observation and model forecast states are considered in the error covariance matrices.

3.2.3.2 Assimilating SMOS only

Both EnKF and EnKS were employed to assimilate SMOS-derived SM data in the W3 model. The model states x for update were the W3 simulated top- and shallow-layer soil water storage for two HRUs (shallow-rooted and deep-rooted vegetation, i.e. S_{0hru1}, S_{0hru2}, S_{Shru1}, S_{Shru2}). The SMOS observations impact on the model-simulated deeper soil water storage indirectly through the percolation process from the top soil layer and directly through the adjustments from the error correlation structure in the analysis step. The model states of each grid cell were updated independently without considering neighboring grid cells. The analysis increments of two HRUs for each grid cell were calculated separately.

Before the assimilation, SM observations were rescaled to remove systematic difference between the model and observations (Reichle and Koster, 2004; Renzullo et al., 2014; Koster et al., 2009). This is mainly because the W3 model simulates soil water storage in equivalent water height but SMOS SM retrievals are in volumetric water content. Scaling was done by a mean and variance matching, which ensures the same statistical distribution between model and observations for an effective adjustment of the model estimates. The observations were transformed into model space without modifying the dynamics of the data.

The observation operator $\mathcal{H}$ was the relative wetness ω in this case, due to the inconsistency in units and soil layer thickness between the SMOS observations and W3 model. Relative wetness was calculated as

$$\mathcal{H} = \omega = (1 - f_{sat})\omega_0 + f_{sat}, \tag{3.5}$$

where ω_0 is the relative wetness of the unsaturated soil column, derived by scaling the top soil layer water storage by the field capacity (i.e. S_0/S_{0FC}) for each HRU, and f_{sat} is the fraction saturated area.

To avoid ensemble collapse and to optimize the use of observations, the covariance inflation technique introduced by Anderson and Anderson (1999) was applied to the top soil layer water storage estimates. Instead of applying a fixed inflation factor all the time, we inflated the ensemble only when the model error was less than 5%. This rational was used to ensure model uncertainties competitive with SMOS uncertainties to allow SMOS to impact on the model states. The inflation factor was calculated dynamically from the variance of the top-layer storage estimates based on error propagation theory. This procedure eliminated the under-estimation of the model error, especially during low or zero rainfall period. Without covariance inflation, error variance would decrease in time to low values, and therefore the observation would not impart constraint on the model estimates (Houtekamer and Mitchell, 2005).

In the EnKF, the states were updated instantaneously when the SMOS observation was available. In the EnKS, by contrast, all of forecast states in a month were entered in one vector and updated jointly on the last day of a month. The temporal and spatial varying observation errors used in the assimilation were derived from the uncertainties of the SM provided along with the SMOS product. Since the observations were transformed to relative wetness instead of absolute values, the uncertainties of the relative wetness derived from SMOS were transformed using the same scaling factor applied to the original SMOS SM data.

3.2.3.3 Assimilating GRACE only

GRACE TWS change estimates represent the average TWS change over a month. The W3 model, however, simulates TWS at a daily time step. We used the EnKS with a one-month assimilation window to assimilate GRACE TWS change. The long-term TWS mean from the open-loop model simulation was added to GRACE TWS anomalies to obtain the absolute TWS estimates. The water storage components from the W3 model comprised the system states, and were updated individually with GRACE estimates. We used the 3° mascon solutions with a spatial sampling at 0.5° resolution, without considering the spatial correlation between neighboring grids. Thus, there was no variation in TWS anomalies inside the grid cells corresponding to each 3° mascon. GRACE TWS signals were disaggregated vertically into changes in the individual water stores and temporally into daily variations through the assimilation process.

$$\begin{aligned}\mathcal{H} =& \frac{1}{N}\sum_{n=1}^{N}[f_{HRU1}(S^n_{0,hru1} + S^n_{S,hru1} + S^n_{d,hru1} + S^n_{snow,hru1} + S^n_{veg,hru1}) \\ &+ f_{HRU1}(S^n_{0,hru1} + S^n_{S,hru1} + S^n_{d,hru1} + S^n_{snowhru1} + S^n_{veghru1}) + S^n_g + S^n_r],\end{aligned} \tag{3.6}$$

We calculated model predicted monthly-averaged TWS using all the daily TWS estimates in a month as the observation operator $\mathcal{H}$ (Equation 3.6). Since the water stores associated with the soil (three layers), snow and vegetation water are simulated independently with two HRUs, and groundwater and surface water are simulated at the grid scale, all the daily states in a month were gathered in a $(5 \times 2 + 2)$ $12N \times 1$ state vector for each ensemble member (i.e. 12 states per day for N days in a month). The N-day state error variance and observation state error covariance were computed, and then used to compute the analysis increments for individual daily water stores. In the assimilation, the ensemble of forecast states was established using all daily forecasts in the month. The smoother was applied at the end of the month and updated all

states back to the first day of the month through the temporal error correlation. Next, the states of the first day from the next month were initialized with the analysis states of the last day from the previous month. The perturbation of the observations was temporally and spatially independent using the uncertainties provided with the JPL-RLM05 product.

3.2.3.4 Joint assimilation

Different from the single-observation assimilation experiments, joint assimilation provides multiple constraints to the W3 model estimates. We applied an EnKS with a one-month assimilation window to assimilate the SMOS SM and GRACE TWS observations into the W3 model. The state vector was the same as for the GRACE-only experiment, including all daily water storage compartments for a month. The observation vector was established with all available SMOS observations during the month and a single monthly GRACE observation. The observation operator in the joint assimilation combined the operator for the assimilation of SMOS and GRACE data, respectively. The model-predicted daily relative wetness of the top soil layer was calculated as explained in Section 3.2.3.2, while model-predicted TWS was treated identically as the GRACE-only experiment (see Section 3.2.3.3). The analysis increments of the states were calculated from both SMOS and GRACE data based on the error variance and covariance matrices (Equation 3.3). Therefore, the degree of influence from the observations on the model states is related to the relative error magnitudes of the model and both SMOS and GRACE observations.

The mismatch in dynamic range and observation frequency required special attention. There were two orders of magnitude difference between the units of SM and TWS, resulting in large differences in the magnitude of uncertainties (i.e. ~ 0.04 m^3/m^3 for SM and ~ 20 mm for TWS). The large observation uncertainties of GRACE assigned the corresponding elements a relatively smaller value in the Kalman gain matrix, resulting in less weight given to the GRACE observations. There were about 10 SMOS observations per month and only

1 monthly GRACE observation, thus the analysis increment for each individual state was impacted by 10 SM observations and 1 TWS observations. Left unaddressed, the analysis increments gained from SMOS and GRACE data would therefore be imbalanced, leading SMOS to unduly dominate the model estimates. To account for this unit disparity, and to ensure neither observations inappropriately dominated the model estimate, a weighting factor was applied to the observation uncertainties. We conducted several experiments with different scaling factors for the observation uncertainties to allow SMOS and GRACE to have approximately equal weighting in the state vector updating process. Three of those experiments are described here, i.e. assimilation with original observation uncertainties, multiplying SMOS uncertainties by 2 and multiplying GRACE uncertainties by 0.5, respectively.

3.2.4 Model evaluation

We used GRACE observed TWS anomalies to validate the TWS estimates updated by the SMOS-only assimilation, and SMOS SM to validate SM estimates updated by assimilation of GRACE only. This analysis was helpful to evaluate the performance of the single-observation assimilation and to investigate whether there was any conflicting information imparted by the two observations. In addition, *in situ* measurements of near-surface SM, root-zone SM, groundwater level, evapotranspiration and streamflow were used to validate related model-simulated water balance variables in comparison to the open-loop model simulation. These measurements are described in the following sections.

3.2.4.1 Soil moisture observations

Three separate Australian networks of *in situ* SM sensors were used in the evaluation of our modeling results: OzNet, OzFlux and CosmOz (Holgate et al., 2016) (Figure 3-1(a)). OzFlux and CosmOz sites are spread across Australia, while OzNet provides dense measurements for one catchment (that

of the Murrumbidgee River) in southeast Australia. OzFlux is a national ecosystem research network providing observations of energy, carbon and water exchange between the atmosphere (http://www.ozflux.org.au). CosmOz is a network of cosmic-ray sensors containing 10 calibrated stations out of 14 total stations across Australia (http://cosmoz.csiro.au). OzNet contains 63 monitoring stations in the Murrumbidgee River catchment in New South Wales, Australia (Smith et al., 2012). Most OzNet and OzFlux stations use Campbell Scientific water content reflectometry probes and provide SM at depths from 0 to up to 90cm. Unlike the point measurements from other networks, the measurement scale of the CosmOz cosmic ray probes have a signal source area with an approximately 600m radius, *i.e.* ∼30 ha (Desilets and Zreda, 2013). The signal depth is influenced by water content itself; from ∼10 cm depth in saturated soil to ∼50 cm in very dry soil (Franz et al., 2012).

We evaluated model-simulated near-surface SM using all available *in situ* measurements (OzNet, OzFlux, CosmOz) at 0-10 cm from 2010 to 2013. The CosmOz measurements were used to evaluate surface SM, due to the depth of CosmOz measurements being generally 6-15 cm in wet soil (Hawdon et al., 2014). Furthermore, measurements from 37 OzNet probes measurements during our assimilation period were used for evaluation of root-zone SM at 0-30 cm and 0-90 cm depth. For each OzNet, OzFlux and CosmOz probe, daily SM were computed by averaging all the measurements within the 24 hours. The mean of all measurements within a model grid cell was used if these contained multiple probes (locations are available at Table S1). We provisionally assumed these daily-averaged measurement to be representative for the coincident model grid cell. Since the averaged effective depth of CosmOz sites are around 10-15cm, the CosmOz sites were included in the evaluation of top-layer soil moisture. In total, there were *in situ* data for 39 grid cells to evaluate the top-layer SM estimates and 9 grid cells to evaluate the shallow-layer SM estimates. Correlations between *in situ* data and model-simulated soil water storage at the same depth were calculated to evaluate the accuracy of the esti-

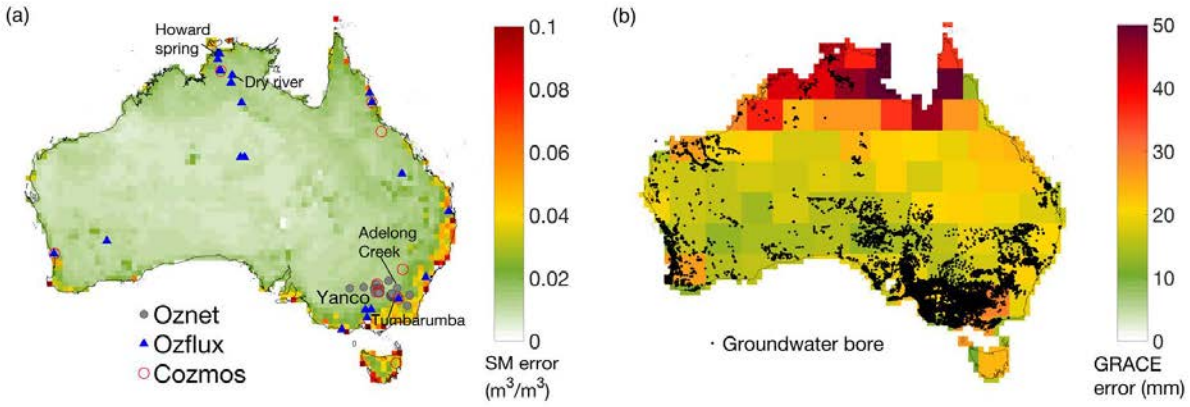

Figure 3-1: In-situ observation networks for validation: (a) locations of soil moisture probes from OzNet, OzFlux and CosmOz with a background of temporally-averaged error estimates in SMOS soil moisture retrievals; (b) groundwater bores with a background of temporally-averaged error estimates of GRACE mascon TWS change estimates.

mation, to circumvent the difference in units between model simulations (mm extractable water) and *in situ* measurements (soil volume %).

3.2.4.2 Groundwater observations

There are around 800,000 groundwater monitoring bores spread unevenly across Australia, providing point-scale groundwater level change over time (Figure 3-1(b)). The groundwater level data from the Australian Groundwater Explorer (Bureau of Meteorology, http://www.bom.gov.au/water/groundwater/explorer) were collected. We chose

bores that had more than 24 observations and at least 4 consecutive months over the period of January 2002 to December 2013. Water level was reported as either depth to water (DTW, depth below a reference point on the bore), standing water level (SWL, distance from the top of the ground surface to the groundwater) or reduced standing water level (RSWL, groundwater elevation above Australian Height Datum). We calculated groundwater level anomalies from these measurements and aggregated them to 309 values on 0.5° grid cells to enable a comparison to model-estimated groundwater storage anomalies. The mean of all the measurements in a grid cell was assumed to be representative of the grid cell, since GRACE detected the average water change inside its footprint and cannot distinguish the difference between aquifers. The number of bores in each grid cell varies from 1 to > 4000; most grid cells with high bore density were located in south-east Australia. Monthly groundwater level anomalies were computed by averaging all the measurements during a month and compared with model simulations owing to the difference of water level baseline for each bore. Specific yield values were not applied to the water level measurements because we only evaluated correlation between groundwater level anomalies and groundwater storage estimates. This avoids errors from assumed specific yield values to contaminate the comparison.

3.2.4.3 Evapotranspiration observations

Observations from the OzFlux network (http://www.ozflux.org.au) were used to evaluate model estimates of daily evapotranspiration (ET) from January 2010 to December 2011. The coincident model grid cell was compared with observations from 16 flux towers. Observations were converted from latent heat flux measurement, integrated over the 24-hour period, into model units of mm per day using the latent heat of vaporisation (i.e. 2.45 MJ/kg).

3.2.4.4 Streamflow observations

Streamflow observations from 780 unregulated catchments across Australia (Zhang et al., 2013) were used in the evaluation of monthly modelled streamflow. Where catchment boundaries overlapped serval model cells, corresponding cells were averaged to give representative model estimates. Similarly, where several catchments were within a single model cell, the streamflow data were averaged. The catchment boundaries and their coincident model grid cells are shown in Figure S1 of the supplementary data. In total, there were 84 aggregated catchments available from January 2010 to December 2011 for use in the evaluation of model-simulated streamflow before and after the assimilation.

3.3 Results

3.3.1 Contributions of SMOS and GRACE data to different water stores

The analysis increments were calculated as percentages to investigate the contributions to different water stores from SMOS data and GRACE data. Figure 3-2 shows the averaged analysis increments of March and September from three assimilation experiments: the SMOS-only assimilation (EnKF), GRACE-only assimilation and joint assimilation, respectively. The analysis increments to the top-layer soil water from SMOS-only assimilation was the largest among the three with around 30% (Figure 3-2(a)). GRACE data were less correlated with top-layer soil water storage and led to moderate analysis increments (Figure 3-2(b)). This appears to be a result of the high variability of near-surface SM in both time and space and the incongruity between daily precipitation and monthly GRACE TWS change observations. Also, the monthly TWS change provided the information of integrated water storage change over a period and may attenuate or cancel out the small magnitude change of sur-

face soil water through the averaging. However, SMOS and GRACE data imparted opposite water variations in east Australia, where SMOS decreased the soil moisture and GRACE increased the soil moisture. Similar conflicting increments were found for the shallow- and deep-layer soil moisture between GRACE and SMOS data. Figure 3-2(c) shows the analysis increments from both SMOS and GRACE through joint assimilation. The adjustments of top- and shallow layer soil water storage were dominated by SMOS data, similar to SMOS-only assimilation trends but with a reduced amplitude of change. This is probably because the EnKS smoothed the adjustments over a month instead of providing an instantaneously update.

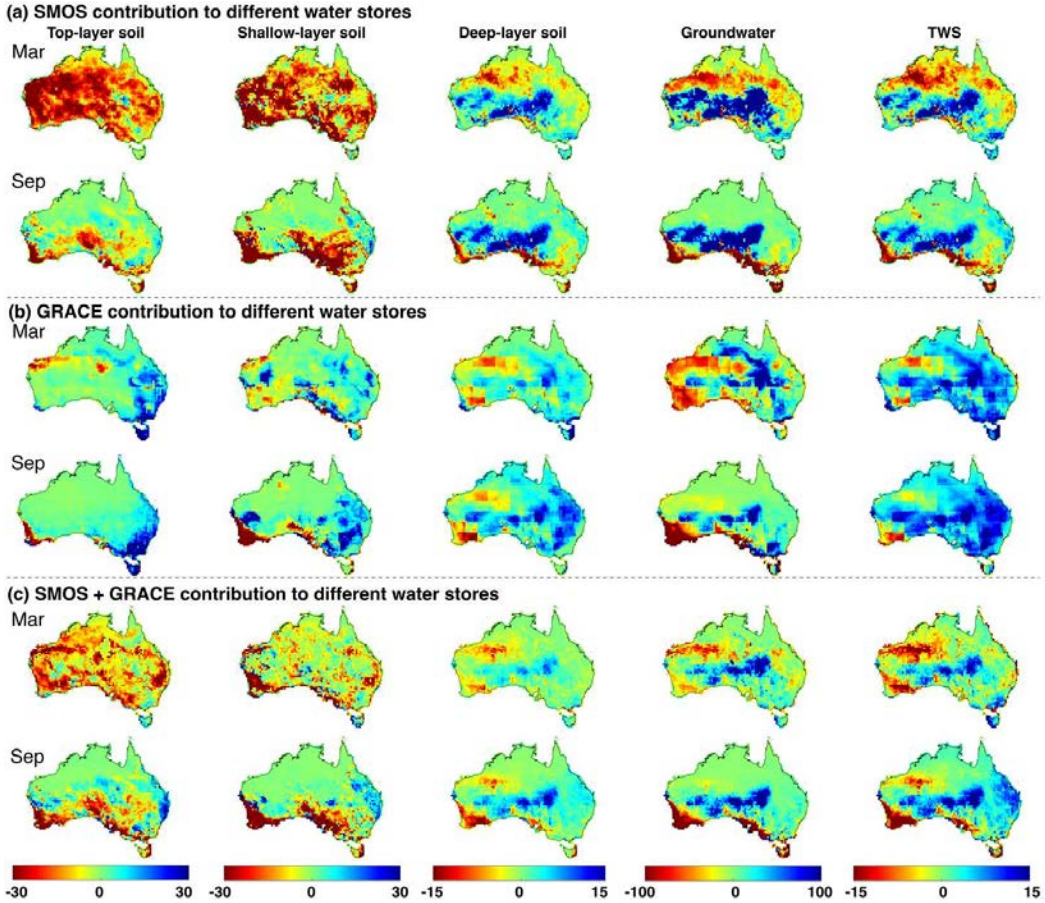

Figure 3-2: Averaged analysis increments to individual water storage components (top-, shallow-, deep-layer soil water, groundwater storage, and total water storage) in percentage $(x^a\text{-}x^o)/x^o$ in March and September: (a) contributions of SMOS data ; (b) contributions of GRACE data; and (c) contributions of the combination of SMOS and GRACE data.

In the SMOS-only assimilation, groundwater storage was not included in the state vector. The analysis increments of groundwater and TWS were caused by the other updated states and model physics. Therefore, assimilating SMOS data alone can greatly impact other states such as groundwater and TWS. However, the analysis increments for groundwater and TWS from the joint assimilation were similar to the increments from GRACE-only assimilation. The magnitude of increments of the joint assimilation was slightly smaller than the GRACE-only assimilation, owing to the inconsistent increments from SMOS data. Thus, assimilating SMOS or GRACE data alone can lead to different water variations for different water layers. Overall, SMOS mainly contributed to update the top- and shallow-layer soil water estimates, while GRACE dominated groundwater and TWS estimates.

3.3.2 Consistency with satellite retrievals

The top soil layer relative wetness estimated from open-loop model simulation and different assimilation experiments were compared with SMOS-derived near-surface SM (Figure 3-3(a)). GRACE-derived TWS anomalies were compared to model-simulated monthly TWS anomalies with and without the assimilation of satellite observations (Figure 3-3(b)). The 0.5° model-simulated TWS anomalies were aggregated over each 3° mascon to compare with GRACE data. It is expected that the assimilation of observations would bring model estimates closer to the observations and 99% of correlations passed the significance test. The averaged correlation of SM from SMOS-only assimilation and SMOS data improved to 0.88 and 0.86 for EnKF-SMOS and EnKS-SMOS, respectively (Table 3.1). Similarly, the correlation of TWS from GRACE-only assimilation and GRACE data improved from 0.57 to 0.75 and the root mean square (RMS) error was reduced by 15 mm on average. This merely demonstrates that the assimilation had the intended effect.

The SM estimates from the GRACE-only assimilation can be compared with SMOS data as an independent evaluation to investigate any potential

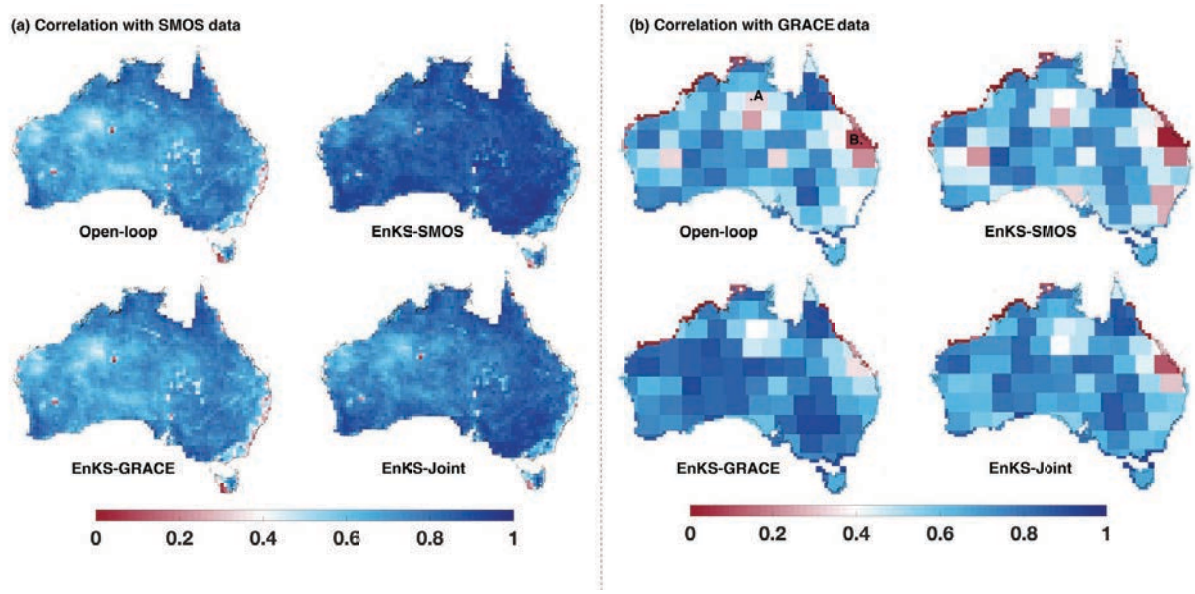

Figure 3-3: Consistency with SMOS and GRACE data: (a) correlations of model-simulated top-layer soil relative wetness with SMOS data; (b) correlations of model-simulated TWS anomalies with GRACE data (Open-loop: open-loop model simulation; EnKS-SMOS: assimilation of SMOS only using EnKS; EnKS-GRACE: assimilation of only GRACE using EnKS; EnKS-Joint: joint assimilation. Time series for point A and B are shown in Figure 5.)

degradation of GRACE data on surface soil moisture estimation. The results showed that assimilating GRACE data alone overall had no improvement on estimating surface SM and slightly degraded the correlation of SMOS data for more than half of the grid cells (Table 3.1), compared with the open-loop model simulation. Therefore, assimilating only GRACE data did not produce more accurate estimates of surface soil moisture. On the other hand, assimilating only SMOS data degraded correlation with GRACE TWSA compared to open-loop estimates, with only 30% of the grid cells showing an improved correlation (Table 3.1). Evidently, assimilation of SMOS data alone also did not improve

Table 3.1: Spatial-averaged correlation of relative wetness and TWS with SMOS and GRACE data for open-loop model simulation and different data assimilation experiments over the Australian continent

	Open-loop	EnKF SMOS	EnKS SMOS	EnKS GRACE	Joint (ϵ,ζ)	Joint (2ϵ,ζ)	Joint (2ϵ,0.5ζ)
Mean r_ω	0.69	0.88	0.86	0.69	0.84	0.81	0.8
Mean $rmse_\omega$ (%)	0.21	0.12	0.13	0.22	0.14	0.15	0.16
$r^a_\omega > r^o_\omega$(%)	NA	94	94	35	94	93	93
Mean r_{tws}	0.57	0.39	0.55	0.75	0.64	0.69	0.76
Mean $rmse_{tws}$ (cm)	6.80	7.28	6.64	5.04	6.27	5.98	5.47
$r^a_{tws} > r^o_{tws}$ (%)	NA	30	46	97	70	85	95

$r_\omega/rmse_\omega$: correlation/root mean square error of relative wetness;
$r_{tws}/rmse_{tws}$: correlation/root mean square error of TWS;
$r^a - r^o$: correlation improvement against open-loop model simulations.
ϵ: SMOS error; ζ :GRACE error.

the estimation of TWS, with a decrease of 0.16 in averaged correlation when the EnKF was used. Therefore, assimilating SMOS data alone can considerably degrade the estimation of TWS.

The joint assimilation achieved similarly good agreement with SMOS data and GRACE data as the SMOS-only assimilation and the GRACE-only assimilation, respectively. Figure 3-4(a) and (b) shows the time series of the top soil layer relative wetness and TWSA before and after the assimilation at Yanco (located in the south of the Murray-Darling Basin), illustrating the improvement in consistency with SMOS and GRACE data. The joint assimilation sometimes showed less agreement with GRACE data than GRACE-only assimilation, such as Point B in Figure 3-3(b). In other cases, the consistency was improved with the joint assimilation at Point A. The decrease in correlation could be caused by the inconsistent trends between rainfall, SMOS and GRACE, as shown in Figure 3-5(a)-(c). Figure 3-5(e)-(h) shows time series of GRACE, SMOS, rainfall and model-simulated TWS at Points A and B. The results show that the same trends between rainfall, SMOS and GRACE can result in improved agreement with GRACE data. However the agreement degraded at Point B, where GRACE observed TWS increased but no precipi-

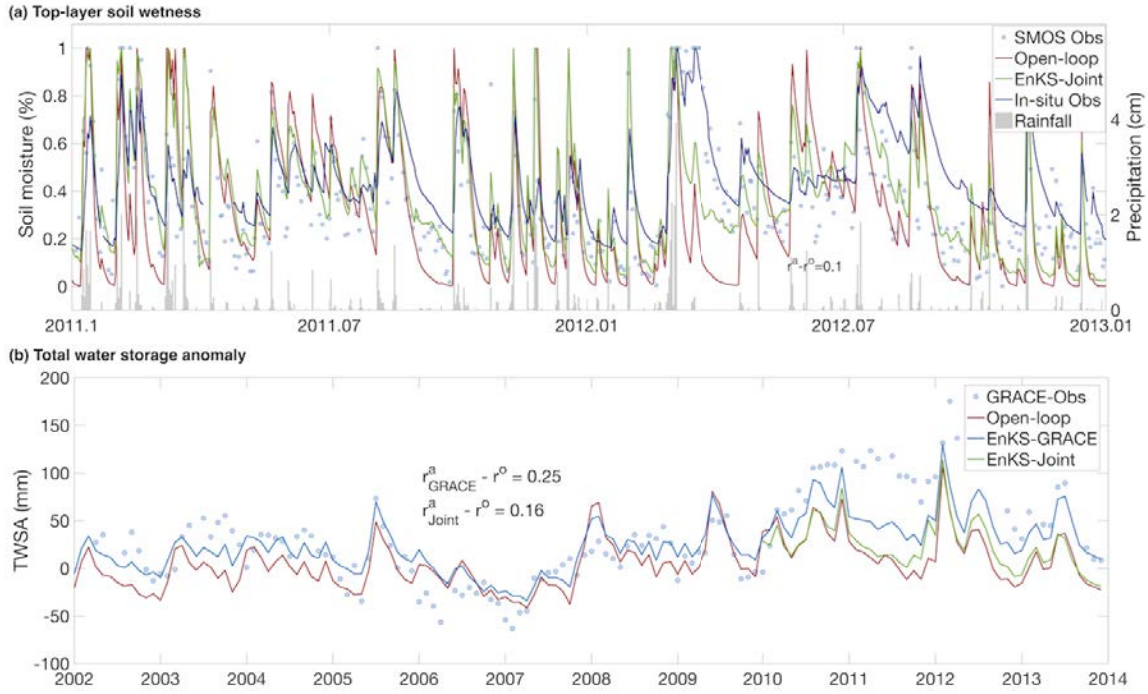

Figure 3-4: Time series of SM and TWSA for Yanco before and after the assimilation: (a) model simulated top-layer soil relative wetness and its consistency with SMOS retrievals, in-situ soil moisture measurements and rainfall data; (b) consistency between model-simulated TWS anomalies and GRACE data.

tation and soil moisture increased over time.

3.3.3 Evaluation against near-surface soil moisture measurements

Model-simulated top soil layer relative wetness values were compared with *in situ* measurements of SM at 5-10 cm depth. Assimilating only SMOS data significantly improved model-estimated near-surface SM compared to the open-loop estimates, by up to 0.32 in correlation (Figure 3-6(a)), but a few sites located close to the water body or in densely vegetated areas showed slightly lower correlations after assimilation. SMOS observations in these locations (e.g. Dry River, Howard Spring and Tumbarumba) showed poor correlation with the *in situ* measurements. Overall, the EnKS produced slightly better correlations with *in situ* observations than the EnKF.

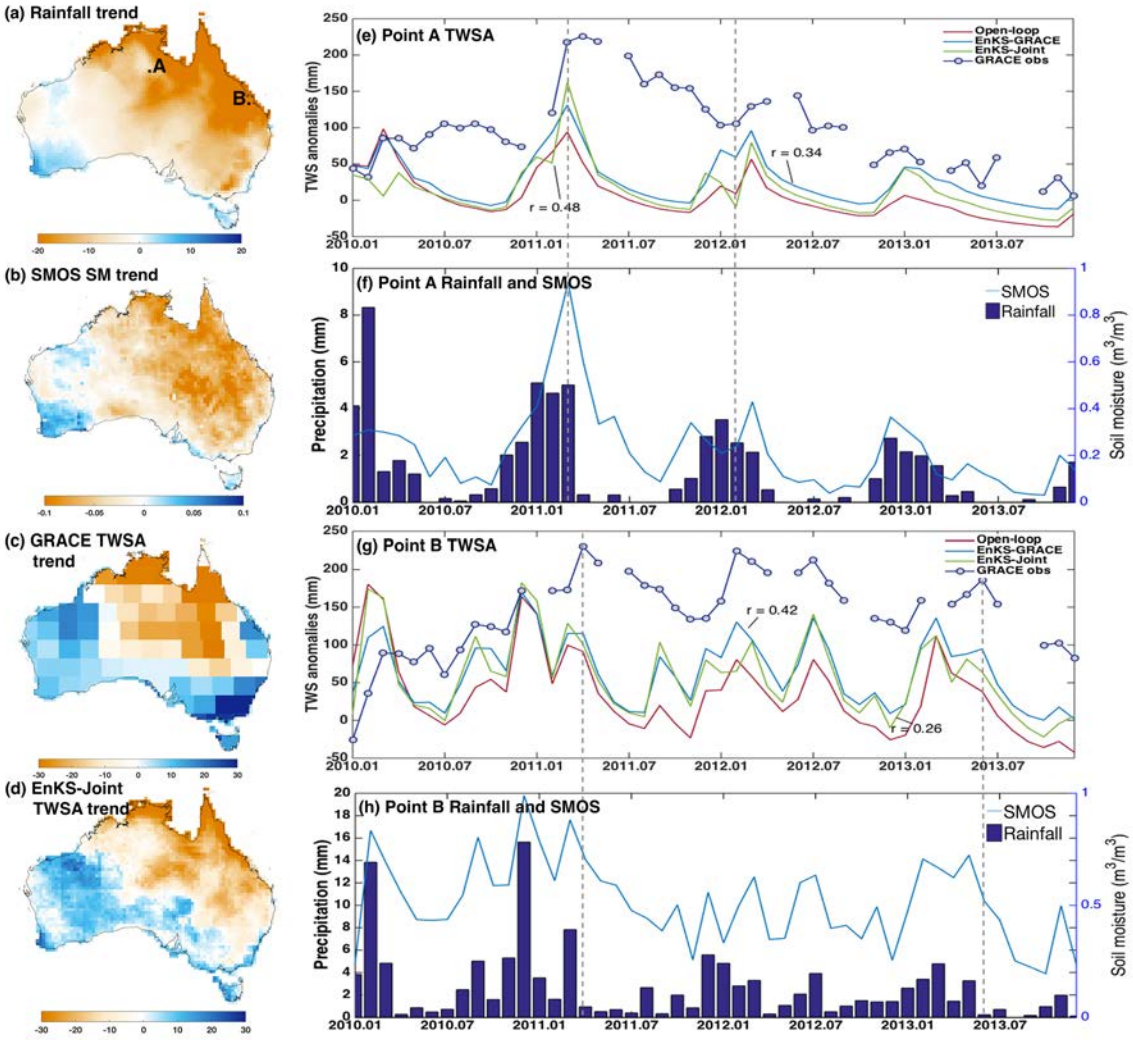

Figure 3-5: Inconsistent trends between rainfall, SMOS and GRACE data over 2010 to 2013: (a) annual trend of rainfall; (b) annual trend of SMOS observed soil relative wetness; (c) annual trend of GRACE observed TWSA; (d) annual trend of model-simulated TWSA through joint assimilation; (e) GRACE observed TWSA compared with model simulated TWSA at point A; (f) SMOS SM and rainfall observations at Point A; (g) GRACE observed TWSA compared with model simulated TWSA at point B; (h) SMOS and rainfall observations at Point B.

The assimilation of only GRACE data did not strongly change the correlation of surface SM with the *in-situ* measurements and was overall not beneficial. Only one grid cell (Adelong Creek; Figure 3-1) showed better correlation than other assimilation experiments. This may have been the standing water effect on SMOS SM retrieval. Since microwave brightness temperature

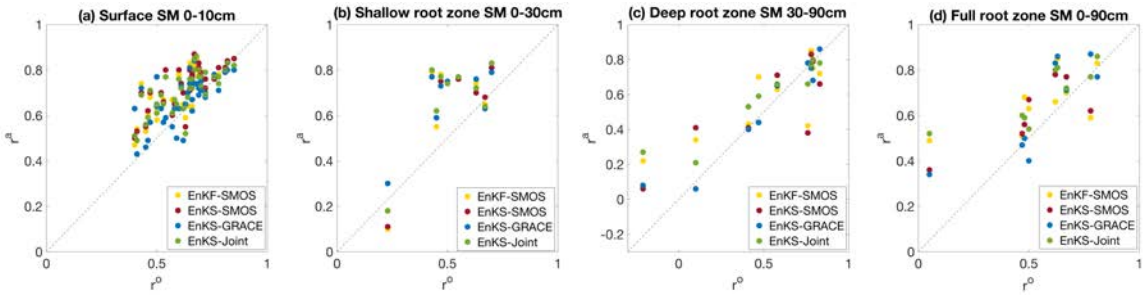

Figure 3-6: Correlation of model-simulated soil moisture with in-situ observations (r^o: correlation of open-loop model simulation; r^a: correlation after assimilation; yellow dots: the assimilation of SMOS only using EnKF; red dots: the assimilation of SMOS only using EnKS; blue dots: the assimilation of GRACE only; green dots: joint assimilation): (a) correlation of surface soil moisture at 0-10 cm against in-situ measurements from OzFlux, OzNet and CosmOz network; (b) correlation of shallow root zone soil moisture at 0-30 cm against in-situ measurements from OzNet; (c) correlation of deep root zone soil moisture at 30-90 cm against in-situ measurements from OzNet; (d) correlation of full root zone soil moisture at 0-90 cm against in-situ measurements from OzNet.

has a high sensitivity to open water, a small fraction of water bodies within the footprint can result in a considerable overestimation of retrieved SM (Ye et al., 2015). Joint assimilation generally improved the near-surface SM estimates in most locations, with the same efficiency as the SMOS-only assimilation. The largest improvement was up to 0.27 (Figure 3-6(a); Table S2). Only one grid cell showed a decrease in correlation by 0.1 when compared with the open-loop simulation (CosmOz Tumbarumba site located in a wet forest environment Figure 3-1).

3.3.4 Evaluation against root-zone soil moisture measurements

Root-zone SM measurements from the OzNet Network at 0-30 cm, 30-90 cm and 0-90 cm depths were used to evaluate the model-simulated shallow- and deep-layer soil water storage estimates. Figure 3-6(b-d) show that assimilating surface SM data from SMOS led to improved soil moisture at different depths, in particular shallow layer soil moisture estimates. An average increase in

correlation of 0.15 (Table S3) was found at shallow root zone SM estimates with both EnKF and EnKS. Assimilation of GRACE data only showed more impacts on improving root zone SM than surface SM estimation, with an increase in correlation by up to 0.29 (Figure 3-6(d), Table S3). The joint assimilation combined the information of both surface SM and TWS variation and showed its capability to estimate the shallow-layer soil moisture better than the other three assimilation experiments. The resulting SM estimates showed an increase of 0.1 in correlation at both shallow and deep layer soil, as well as the full root zone.

3.3.5 Evaluation against groundwater level measurements

Assimilating only GRACE significantly improved the correlation with groundwater level measurements against model open-loop, as shown in Figure 3-7(a). The correlation is increased by an average 0.1 and up to as much as 0.9 for individual grid cells. Improved agreement between model-estimated groundwater storage change and groundwater level measurements further emphasised the benefit of GRACE TWS assimilation for deeper water stores. Figure 3-7(c) illustrates the improvement of the groundwater storage anomalies estimated for the Murray-Darling Basin after assimilation of GRACE data for an extended 12-year period. The magnitude of the groundwater storage changes is intensified due to the assimilation of GRACE data, with greater depletion in dry periods (2006 to 2010) and greater increases during wet periods (2010 to 2013) over the basin. The correlation was improved from 0.50 to 0.80. Note that the actual units vary between the assimilation results and bore data, since specific yield was too uncertain to attempt a conversion from water storage to groundwater level.

Figure 3-7(b) shows the locations where the joint assimilation performed better than the GRACE-only assimilation. The majority of grids showed improved correlation than GRACE-only assimilation with an improvement in correlation by up to 0.4. In particular, improved correlation was found in

the areas where opposing trends in SMOS SM and GRACE TWS were observed. This indicated the potential to simulate the water loss caused by the groundwater extraction, which is not represented in the model. Figure 3-7(d) shows the comparison of simulated groundwater storage change from the GRACE-only assimilation and the joint assimilation at Point C in Figure 3-7(b). This point is located in the agriculture area and has moderate rainfall. However, the relative wetness of soil is over 0.6 at all time (Figure 3-7(d) top panel). Groundwater bore data showed a decrease in water level during January to April 2011, while GRACE observed no significant change in TWS and the soil moisture increased. The joint assimilation picked up this decrease in groundwater but no decrease was estimated with the assimilation of only GRACE data. Events with a similar decrease occurred in January to April 2012 and July to September 2012, and a larger magnitude of groundwater decrease occurred in the joint assimilation than in the GRACE-only assimilation. Overall, joint assimilation appeared to impart the benefits of the combination of GRACE TWS and SMOS SM as constraints and improved the accuracy of the model-simulated groundwater storage dynamics.

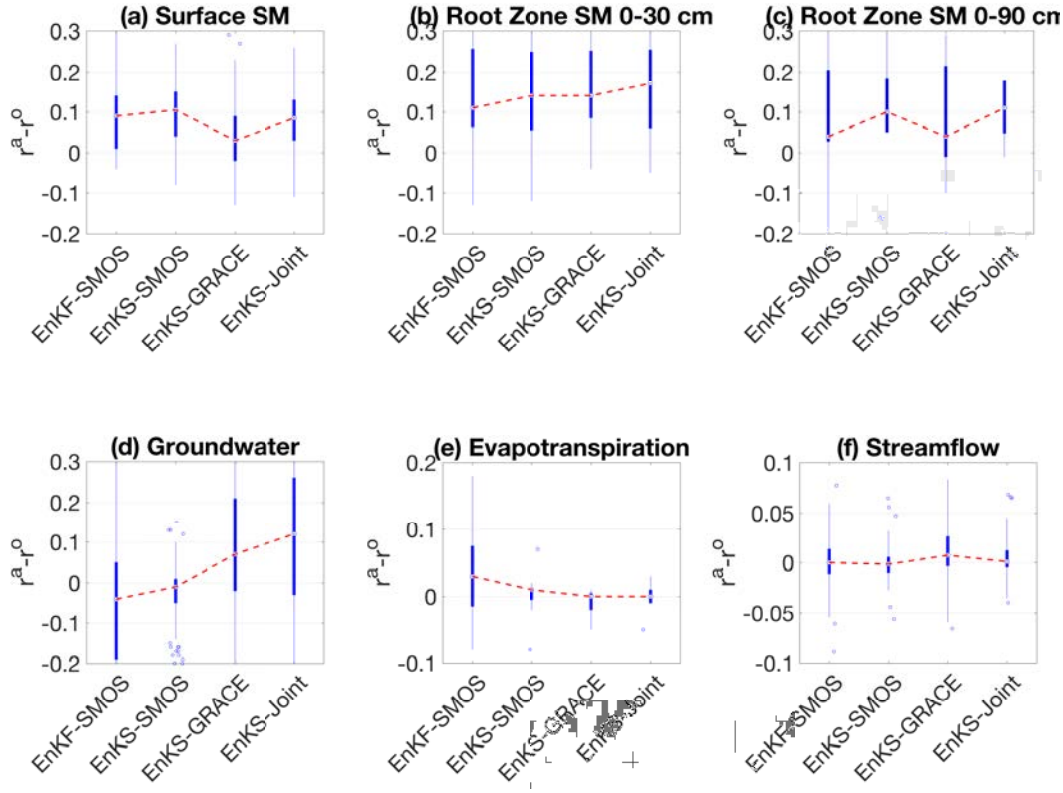

Figure 3-7: Correlation increments (r^a-r^o) of model-simulated groundwater storage anomalies with in-situ water level measurements: (a) the correlation increments of the assimilation of GRACE data alone compared to model open-loop run (blue: improved; red: degraded;); (b) correlation increments of the joint assimilation compared to the assimilation of GRACE data alone; (c) time series of averaged groundwater storage simulation of Murray-Darling Basin and in-situ water level measurements; (d) improvement of joint assimilation compared with the assimilation of GRACE data alone at Point C (top panel: GRACE observed TWSA and SMOS observed relative wetness; bottom panel: model-simulated groundwater storage anomalies and in-situ water level measurements).

3.3.6 Evaluation of evapotranspiration and streamflow

Assimilating SMOS data at daily time step (EnKF-SMOS) showed the biggest impact on improving ET estimates compared to other experiments with an average correlation of 0.83 (Table S4). Conversely, assimilating GRACE data slightly degraded the correlation for most of the points (i.e. 56%). Although the joint assimilation did not significantly improve the ET, the proportion of degradation was reduced compared with other experiments. Assim-

ilating SMOS and GRACE data slightly improved the accuracy of streamflow simulation with average correlation of 0.86 from 0.81 (Table S4). The joint assimilation showed improved correlation for 70% of the grid cells and the correlation increased by up to 0.17 against model open-loop simulation.

In this section, model simulated surface soil moisture, root-zone soil moisture, groundwater, TWS, ET and streamflow were evaluated with both *in situ* and satellite observations. Figure 3-8 summarises the independent evaluation of individual water balance component. Overall, joint assimilation resulted in more accurate estimation of soil moisture profile at different depths, unlike the assimilation of only one of the two data sets. (Figure 3-8(a-c)). Assimilating GRACE data only did not always produce accurate soil moisture estimates and overall less beneficial than either joint or SMOS-only assimilation. Assimilating SMOS SM did not improve the correlation between the model-simulated groundwater storage and the *in situ* water level measurements. Indeed, the correlation reduced for most of the grid cells compared to the open-loop estimates (Figure 3-8(d)). The joint assimilation show marginal improvement on ET and streamflow. Notably, though, the joint assimilation had reduced impact on ET and streamflow performance than single-source data assimilation (i.e. reduced proportion of correlation decrease).

3.4 Discussion

3.4.1 Disaggregation of monthly integrated water storage

The objective of the joint assimilation was to combine the information from both SMOS and GRACE data to better estimate the water budget and its variations. An important challenge in the assimilation was to allow for the disparity in temporal resolution and spatial resolution at both the vertical and horizontal scales between SMOS data, GRACE data and model states. In this study, the EnKS-based assimilation framework with a one-month assimilation window successfully disaggregated the monthly GRACE signals into

daily analysis increments for each water store. Unlike the (GRACE-only) data assimilation using a filter-based approach (Eicker et al., 2014; Tangdamrongsub et al., 2015) to update model estimates monthly or update daily estimates by interpolating GRACE data, our EnKS-based assimilation simultaneously updates all daily model states in a month using the monthly GRACE data. Different from the approaches of Zaitchik et al. (2008) and Li et al. (2012) with an even increment for each day, the increments applied over each day of the month were different, thus accounting for temporal error correlations in our method.

The assimilation of GRACE data improved the consistency between model-estimated and GRACE TWS. The clearest improvements were seen in western and southeastern Australia (Figure 3-3(b)). The magnitude of TWS change derived from GRACE was larger than modeled estimates. Hence, assimilating GRACE TWS amplified changes in storage and made trends in water loss or gain more distinct (Figure 3-4(b)). The joint assimilation of SMOS and GRACE data sometimes led to reduced agreement with GRACE data due to the conflicting constraints. Houborg et al. (2012) also found that the average amplitude of the TWS change from the open-loop model was smaller than the GRACE TWS observations and the adjustments of water can be subdued by a limited water storage capacity in the model to accommodate the adjustments. The integrated water storage change estimates from GRACE data were partitioned into increments for different water stores through the error correlation structure (Figure 3-2). In the joint assimilation, the adjustments of soil water stores were dominated by SMOS data, while the contributions to groundwater and TWS were mainly from GRACE data. However, assimilation of SMOS alone can result in considerable changes in TWS. Our study appears to be the first to compare GRACE TWS with TWS estimates after the assimilation of near-surface SM only. The results illustrate that introducing SM observations may lead to improved near-surface and shallow SM estimates, but degraded deeper SM, groundwater and total TWS estimates. Thus, the relative weight-

ing between SMOS and GRACE data is critical in the joint assimilation. In the experiment of changing the relative weighing between two data sets, we found that model-simulated TWS was sensitive to both SMOS and GRACE data (Table 3.1). Amplifying SMOS uncertainty and attenuating GRACE uncertainty to accommodate their different dynamic range and observation frequency resulted in a better consistency with GRACE data: the correlation increased from 0.64 to 0.76 and another 25% additional grid cells achieved better correlation than the open-loop simulation. This suggested that SMOS data dominated the original analysis adjustments in the joint assimilation configuration. One likely reason is that the adjustments of TWS came from 10 SMOS observations per month but only one GRACE observation. It also appears that SMOS SM errors may be greater than indicated by the retrieval error estimates. The relative weighting between SMOS and GRACE data needs to be further investigated to optimize their combined use.

In this study, $3^\circ \times 3^\circ$ GRACE mascon solutions were used, but the TWS and groundwater change can be highly heterogeneous inside each mascon. Figure 3-5(c) and (d) compare the annual trend of TWS variation from GRACE and the joint assimilation. The results demonstrated that the joint assimilation produced more detailed spatial variability compared with GRACE mascon data. This is due to the model forward run with high resolution forcing data and the constraints from SMOS data. The joint assimilation showed good consistency with GRACE data, except for east coast Australia where GRACE uncertainties were relatively large. The joint assimilation also showed better correlation with GRACE TWS in north central Australia compared to the assimilation of only GRACE. This is illustrated in Figure 3-5(e) and (f): the dashed line indicates that SMOS assimilation enhances the analysis by adding or removing more water in the system when SMOS has the same trend in TWS as GRACE. This occurs if the TWS change is mainly due to the soil water variation. Therefore, assimilating SMOS and GRACE together appears to impart more detailed spatial information on the distribution of water, in-

ducing the downscaling of coarse GRACE signals. The TWS estimates with improved spatial resolution from the joint assimilation offers a new tool for monitoring total water storage change with distinct benefits over the original GRACE data.

3.4.2 Impact on soil moisture profile estimates

The joint assimilation was able to improve the soil moisture estimation in different layers (Figure 3-8(a)-(d)). The improved SM correlation at four contrasting depths demonstrates the benefits of joint assimilation on improving the vertical soil moisture profile estimates. In particular, the joint assimilation stood out from the assimilation of only either SMOS or GRACE data in improving root-zone SM estimates. Assimilating SMOS data with EnKF was less robust than EnKS in improving shallow- and deep-layer soil moisture. The EnKF corrected the model states instantly as observations became available, while the EnKS updated all previous states back to the first day of the month. The EnKS smoothed water storage estimates over the month, preventing incurring spikes in the updated states and eliminating the impact of noisy observations. Moreover, deeper layer soil water storage or TWS responded slower to precipitation than surface SM, resulting in a time lag with the variation of surface SM. The EnKS with an assimilation window therefore appears more suitable for correcting the states that respond over the course of days or months, such as deep soil water, groundwater and TWS.

SMOS observations can also provide supplementary information about the water inputs and can mitigate errors in precipitation estimates for areas with sparse monitoring stations. As illustrated in Figure 3-5(a), the positive trend in rainfall evident in north-west Australia was less than observed in both SMOS and GRACE (Figure 3-5(b)-(c)), suggesting the error lay in the precipitation data (there are very few rain gauges in this dry and sparsely populated region). An example of comparison between precipitation, *in-situ* measurements and SMOS data at Yanco in Figure 3-4(a) showed that the joint assim-

ilation resulted in a higher more soil moisture predicion during July-October as well as January-April in both 2010 and 2012, consistent with *in-situ* measurements. However, no significant rainfall events were recorded, indicating an error in precipitation estimates or that there was another source inputs water from such as irrigation. Therefore it appears feasible that the SMOS data can correct errors in the precipitation estimates and detect other source of water inputs, resulting in more accurate estimates of the soil moisture profile. This may have considerable value for agricultural water resource management and drought monitoring.

3.4.3 Impact on groundwater estimates

Similar to Zaitchik et al. (2008), Houborg et al. (2012), and Tangdamrongsub et al. (2015), we found that assimilating GRACE data successfully mitigated the model deficiency in groundwater simulation and led to major improvements in estimating groundwater storage. The correlation with *in-situ* groundwater level measurements was further improved for the majority of grid cells by the joint assimilation, compared to the GRACE-only assimilation. Integrating SMOS data most likely constrained the magnitude of groundwater storage change from TWS changes with more accurate soil water storage estimates. Where they occurred, the opposite trends between GRACE and SMOS provided extra information on the exchanges between soil water and groundwater. This may help quantify groundwater extraction over large areas (Rodell et al., 2009). In addition, the SMOS data helped to refine the spatial pattern of soil and groundwater storage changes derived from GRACE data. Long et al. (2016) found that groundwater depletion estimated from GRACE is likely to be overestimated. They highlighted the importance of incorporating a priori information to refine spatial patterns of GRACE signals. The joint assimilation is less efficient if large water storage changes occur as a result of lateral flow from neighboring cells, e.g. through large rivers or ice mass changes. In such cases, the responsible processes need to be quantified and in-

cluded (van Dijk et al., 2014a). Overall joint assimilation efficiently improved estimates of groundwater change, potentially resolving the lack of groundwater observations at large scales over much of the world.

3.4.4 Impact on evapotranspiration and streamflow

The joint assimilation framework proposed in this study explicitly acknowledges uncertainty in the model forcing data (precipitation, temperature and radiation) and does not conserve mass and energy with respect to the original estimates. While the lack of water balance is not a problem for some applications, there is potential that estimates of other water balance terms may be degraded through data assimilation to compensate for model structural and/or input errors. To investigate this, we evaluated the resulting streamflow and ET with *in-situ* measurements. We found no degradation on both ET and streamflow estimates after the joint assimilation (Table S4), Figure 3-8(e)-(f)). Despite differences in scale, for most locations there was in fact a slight improvement in correlation with ET and streamflow observations and reduced degradation after the joint assimilation as compared to single-observation assimilation experiments (i.e. from 56% to 18% and 31% to 23%, Table S4). The differences of ET and streamflow between assimilation results and open-loop are small, since the fluxes are often reproduced reasonably well in model open-loop with an average correlation of 0.78 and 0.81, respectively (Table S4). The overall marginal improvement may be due to several factors, including a lack of analysis update on water flux terms, weak coupling strength with soil water storage, and 'smoothed' variation in the monthly data evaluation.

Evapotranspiration estimates were observed to improve in the EnkF-SMOS experiment with an increase in correlation of up to 0.44 (i.e. from 0.46 to 0.90) compared to open-loop estimates. This is likely because the ET estimates were updated indirectly through updated analysis of soil moisture at daily time step, while they were only adjusted at the beginning of a month with the analysis states at the end of thee month in the EnKS. Assimilating

GRACE data alone had no positive impacts on the estimation of ET with a slight degradation for most of the locations. Tangdamrongsub et al. (2015) also found that assimilating GRACE data had no significant impact on streamflow estimation, since monthly GRACE data cannot help to capture the larger peaks of individual streamflow events. To further improve other variables in the water cycle, an approach incorporating the ET, runoff and precipitation in the adjustment would be considered in future work.

3.5 Conclusions

The accuracy of vertical soil moisture profile, groundwater storage and total water storage estimates from hydrological modeling was significantly improved through the joint assimilation of satellite-observed near-surface SM from SMOS and TWS from GRACE. The joint assimilation produced more accurate estimates of the key elements of water cycle than the assimilation of only one of the satellite observations, without degradation of streamflow and ET estimates. It improved the performance of GRACE-only assimilation by integrating near-surface water distribution at a finer scale from SMOS, while limiting the degradation of deeper storage estimates caused by the assimilation of SMOS alone.

All of the individual water storage components for different land cover types were updated at daily time steps over a one-month assimilation window, incorporating the information from both GRACE and SMOS data through temporal error correlations. SMOS provided temporal and spatial varying constraints on near-surface SM and shallow-layer SM estimates from the model. However, assimilating only SMOS SM data degrades the correlation with GRACE TWS data and *in situ* groundwater level measurements, especially when an EnKF is used. GRACE TWS data mostly contributed to correcting model simulated deep-layer SM and groundwater storage values in the assimilation, also imparting overall constraints on monthly TWS estimates.

Moreover, having constraints on both TWS and near-surface SM can help to mitigate the lack of rain gauges in remote areas and may even help to quantify the impacts of large-scale groundwater extraction. We found that the error in the precipitation data used to force the hydrological model can be corrected through the use of higher resolution SMOS SM observations when both TWS and SMOS show similar increase trends but there was no or low precipitation observed, resulting in more detailed spatial patterns of near-surface soil water variations. The joint assimilation can also detect groundwater loss due to extraction for irrigation purpose, if SMOS shows strong increase in soil wetness but there is no increase in TWS and precipitation.

Integrating SMOS SM and GRACE TWS together successfully combined the strengths of each information source and largely mitigated against their weaknesses. The improved individual water storage estimates offer potential for drought and groundwater monitoring, as well as water cycle reanalysis applications.

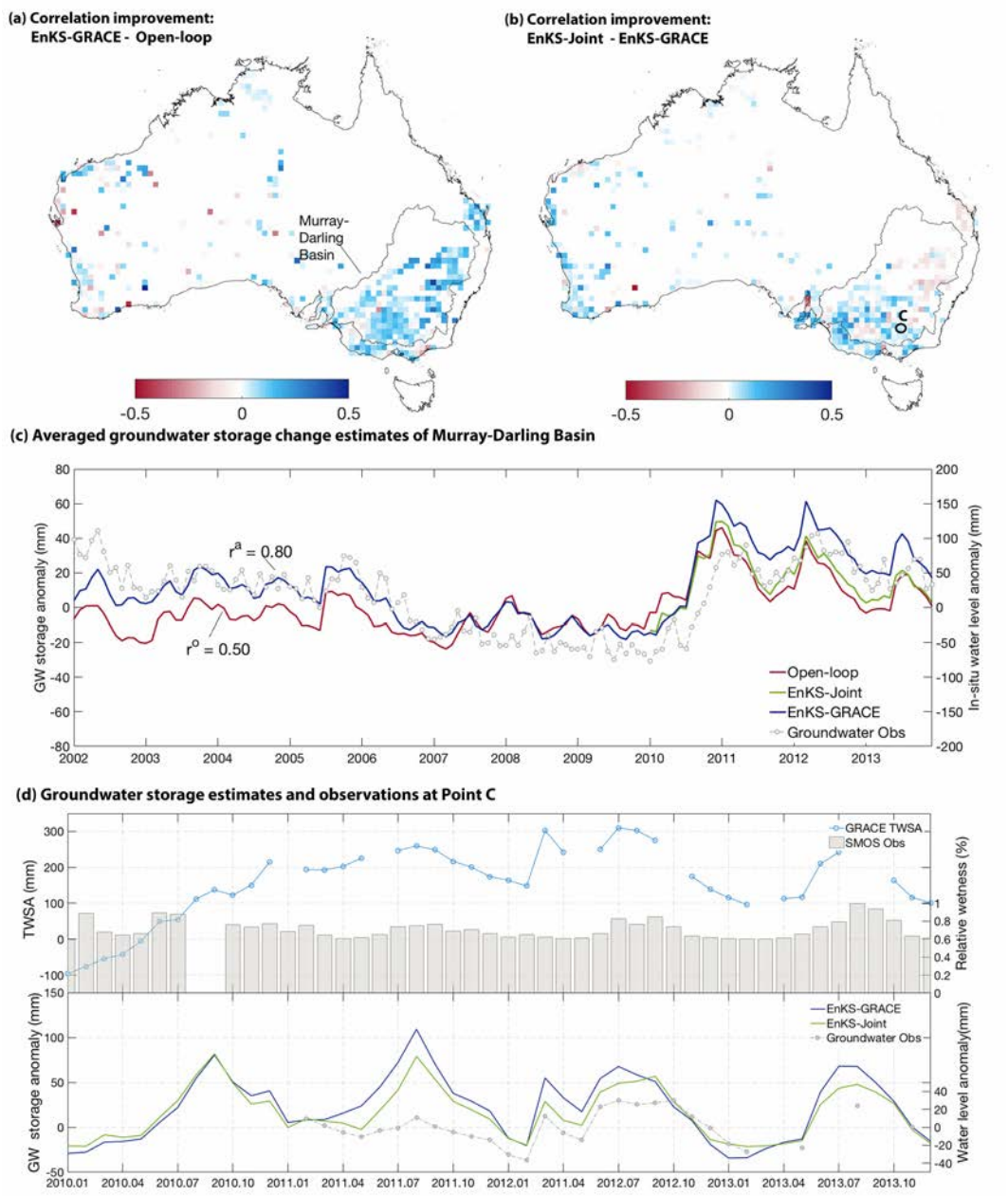

Figure 3-8: Performance of four assimilation experiments on improving different water balance components and statistics of correlation increments (difference between assimilation and open-loop model simulation) (a) surface soil moisture, (b)-(c) root zone soil moisture at different depths, (d) groundwater, (e) evapotranspiration and (f) streamflow. (The red lines connect the median value of the correlation increments; the blue bars show the interquartile range and the range of correlation increments.)

Chapter 4

Improved global root-zone soil moisture estimates

Most ecohydrological and agricultural dynamics are related to, and often depend upon the root-zone soil moisture. Accurate estimation of global root-zone soil moisture is critical for predicting vegetation conditions but challenging without direct measurements. Since significant improvements in root-zone soil moisture estimation are found in Australia after the joint assimilation of GRACE and SMOS data, we implemented our proposed joint assimilation framework globally with further amendment in method and spatial resolution. This chapter shows the global results of the joint assimilation of GRACE and SMOS retrievals. The accurate estimation of root-zone soil moisture through joint assimilation is of potentially great value for anticipating vegetation greenness and productivity. This chapter is based on the material published in Hydrology and Earth System Sciences:

Tian, S., Renzullo, L. J., van Dijk, A. I., Tregoning, P., Walker, J. P. (2019). Global joint assimilation of GRACE and SMOS for improved estimation of root-zone soil moisture and vegetation response. Hydrology and Earth System Sciences, 23(2), 1067–1081

Abstract

The lack of direct measurement of root-zone soil moisture poses a challenge to the large-scale prediction of ecosystem response to variation in soil water. Microwave remote sensing capability is limited to measuring moisture content in the uppermost few centimetres of soil. GRACE (Gravity Recovery and Climate Experiment) mission detected the variability in storage within the total water column. However, root-zone soil moisture cannot be separated from GRACE-observed total water storage anomalies without ancillary information on surface water and groundwater changes. In this study, GRACE total water storage anomalies and SMOS near-surface soil moisture were jointly assimilated into a hydrological model globally to better estimate the impact of changes in root-zone soil moisture on vegetation vigour. Overall, the accuracy of root-zone soil moisture estimates through the joint assimilation of surface soil moisture and total water storage retrievals showed improved consistency with ground-based soil moisture measurements and satellite-observed greenness when compared to open-loop estimates (i.e. without assimilation). For example, the correlation between modelled and in situ measurements of root-zone moisture increased by 0.1 (from 0.48 to 0.58) and 0.12 (from 0.53 to 0.65) on average for grasslands and croplands, respectively. Improved correlations were found between vegetation greenness and soil water storage on both seasonal variability and anomalies over water-limited regions. Joint assimilation results show a more severe deficit in soil water anomalies in eastern Australia, southern India and eastern Brazil over the period of 2010 to 2016 than the open-loop, consistent with the satellite-observed vegetation greenness anomalies. The assimilation of satellite-observed water content contributes to more accurate knowledge of soil water availability, providing new insights for monitoring hidden water stress and vegetation conditions.

4.1 introduction

Water is a growth-limiting resource that impacts over 40% of Earth's vegetated surface (Nemani et al., 2003). Vegetation productivity and water stress are strongly coupled by the interactions between soil moisture, photosynthesis, transpiration, interception and hydraulic redistribution (Porporato et al., 2004). The amount of water available to support plant growth and buffer against rainfall deficiencies largely determines the length of the growing period (Leenaars et al., 2018). Rooting depth as an essential parameter in hydrologcial modeling to regulate correct simulation of subsurface processes have been estimated based on various scientific hypotheses due to the lack of direct measurements (Wang-Erlandsson et al., 2016; Yang et al., 2016). Although some vegetation species have roots that can grow to tens of metress depth (Canadell et al., 1996), most plants have roots that are contained in the upper 2m of the soil column, and thus cannot access the deeper water stores (Tokumoto et al., 2014). For example, Dunne and Willmott (1996) derived a global distribution map of plant-extractable soil water capacity based on soil-water retention properties, soil texture and organic content estimates and found that less than 150 mm of the water capacity can be accessed by the plants over 90% of the vegetated area. The duration of water stress and the vertical distribution of soil moisture determine the vegetation vigour to a large extent in drylands (Canadell et al., 1996). Stress due to limited soil water can trigger a reduction in photosynthesis, which in turn leads to reduced productivity and increased vegetation mortality. The increasing deficit in deep soil water under a changing climate may further intensify ecological droughts during the growing season (Schlaepfer et al., 2017). There is a compelling need to quantify the vegetation responses to water scarcity for improved assessment of climate change impacts at large scales (Breshears et al., 2005).

Wang et al. (2007) and Santos et al. (2014) investigated different responses of vegetation vigor to ground-based root-zone soil moisture observations at dif-

ferent depths. There are limited studies on the impacts of soil water availability on the functions in terrestrial ecosystems at regional to global scale due to the absence of widespread direct observations of root-zone soil moisture. Soil moisture simulations and satellite water content observations from the uppermost soil layer to the total water column have been used to quantify the water driven surface vegetation greenness variability (Laio et al., 2001; Wang et al., 2007; Andela et al., 2013; Chen et al., 2014; Yang et al., 2014; Xie et al., 2016a). However, model-simulated soil moisture profile estimates are highly uncertain due to the necessary simplification of processes and parameterization (Porporato et al., 2004). Soil moisture observations from in situ monitoring networks or satellite observations are generally spatially, vertically and temporally constrained by the instruments. Satellite soil moisture retrievals from microwave sensors such as SMOS (Soil Moisture and Ocean Salinity) only provide the soil moisture in the uppermost soil layer and are limited by the errors introduced by soil type, canopy cover and surface roughness (Houser et al., 1998; Narayan et al., 2004). In contrast, the GRACE (Gravity Recovery and Climate Experiment) mission provided integrated water storage change including water above and under the surface through mapping anomalies in the changing Earth's gravity field (Tapley et al., 2004). It has been demonstrated that GRACE-observed total water storage anomalies can explain changes in surface greenness both interannually and seasonally without time lag over Australia (Yang et al., 2014). Conversely, Chen et al. (2014) found that vegetation greenness typically lags soil moisture at less than 10 cm depth by one month over mainland Australia using merged satellite soil moisture products (Liu et al., 2012b). This discrepancy in the time lags indicates that vegetation responds differently to variations in surface soil moisture and total water storage. The quantification of vegetation response to soil water availability at large scale therefore remains challenging without accurate soil moisture profile estimations.

Observations of near-surface soil moisture have been successfully inte-

grated into land surface models to correct model deficiencies on simulating soil moisture using various assimilation techniques (Walker and Houser, 2001b; Sabater et al., 2007; Crow et al., 2008; Renzullo et al., 2014; Dumedah et al., 2015). Active/radar and passive/radiometer observations were jointly assimilated to improve surface soil moisture and root-zone soil moisture with optimal accuracy and spatial coverage by Draper et al. (2012) and Lievens et al. (2017). Significant improvements were mainly found for shallow root-zone estimation at 0-30 cm (Draper et al., 2012; Renzullo et al., 2014), with less benefit for deeper soil layers. Conversely, GRACE-observed total water storage anomalies were successfully assimilated or otherwise combined with model simulations for improved deep soil and groundwater estimation (Zaitchik et al., 2008; van Dijk et al., 2014a; Tangdamrongsub et al., 2015; Khaki et al., 2017; Schumacher et al., 2018; Girotto et al., 2017; Tangdamrongsub et al., 2018), but with typically marginal improvements for surface and shallow soil moisture (Li et al., 2012; Girotto et al., 2017; Tian et al., 2017; Tangdamrongsub et al., 2018; Shokri et al., 2018). This is due to the highly variable nature of near-surface and shallow soil moisture in space and time, which has little influence on the GRACE signal. Recently, near-surface soil moisture and total water storage observations were jointly assimilated into a water balance model over Australia and demonstrated to consistently improve water storage profile estimates, especially in the root-zone soil moisture estimates (Tian et al., 2017). The use of satellite-observed daily near-surface soil moisture has been demonstrated to better disaggregate shallow soil moisture and groundwater change from GRACE-observed total water storage change because of the different temporal dynamics.

In this study, satellite-observed soil moisture and changes in total water storage were jointly assimilated into a global water balance model following the approach of Tian et al. (2017) and extended with several further innovations. We investigated the impacts of assimilating satellite water content retrievals on the estimation of surface and root-zone soil moisture and evalu-

ated with ground-based soil moisture measurements. The relationship between vegetation vigor and soil water availability was assessed with satellite-observed greenness and root-zone soil moisture estimates for different vegetation types. The performance of the joint assimilation is compared against the open-loop model and alternative assimilation methods. The annual trends of root-zone soil water storage anomalies are compared with the trends in vegetation greenness anomalies to investigate the potential of using accurate information of soil water availability for explaining and anticipating vegetation greenness and productivity.

4.2 Materials

4.2.1 Ecohydrological model

The World-Wide Water (W3) model (van Dijk et al., 2013a) (available at http://wald.anu.science) is a one-dimensional, grid-based distributed ecohydrological model that simulates water balance and water-related vegetation dynamics. It was adapted from the Australian Water Resources Assessment Landscape (AWRA-L) model (van Dijk, 2010a; Frost et al., 2016). Precipitation is assumed to be the only water input into the system. The precipitation enters the grid cell through the vegetation and soil moisture stores and exits the grid cell through evapotranspiration, run-off or groundwater discharge (Frost et al., 2016). Each grid cell contains a mix of land cover classes (Hydrological Response Units; HRUs) and is conceptualized as a catchment that does not laterally exchange water with neighbouring cells. Different vegetation has different degrees of access to soil water. Soil and vegetation water and energy fluxes were simulated separately for deep-rooted and shallow-rooted vegetation to consider different rooting and water uptake behaviour. The soil water store was partitioned into three layers, namely, top, shallow and deep soil to describe the plant available water, approximately 0–5cm, 0.05–1m, and 1–10m in depth respectively. A simple groundwater model is used to simulate uncon-

fined groundwater storage considering deep drainage from soil water, capillary rise and groundwater evaporation and discharge. The unconfined groundwater and surface water stores were simulated at grid cell level.

A $0.25° \times 0.25°$ global gridded Multi-Source Weighted-Ensemble Precipitation (MSWEP) data set derived by merging gauge, satellite and reanalysis data (Beck et al., 2017) was used as the only water input in the system. The $0.5° \times 0.5°$ WFDEI (WATCH Forcing Data methodology applied to ERAâĂŘInterim) meteorological forcing data set (Weedon et al., 2014) used in this study including radiation, air temperature, wind speed, and surface pressure, and these were resampled to be consistent with the resolution of precipitation at 0.25°. The soil water balance of the W3 model was simulated globally on a daily basis with a spatial resolution of $0.25° \times 0.25°$.

4.2.2 Land cover types

The 2010 land cover types of each pixel were characterized by the MODIS (Moderate Resolution Imaging Spectroradiometer) global IGBP (International GeosphereâĂŞBiosphere Programme) land cover classifications (MCD12Q1) at $5' \times 5'$ resolution (Channan et al., 2014). The number of pixels at $5' \times 5'$ resolution for each land cover type in the entire corresponding $0.25° \times 0.25°$ grid cells were counted to determine the sub-pixel heterogeneity. If the land cover type is identical for the corresponding model grid cell, the land cover type of this model grid cell is considered to be homogeneous. Model grid cells with multiple land cover types and over 60% grassland were defined as grassland-dominated mixed vegetation. Similarly, model grid cells with mostly forest were classified as forest-dominated pixels. Grid cells with multiple different land covers were classified as mixed land cover. The forest cover of each $0.25° \times 0.25°$ grid cell was calculated with the percentage of forest (including evergreen, deciduous and mixed forest) pixels to investigate the impact of woody vegetation on soil moisture estimation.

4.2.3 Satellite-observed water content

Satellite-observed near-surface soil moisture from SMOS and total water storage from GRACE were used in this study. GRACE tracked the water movement from space by measuring the changes in the distance between the twin satellites caused by surface mass variations (Tapley et al., 2004). The JPL RL05M mass concentration (mascon) GRACE solutions (Watkins et al., 2015) were used to constrain model-simulated total water storage (i.e. the integration of surface water, soil water at three layers and groundwater stores). The GRACE data were represented on a 0.25° grid but they represent native resolution of 3° × 3° equal-area caps. In contrast with sensing the integrated water content, SMOS characterizes global temporal change of near-surface (0 - 5 cm) soil moisture from the microwave brightness temperature observations every three days (Kerr et al., 2010). The 0.25° Level-3 global daily soil moisture retrievals from CADTS (Centre Aval de Traitement des DonnÃľes SMOS, https://www.catds.fr) (Jacquette et al., 2010; Kerr et al., 2013) for ascending and descending orbits were averaged over the overlapping area. The temporally and spatially varying uncertainties of GRACE and SMOS retrievals were provided as part of their respective products, and were used to investigate observation error variance-covariance matrices in the assimilation method. The relative error was calculated as the ratio of the uncertainty over the absolute value for both GRACE and SMOS retrievals for each grid cell at each time step. The average uncertainties for SMOS and GRACE observations were categorized based on land cover types to investigate the relative weighting between observations in the assimilation (Fig. 4-1).

4.2.4 International Soil Moisture Network

Iin situ soil moisture observations at different depths available from the International Soil Moisture Network (ISMN) (Dorigo et al., 2011) were used to evaluate the performance of model-simulated soil moisture for the uppermost

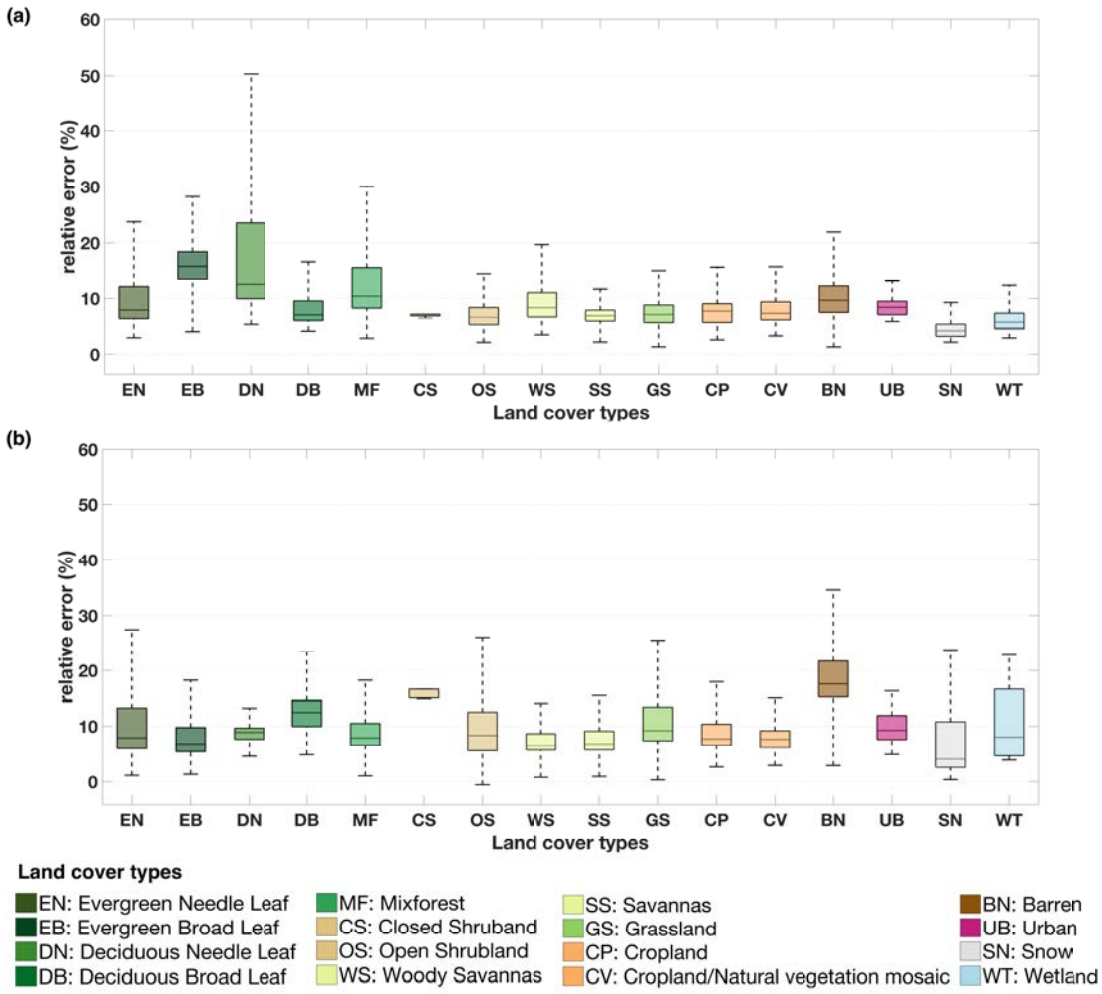

Figure 4-1: Averaged relative error of satellite-observed water content in different land cover types for: (a) SMOS-derived soil moisture; (b) GRACE-derived total water storage.

soil layer and root-zone. An additional level of quality control was imposed here on the ISMN data to eliminate those sites with less than 2 years data record, having persistently low or high values, or possessing inexplicable spikes or breaks in the time series. In total 164 stations from 19 measurement networks provided near-surface (0 – 5 cm) soil moisture observation globally, while 197 station from 15 networks provided root-zone soil moisture at 0 – 1 m (Fig. 4-2). Hourly observations were averaged over a 24-hour period to give daily moisture measurements. Stations with multiple measurements for soil moisture

within 1 m depth were aggregated to soil moisture at 0–1 m. The 98^{th} and 2^{nd} percentiles of the data records for each site were assumed to represent the field capacity and wilting point required for the calculation of relative wetness.

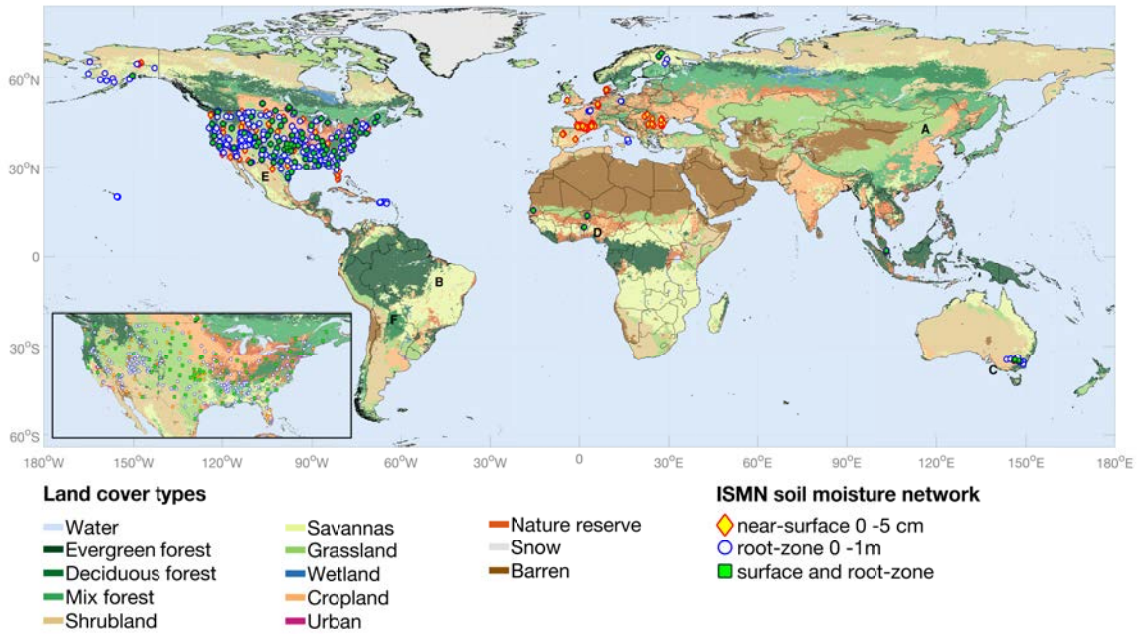

Figure 4-2: Distribution of in situ near-surface and root-zone soil moisture sites from the International Soil Moisture Network (ISMN) overlaid on the background of MODIS IGBP (International GeosphereâĂŞBiosphere Programme) land cover classifications (MCD12Q1).

4.2.5 Satellite-observed greenness

The MODIS 0.05° monthly normalized difference vegetation index (NDVI) product (MOD13C2) (Didan, 2015) derived from atmospherically-corrected reflectance in red and near-infrared wavelengths were used as a simple and robust indicator for vegetation greenness. The MOD13C2 NDVI data were aggregated to 0.25° to be comparable with model simulations from January 2010 to December 2016. Areas of the Earth's surface that never exceeded a maximum NDVI value of 0.2 over this period were masked as barren land.

4.3 Method

4.3.1 Data assimilation

SSatellite-derived total water storage and near-surface soil moisture were jointly assimilated into the global W3 model from 2010 to 2016. Systematic differences between model and observations need to be removed to ensure optimal performance of the assimilation method (Evensen, 1994; Dee, 2005; Renzullo et al., 2014). Since the W3 model only specifies soil water storage in water depth (mm) rather than prescribing a physical thickness of the soil layers and porosity, the model-simulated soil water availability cannot be directly compared with SMOS soil moisture retrievals in volumetric fraction. To resolve the inconsistency between model and satellite observations in representing the near-surface soil water availability, both SMOS retrievals and W3 simulated top-layer soil water storage (θ_t) were converted to relative wetness (w_t) (0-1) with respect to the dry (θ_{wt}) and wet (θ_{fc}) extremes over the 7-year period, calculated as the 2^{nd} and 98^{th} percentiles, respectively (Eq. 4.1).

$$w_t = \frac{\theta_t - \theta_{wt}}{\theta_{fc} - \theta_{wt}} \tag{4.1}$$

For total water storage, it was a simple matter of adding the W3 model-simulated total water storage averaged over 2004 – 2009 to the GRACE-observed water storage anomaly for absolute total water storage values.

Due to the disparity in temporal and spatial resolution and measurement depths between SMOS and GRACE, these contrasting satellite water content observations were assimilated using an ensemble-based Kalman smoother approach with a one-month window, following the approach of Tian et al. (2017). Total water storage together with soil moisture data were used to constrain model-simulated water storage components formed as the state vector x, including vegetation water and soil water (top, shallow, and deep layer) for each hydrological response unit, surface water (rivers, lakes) and unconfined ground-

water. The observation vector y consisted of the available daily SMOS surface soil moisture and the GRACE total water storage in a month at each grid. Model error variance P^f was derived from 100 ensemble members of the state variable, generated through the perturbation of precipitation, radiation and air temperature data. The analysis states x^a were updated with the forecast states x^f and the weighted difference between the observations and forecasts at the end of every month (Eq. 4.2), i.e.,

$$x_i^a = x_i^f + P^f H^T (H P^f H^T + R)^{-1} \left[y - H(x_i^f) + \epsilon_i \right], \quad i = 1, \ldots, 100 \quad (4.2)$$

The matrix $P^f H^T (H P^f H^T + R)^{-1}$ above, known as the Kalman gain, determines the degree of influence that observation y has on changing the model forecast state, x^f.

Spatially and temporally varying uncertainties from GRACE and SMOS products, characterised by R, were used in the assimilation to represent the observation error covariance matrix. Tian et al. (2017) applied an artificial weighting factor to the uncertainties of GRACE and SMOS data to compensate the over-adjustment from SMOS due to the inconsistency in units between SMOS and GRACE data. In this study, the first part of the observation operator H converts SMOS soil moisture retrievals firstly into relative wetness (Eq. 4.1) and then to available water content (in mm) for the upper most soil layer. The field capacity and wilting point from model simulations for the top 5 cm were applied to both soil wetness and uncertainties. No further weighting factor was required between GRACE and SMOS data after converting SMOS data to equivalent water height. Both ascending and descending SMOS soil moisture retrievals were used to improve the spatial coverage. The second part of the observation operator computes the monthly mean from the sum of daily water storage components in the state vector. The state variables for the next time step of the model forward run were initialized with the analysis states.

The open-loop run (without assimilation of any observation), the assimi-

lation of soil moisture alone and the assimilation of total water storage alone were also evaluated to examine different impact of different satellite data on soil moisture profile adjustments. The same ensemble Kalman smoother was applied to the assimilation of SMOS alone (SMOS-only) and the assimilation of GRACE alone (GRACE-only) to compare with the joint assimilation. Since the uncertainty in SMOS data varies considerably between land cover types, another joint assimilation experiment (Joint-landcover) was conducted where SMOS uncertainties were increased by 50% of the reported value over dense forest area (tree cover > 0.7) was implemented to identify any possible underestimation of SMOS uncertainties in forest regions.

4.3.2 Evaluation of soil moisture estimates

Estimates of soil water content in the uppermost soil layer (0–5 cm) and root-zone (0–1 m) after the joint assimilation were evaluated against in situ soil moisture observations from ISMN. The in situ stations within the corresponding model grid cell were aggregated to represent the soil moisture at 0.25° scale. The in situ soil moisture monitoring sites were grouped based on land cover type of the corresponding model grid cell. Both model-simulated and observed soil moisture were transformed to relative wetness to resolve differences in units and depths between model simulations and in situ observations (Eq. 4.1). The performance of soil moisture estimation was statistically evaluated with Pearson correlation (r) and root-mean-square error (RMSE) for the open-loop and different assimilation experiments.

4.3.3 Analysis of vegetation response to root-zone soil moisture

In this study, satellite-observed vegetation greenness were used as an independent evaluation of root-zone soil moisture estimates in water-limited regions. 30 years of monthly potential evapotranspiration and precipitation data

were used to derive the aridity index. The aridity was simply calculated by averaging the fraction of months that potential evapotranspiration exceeded precipitation in a year. The humid regions with aridity index less than 0.4 were masked out in the evaluation. The correlations between satellite-observed vegetation greenness and soil water storage from different sources were calculated for comparison. The deseasonalized NDVI and soil water storage were derived to investigate the impacts of data assimilation on simulating seasonal cycle and anomalies. The estimation of soil water availability used in the comparisons included SMOS soil moisture, GRACE total water storage, model simulated root-zone soil moisture via the joint assimilation, and the precipitation-based soil moisture estimates from the antecedent precipitation index (API). The API was calculated using the MSWEP precipitation data with a constant decay coefficient of 0.9 (Hooke, 1979). API was used as it better represents the cumulative effects of precipitation than individual rainfall events on vegetation response. The statistical improvement in correlation was used as an indicator for enhanced performance on simulating seasonal pattern and the deviation of monthly mean.

The soil water availability at the integrated depth that has the maximum correlation with NDVI best explains the changes in surface greenness at each grid cell, so-called vegetation-accessible storage (Tian et al., 2019). The correlation of monthly NDVI and soil moisture estimates integrated over different depths after joint assimilation were calculated. The soil water storage estimates were integrated at four depths: near-surface (0–5cm), shallow-root zone (0–1m), deep-root zone (0–10m) and total water column. Annual trend of the accessible storage anomalies relative to monthly means were calculated to determine the area under soil water stress. Linear trend analysis was also applied to the annual average NDVI anomalies to investigate the consistency between vegetation greenness and soil water storage. The trends in accessible storage derived from the open-loop and joint assimilation were compared with the trends in NDVI to investigate the change in annual trend after data

assimilation.

4.4 Results

4.4.1 Near-surface and root-zone soil moisture estimation

SMOS soil wetness and W3 top-layer soil wetness from open-loop and data assimilation were compared with the in situ near-surface soil wetness observations from ISMN (Fig. 4-3). Satellite observations of soil moisture (SMOS) were generally better correlated with in situ soil moisture observations over non-forest areas than open-loop simulations (Fig. 4-3a). However, as the fraction of tree cover increases, the relative performance changes and model simulations tend to be better correlated with in situ measurements than SMOS observations. The joint assimilation of both SMOS and GRACE observations (Fig. 4-3b) shows improved correlation with in situ measurements compared with the model open-loop over the majority of the sites where SMOS observations better correlated with in situ measurements. This improvement is due to data assimilation bringing the model and SMOS soil moisture into better agreement for these sites, as illustrated in Fig. 4-3c for a grassland site. On the other hand, joint assimilation largely reduces the degradation on surface soil moisture over forest sites where SMOS retrievals are less accurate than model simulations (dark green dots in Fig. 4-3a and time series in Fig. 4-3d).

The impact of data assimilation on W3 model performance is further illustrated in Fig. 4-4. For near surface soil moisture (Fig. 4-4a), the assimilation of SMOS observations alone (SMOS-only) shows more sites with improved correlations and reduced RMSE against model open-loop. The assimilation of GRACE data alone had little impact on surface soil moisture estimation. Joint assimilation of SMOS and GRACE with SMOS observations down-weighted for ISMN sites in forest (high tree cover) areas (plot labeled 'Joint-landcover')

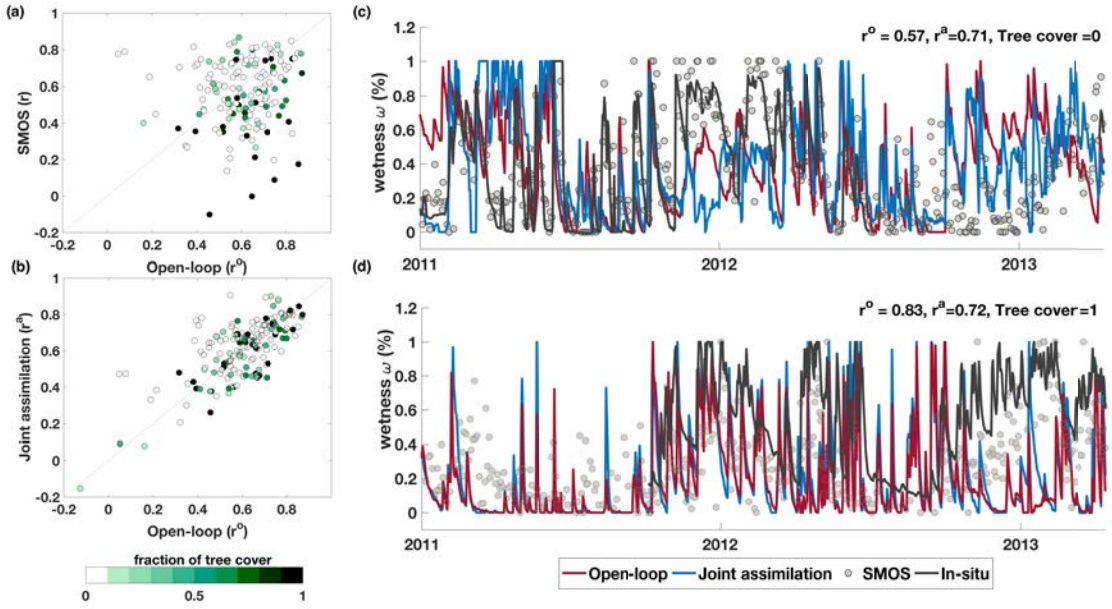

Figure 4-3: Assessment of near-surface soil moisture estimation with ISMN in situ measurements from 2010 to 2015: (a) correlations of SMOS soil moisture retrievals with in situ measurements (y-axis) compared against open-loop (x-axis); (b) correlation of near soil moisture estimates after the joint assimilation with in situ measurements (y-axis) compared against model open-loop (x-axis) ; Each ISMN site is characterised by the fraction of tree cover within the corresponding 0.25° cell. (c) and (d) time series of simulated surface soil moisture before and after the joint assimilation over grassland and forest dominated region.

was observed with less degradation sites than joint assimilation with original SMOS uncertainties ('Joint').

Data assimilation resulted in significant improvements in W3 root-zone soil moisture estimation over the majority of sites (Fig. 4-4b). In contrast to surface soil wetness, SMOS and GRACE observations both impacted deeper soil wetness estimation considerably. Simulation of soil wetness over the root-zone (0–1m) in the joint assimilation was less affected by forest cover compared to the near-surface soil wetness, as evident from the high degree of similarity between the 'Joint' and 'Joint-landcover' plots (Fig. 4-4b). This suggests no significant difference in performance as a result of down-weighting SMOS influence over forest regions.

Table 4.1 summarises W3 model soil moisture estimation performance

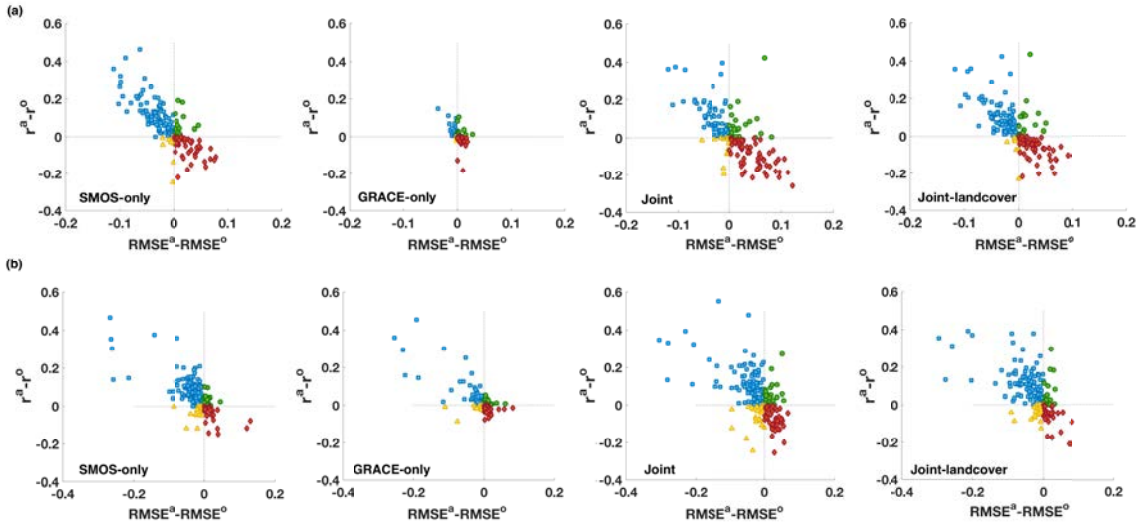

Figure 4-4: Performance of surface and root-zone soil moisture estimates from four data assimilation scenarios against open-loop: correlation (r) and root mean-squared error (RMSE) change after the assimilation($r^a - r^o$, RMSE^a-RMSE^o; ^{a}: after assimilation, ^{o}: open-loop) in (a) surface soil moisture estimation; (b) root-zone soil moisture estimation. The four scenarios include: SMOS-only as the assimilation of SMOS data alone, GRACE-only as the assimilation of GRACE data only, Joint as joint assimilation of SMOS and GRACE, Joint-landcover as increasing SMOS uncertainty in forest regions in the joint assimilation. The points in the scatter plots are colour coded such that: blue indicates ISMN sites where improvement was observed in both correlation and RMSE; green indicates sites where there was improvement in correlation, but not in RMSE; yellow indicates those sites where there was improved RMSE, but not correlation; and red indicating sites where assimilation resulted in degradation in both correlation and RMSE.

for both near-surface and the root-zone for different land cover types. On average, the correlation with in situ observations increased for both surface and root-zone soil moisture estimates compared to model open-loop. The improvements in surface soil moisture estimates were mainly over croplands (i.e. CP and CV) and grassland dominated areas (i.e. GS and GD), with changes in correlation, $r^a - r^o$, as high as 0.44 for cropland. Correlation in model surface soil moisture estimates over savannas and forest areas decreased relative to open-loop simulations. Data assimilation improved root-zone soil moisture estimates for most land cover types with up to 0.38 increase over mix-types areas and an average change in correlation of 0.1 for croplands (from 0.59 to 0.69) and grass-dominated areas (from 0.54 to 0.64).

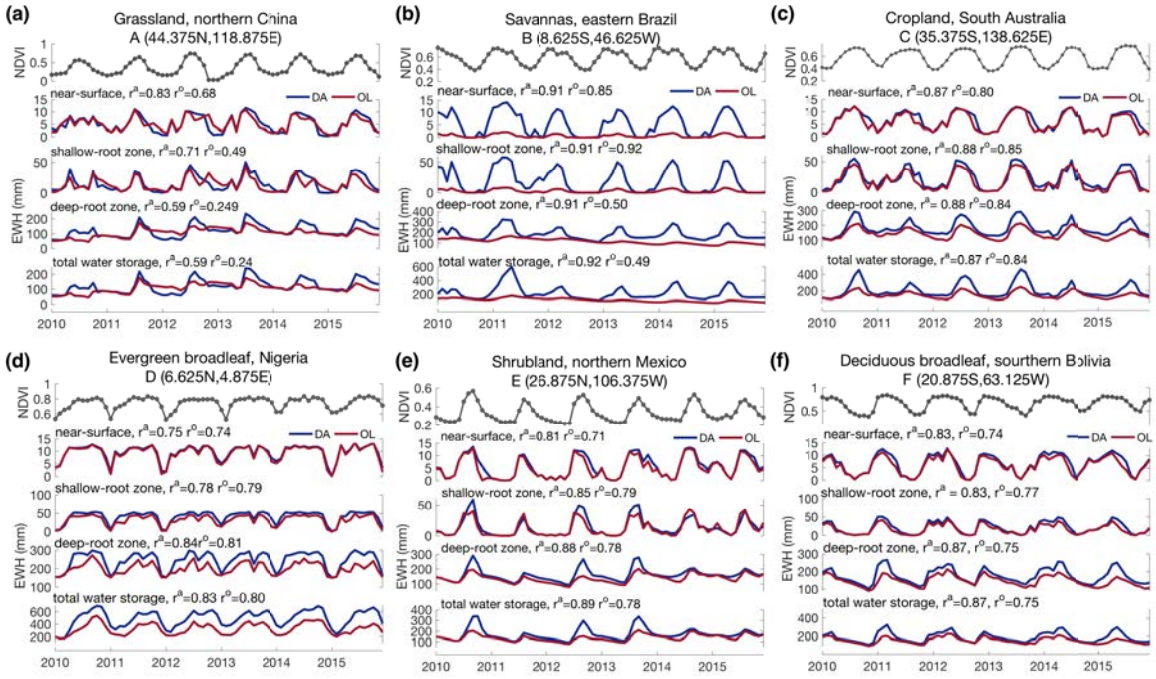

Figure 4-5: Time series of vegetation responses (NDVI) to soil water storage over different integrated depths across land vegetation types before (r^o, red curves) and after the joint assimilation (r^a, blue curves). The location of each site is shown in Figure 1.

4.4.2 Relation between vegetation greenness and soil water availability

Monthly water storage integrated to different depths, from the uppermost soil layer to total soil column, were compared with satellite-observed greenness. The response of vegetation greenness to water storage at different depths is illustrated for selected sites over six land cover types in Fig. 4-5. Significant differences in soil water variability were found between the joint assimilation and open-loop estimates in all sites (Fig.4-5), in particular deep-root zone and total water column. The temporal pattern in greenness and water storage time series was characterized for open-loop and joint assimilation estimates by correlation, r^o and r^a respectively. As an example, the grassland site in northern China responded more strongly to the availability of near-surface soil water (higher correlation) than deep soil water and total water storage (Fig. 4-5a). This suggests a shorter time lag between surface soil water availability and surface greenness. Stronger correlations between NDVI and near surface soil water storage were found to have increased by 0.15 after assimilation (i.e. $r^a - r^o = 0.15$). Greenness of the savannas site in eastern Brazil and the cropland site in southern Australia showed a similar seasonal pattern (correlation) to water storage over all depths (Fig. 4-5b and 4-5c). The largest change in correlation as a result of joint assimilation was observed for the Brazil savannas site (Fig. 4-5b) ($r^a - r^o > 0.4$) for shallow- and deep- water storage. NDVI in shrublands and forest sites with deeper roots showed higher correlation with deep soil water and total water storage availability, such as the evergreen broadleaf forest in Nigeria, shrubland in northern Mexico and deciduous broadleaf forest in southern Bolivia (Fig. 4-5d to 4-5f).

Significant increases in correlation between W3 water storage and vegetation greenness resulted from the joint assimilation of SMOS and GRACE data. Fig. 4-6a shows the maximum change in correlation between the seasonal cycle of NDVI and soil water storage at different integrated depths. Increases

in correlations between the seasonality of NDVI and soil water storage after the joint assimilation were observed globally, most notably in the high latitudes of the northern hemisphere, where increases in correlation over 0.5 were widespread. This is due to the joint assimilation bringing the seasonality of soil water availability into better agreement with greenness. Significant increases in the correlation between NDVI anomalies and root-zone soil water anomalies by 0.2 were widely observed over the semi-arid and arid regions after the joint assimilation (Fig. 4-6b). The result shows that the deviations of root-zone soil water to monthly mean can be better simulated after the joint assimilation with improved consistency with vegetation greenness anomalies.

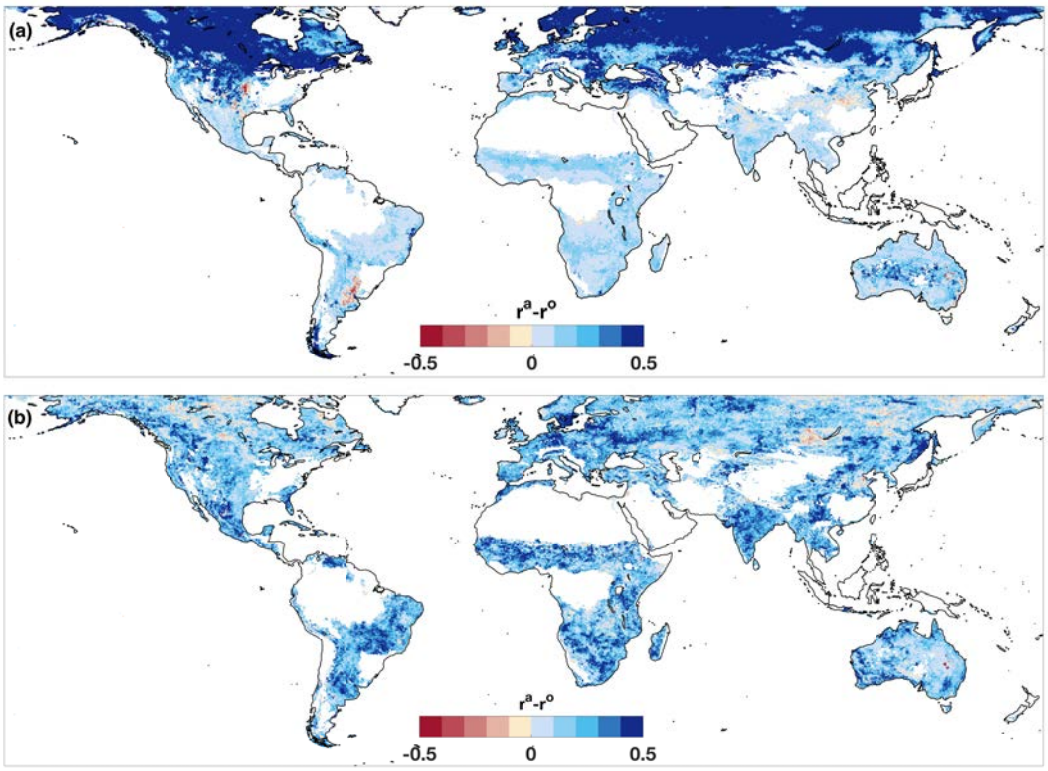

Figure 4-6: Maximum change in correlation ($r^a - r^o$, r^a: joint assimilation, r^o open-loop) of (a) the seasonal cycle of vegetation greenness and soil water storage over different integrated depths; (b) the anomalies of vegetation greenness and soil water storage over different integrated depths.

Having established that joint assimilation improved soil water estimation

and the correlation with vegetation response globally, we explored the sources of the improvements. The correlation between NDVI and soil water content estimates from API, SMOS, GRACE and W3 were computed globally (Fig. 4-7). API showed a correlation with NDVI of $\sim 0.5-0.6$ over major dry lands and high latitude regions, except for western and southern Australia and North America (Fig. 4-7a). Near-surface soil moisture estimates from SMOS showed strong positive correlation with vegetation conditions over tropical grassland and savannas regions, but strong negative correlation over eastern America and Europe (Fig. 4-7b). Vegetation growth over tropical regions showed clear wet and dry seasonal patterns closely related to the variability of total water storage from GRACE (Fig. 4-7c). The correlation of derived accessible soil water storage (from joint assimilation) shows the strongest correlation with NDVI (Fig. 4-7d) in the semi-arid and arid regions compared to other water content estimates. The negative correlations over western Australia between vegetation conditions and precipitation and surface soil moisture were not observed in GRACE-observed total water storage and joint assimilation derived accessible storage. This indicates that the vegetation here mainly responds to the availability of deep soil moisture. The vegetation conditions were found to be less responsive to the soil moisture availability in Europe and North America since water is not the only limiting factor to the vegetation growth.

4.4.3 Trends in soil water availability and vegetation response

The soil water anomalies estimated from the W3 open-loop and joint assimilation from January 2010 to December 2016 was compared with the global vegetation greenness anomalies over the same period and clear differences in the magnitude of soil water storage change and high spatial variability were observed globally (Fig. 4-8a and 4-8b). For example, a decrease of soil water storage was simulated in open-loop simulations over southern Mexico and

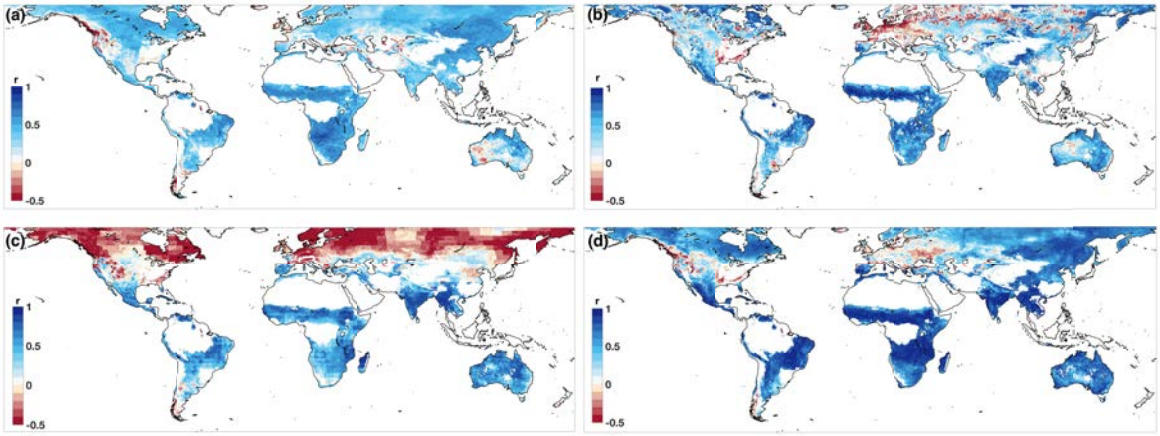

Figure 4-7: Vegetation response to different sources of soil water availability as indicated by: the correlation between monthly NDVI and (a) antecedent precipitation index (API), (b) SMOS surface soil moisture retrievals, (c) GRACE total water storage change retrievals, and (d) vegetation-accessible water storage derived after the joint assimilation.

northeastern China. However joint assimilation results showed an increase in soil water storage anomalies for these same regions. Differences in water storage anomalies change between open-loop and joint assimilation (Fig. 4-8c) could be over 10 mm/yr, and were most noticeable over southeast Asia and Australia.

Clear decreasing trends in NDVI anomalies (more than 0.025 units per year) were observed over central and eastern Australia (Fig. 4-8d), while decreasing trends in soil water availability of over 10 mm/yr were found in both model open-loop and joint assimilation estimates. A greater decrease of soil water storage was inferred in central and eastern Australia through joint assimilation than from the open-loop. Similarly, the deficit in accessible root-zone soil water storage estimated through joint assimilation aligned well with the dramatic decrease in vegetation greenness in eastern Brazil, southern India and southern Africa. The joint assimilation resulted in estimated increases in soil water storage that were globally much more consistent with increased greenness than the open-loop simulations.

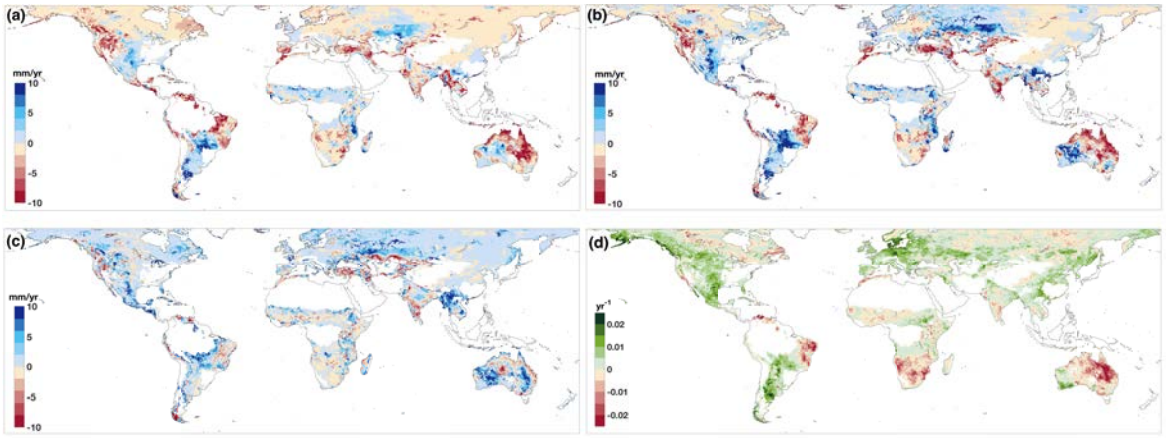

Figure 4-8: Change of soil water availability and vegetation greenness from 2010 to 2016: linear trends of accessible water storage anomalies estimated from (a) model open-loop and (b) joint assimilation; (c) difference in trends between joint assimilation and model open-loop; (d) linear trends of NDVI anomalies.

4.5 Discussion

We found that global modelling of root-zone soil moisture can be improved substantially through the joint assimilation of GRACE total water storage and SMOS soil moisture retrievals. This is consistent with previous findings for Australia (Tian et al., 2017). Corrections to near-surface soil moisture estimates resulted mainly from the assimilation of SMOS soil moisture. Uncertainties in SMOS soil moisture retrievals, e.g. related to errors in surface roughness and vegetation cover characterisation, influenced the accuracy of the estimation through the weights of the Kalman gain (Eq. 4.2). Therefore, in locations where satellite soil moisture estimates were observed to be more accurate than the W3 model open-loop simulations (e.g. grassland and cropland areas), the assimilation of these data improved the agreement between model estimates of near-surface soil moisture and in situ observations. However, assimilation of SMOS degraded model estimation for grid cells dominated by forest or mixed land cover types, most likely due to the underestimated SMOS uncertainties. The SMOS relative errors for each cover type ranged from 7–15% at median values, but was as high as 50% for full forest coverage regions

(Fig. 4-1a). The average relative errors for SMOS for over 50% of the in situ sites with mixed land cover types were only 9% (Table 4.1), indicating a potential under-estimation of SMOS error in those grid cells. By increasing the uncertainty of SMOS observations for forest areas, thus reducing their influence on assimilation, the number of sites with degraded model estimation was reduced (Fig. 4-4a). This suggests that reported uncertainties associated with the SMOS product are likely underestimated for densely vegetated areas.

The suitability of ISMN in situ soil moisture measurements for evaluation needs to be considered in interpretation. The quality of the data records, the sparseness of network coverage, uneven distribution globally (e.g. heavily skewed to North America), as well as the representativeness of a single site, or very small number of sites within a model or satellite pixel ($\sim 0.25^\circ \times 0.25^\circ$) are important contributing factors to the evaluation statistics. For example, there were considerably fewer ISMN sites in dense vegetation cover area (e.g. Table 1 WS, EN,DB and MF) than other cover types (i.e. 11 out of 167), and therefore should be a consideration in comparing average performance metrics across cover types. Also, by careful inspection of the in situ data and removal of any sites with large gaps in the temporal coverage or with unrealistic temporal behaviour (e.g. abrupt changes between dramatically contrasting moisture states), model evaluation could only be conducted with a subset of only 70% of the full complement of ISMN data that was believed to be of better quality. Given the paramount importance of these data in evaluation of model and satellite products in general, it is critical that the ISMN and similar in situ measurement networks are maintained, but rigorous quality control is equally important.

The assimilation of GRACE data had marginal impact on W3 near-surface soil moisture simulation (Fig. 4-4a). In contrast to the SMOS product, uncertainties in GRACE data were less variable in terms of relative error across land cover type, with error between 10–15% on average (Fig. 4-1b). The majority of the modelling grid cells showed improved correlation and reduced RMSE of

root-zone soil moisture as a results of joint assimilation of GRACE and SMOS, not only in the grassland-dominated sites but also for mixed land cover types. The improved root-zone soil water estimation in the joint assimilation could be linked to the Kalman smoother, which used the SMOS (daily) data to temporally disaggregate the GRACE-observed (monthly) total water storage. Therefore, not only does the joint assimilation of SMOS and GRACE observations vertically redistribute the water storage change into different W3 soil layers, it also redistributes the change temporally based on different dynamics of the soil moisture signal at the different depths.

Root-zone soil moisture varies considerably in space, as do plant rooting depth and soil physical properties. This makes it a challenge to compare model estimates over a cell and in situ measurements at point scale. Remotely sensed vegetation greenness can serve as a surrogate for water availability in water-limited regions of the world. MODIS NDVI was used as an independent dataset to evaluate root-zone soil moisture simulations. Significant increases in correlation were found globally after joint assimilation (Fig. 4-6). The improvements over temperate regions are due to better consistency with NDVI seasonality (Fig. 4-6a). The increased correlation between root-zone soil water storage anomalies and vegetation greenness anomalies in semi-arid to arid regions is encouraging as it may result in improved capability for forecasting drought and vegetation productivity in dryland ecosystems.

The response of vegetation to water availability at different depths varies according to vegetation type and climate. For example, grasslands over the western U.S. and northeastern China showed strong correlation with SMOS near-surface soil moisture retrievals and modelled surface soil moisture, but weak correlation with GRACE-observed total water storage (Fig. 4-5a and 4-7). On the other hand, grassland in Sahel showed the same relative response to water availability at different depths but higher correlation with deep soil availability (Fig. 4-7). This appears to be due to the relatively deep root zone and lesser water holding capacity (Leenaars et al., 2018). Identifying

the soil layers that contribute most to the temporal behaviour of vegetation greenness is critical for understanding the impacts of water stress on the terrestrial ecosystem. The variation of soil water storage at plant accessible depths strongly reflected vegetation conditions over most of the globe except for part of North America and Europe (Fig. 4-7d). The SMOS and GRACE observations both showed negative correlation with the surface greenness over Europe and eastern North America, where better correlations were found with precipitation based index (API, in Fig. 4-7a). This is expected, since is water is not the primarily and only limiting factor (Nemani et al., 2003; Wu et al., 2015). Overall, the soil water storage derived from the joint assimilation embodied the best knowledge of available water content not only from meteorological forcing data, but also from the SMOS near-surface soil moisture and GRACE total water storage. Given accurate information of soil water availability, vegetation vigor and productivity can potentially be predicted (Tian et al., 2019).

A number of severe droughts have occurred during the last decade, including the droughts in Sahel, East Africa, California, China and northeastern Australia. The annual trends in NDVI anomalies and root-zone soil water storage anomalies from January 2010 to December 2016 showed consistency in the spatial patterns. After a sharp recovery from the Millennium drought during an extremely wet period from 2010 to 2011 (Leblanc et al., 2009; van Dijk et al., 2013b; Xie et al., 2016b), drought returned to eastern Australia with a decrease in soil water of over 10 mm/yr estimated from both model open-loop and joint assimilation (Fig. 4-8a and 4-8b). A decline in NDVI anomalies of more than 0.025 units per year was observed for the majority of middle and eastern Australia due to the developing soil water deficit (Fig. 4-8d), which is likely due to the widespread rainfall deficits caused by the El Niño 2014-16 and further amplified by the Indian Ocean Dipole 2015. Increases in soil water deficit were enhanced as a result of assimilating GRACE and SMOS over eastern Brazil, California and southern India and this was consistent with a decrease in vegetation greenness in these areas. The stronger signal of water

storage deficiency compared to the open-loop is mainly attributed to GRACE-observed decreasing total water storage in agreement with the water storage deficit observed by GRACE data only Rodell et al. (2018). The severity of groundwater depletion for irrigation in northern and southern India, as observed by GRACE (Rodell et al., 2009), was also better captured by through the assimilation of GRACE (Fig. 4-8b). Joint assimilation of GRACE and SMOS sometimes reversed the direction of change in soil water storage, compared to the open-loop, resulting in better agreement with trends of temporal pattern in NDVI, particularly in southern Mexico and northeastern China.

4.6 Conclusions

This work has demonstrated that the joint assimilation of GRACE and SMOS data into an ecohydrological model resulted in a spatial and temporal redistribution of water storage that significantly improved root-zone soil moisture estimation over different land cover types globally. In particular, significant improvements were found in the estimation of root-zone soil water availability over grassland and cropland. The joint assimilation optimally integrated the water dynamics information from SMOS and GRACE and mitigated the deficiencies of the individual sources of observation.

Vegetation response to soil water availability at different depths was found to vary according to ecosystem and climate. The close relationship between vegetation growth and soil water availability was quantified firstly with the root-zone soil water estimates through the assimilation of satellite soil moisture and total water storage retrievals simultaneously. The improved agreement between vegetation vigor and soil water availability indicates the potential for improving ecohydrological modelling and forecasting vegetation condition. Accurate characterization of vegetation response to soil water availability also provides new insights to help improve monitoring and forecasting drought impacts on ecosystems.

Table 4.1: Evaluation of near-surface and root-zone soil moisture estimation with ISMN in situ soil moisture observation across land cover types

	GS	**OS**	**WS**	**SS**	**CP**	**CV**	**EN**	**DB**	**MF**	**GD**	**FD**	**ML**
near-surface soil moisture 0-5cm												
Number of grid cells	31	6	6	2	26	4	2	0	2	23	7	55
Average SMOS uncertainty	6%	8%	12%	7%	6%	11%	11%	7%	17%	7%	24%	9%
Average GRACE uncertainty	9%	12%	12%	6%	9%	9%	5%	10%	9%	9%	7%	10%
Max correlation change $r^a - r^o$	0.36	0.03	0.11	-0.12	0.44	0.12	0.03	n/a	0.11	0.22	0.06	0.29
Average correlation change $r^a - r^o$	0.07	-0.04	0.02	-0.14	0.10	0.04	0.02	n/a	0.06	0.07	0	-0.01
Average open-loop correlation r^o	0.57	0.64	0.57	0.84	0.54	0.54	0.60	n/a	0.61	0.59	0.65	0.61
Average joint DA correlation r^a	0.64	0.60	0.59	0.70	0.64	0.58	0.62	n/a	0.67	0.66	0.65	0.60
root-zone soil moisture 0-1m												
Number of grid cells	33	6	3	1	22	7	4	2	2	30	13	74
Average SMOS uncertainty	6%	8%	12%	7%	5%	10%	11%	8%	13%	7%	18%	9%
Average GRACE uncertainty	9%	9%	9%	6%	7%	8%	6%	8%	9%	8%	8%	10%
Max correlation change $r^a - r^o$	0.34	0.10	0.15	0	0.31	0.16	0.10	-0.04	0.14	0.39	0.18	0.38
Average correlation change $r^a - r^o$	0.10	0	0.06	0	0.12	0.07	0.01	-0.04	0.03	0.08	0.04	0.06
Average open-loop correlation r^o	0.48	0.54	0.75	0.86	0.53	0.65	0.76	0.65	0.47	0.60	0.61	0.56
Average joint DA correlation r^a	0.58	0.54	0.82	0.86	0.65	0.72	0.77	0.61	0.50	0.68	0.65	0.62

Land cover types:

GS: grassland OS: open shrubland WS: woody savannas SS: savannas CP: cropland CV: cropland/natural vegetation EN: evergreen needle leaf forest

DB: deciduous broad leaf forest MF: mix forest GD: grassland-dominated mix types FD: forest dominated mix types ML: mixed land covers

Chapter 5

Forecasting dryland vegetation conditions months in advance

Forecasting vegetation vigor in advance is important for effective drought preparedness, especially in arid regions. Root-zone soil moisture, as a strong regulator of vegetation growth in water-limited areas may be used as a predictor for vegetation condition. Compared to traditional precipitation-based predictors, soil moisture can reflect climate conditions over a longer number of months. The time lag between available soil water storage and vegetation greenness provides unique benefit to forecast vegetation conditions months in advance. Using the global root-zone soil moisture estimation approach derived in Chapter 4, we assess the capability of using soil moisture in forecasting dryland vegetation conditions. The content of this chapter is based on the material published in Nature Communications:

Tian, S., van Dijk, A. I., Tregoning, P.,& Renzullo, L. J. (2019) Forecasting dryland vegetation conditions months in advance through satellite data assimilation. Nature Communications, 10(1), 469

Abstract

Dryland ecosystems are characterised by rainfall variability and strong vegetation response to changes in water availability over a range of timescales. Forecasting dryland vegetation condition can be of great value in planning agricultural decisions, drought relief, land management and fire preparedness. At monthly to seasonal time scales, knowledge of water stored in the system contributes more to predictability than knowledge of the climate system state. However, realising forecast skill requires knowledge of the vertical distribution of moisture below the surface and the capacity of the vegetation to access this moisture. Here, we demonstrate that contrasting satellite observations of water presence over different vertical domains can be assimilated into an eco-hydrological model and combined with vegetation observations to infer an apparent vegetation-accessible water storage (hereafter called accessible storage). Provided this variable is considered explicitly, skilful forecasts of vegetation condition are achievable several months in advance for most of the worldâĂŹs drylands.

5.1 Main text

The majority of ecosystems globally are persistently or seasonally limited by water availability (Nemani et al., 2003). Dryland vegetation responds to rainfall variability in contrasting ways, depending on the timescale of rainfall variability and the way that this interacts with soil hydraulic properties and vegetation rooting patterns (Porporato et al., 2004; Wang et al., 2001; Reyer et al., 2013). Together, these factors determine the vegetationaccessible water storage capacity. Variations in water availability affect the growth and condition of grazing land, dryland crops and planted forests, as well as native vegetation. Vegetation condition, in turn, affects fire risk (Yebra et al., 2008) and soil health (D'Odorico et al., 2007) and can contribute to heatwaves through landâĂŞatmosphere feedback processes (Seneviratne et al., 2010). Forecast-

ing vegetation condition in response to water availability months ahead would therefore be of great value for timely mitigation of such impacts.

Unfortunately, for most of the worldâĂŹs dryland areas, rainfall is very unpredictable (Reynolds et al., 2007) or with low forecast skill at monthly timescale and beyond. Most climate modes do not persist very long and those that do, such as the El NiÃśo Southern Oscillation and Indian Ocean Dipole, tend to achieve comparatively less skill in drier regions (Saji et al., 1999). However, water stored at and below the surface provides a source of forecasting skill that can be more influential over longer periods, as has been demonstrated for streamflow10,11. Soil moisture has a memory that persists for weeks to months, depending on the relative magnitude of vegetation-accessible storage and precipitation variability (van Dijk et al., 2013c; Koster et al., 2010). This suggests the potential to use root-zone soil water availability to forecast vegetation condition at large scale. So far, this potential remains unexplored. This is likely in part because of the lack of accurate knowledge of accessible storage capacity and the low fidelity of hydrological models in estimating vertical moisture distribution (Jackson et al., 1996; Kleidon, 2004; Fan et al., 2017). In weather forecasting, assimilation of atmospheric satellite observations mitigates model deficiencies to provide better estimates of system state, and this has been the main driver of remarkable enhancements of weather forecast skill and lead time (Bauer et al., 2015). Here, we demonstrate that data assimilation can produce similar benefits in ecohydrological forecasting.

Satellite remote sensing has been pivotal to deepening our understanding of water availability and climate change at regional-to-global scale, and has helped to advance predictive models and decision making (Rodell et al., 2018). However, satellite observations of water presence are limited to either the surface (up to 5 cm for soil moisture, e.g., Soil Moisture and Ocean Salinity (SMOS) mission) or total water column (Gravity Recovery and Climate Experiment (GRACE) mission). The quantification of the vertical distribution of water storage is extremely difficult over large spatial and time domains due

to the lack of direct measurement of root-zone soil moisture and groundwater storage. The accuracy of soil moisture or groundwater storage estimates separated from total water storage is limited without ancillary data and the consideration of data uncertainties (Tangdamrongsub et al., 2018). We assimilated MODIS (Moderate Resolution Imaging Spectroradiometer) satellite instrument-derived surface water extent (Van Dijk et al., 2016), SMOS near-surface soil moisture (Kerr et al., 2010) and GRACE total column water storage (Tapley et al., 2004) into a global ecohydrological model (van Dijk et al., 2013c) and estimated the vertical distribution of water at the surface (Van Dijk et al., 2016), in the near-surface soil, shallow root zone (<1 m), deep root zone (>1 m) and in groundwater Tian et al. (2017) (see Methods). Satellite-derived vegetation greenness (i.e., the Normalised Difference Vegetation Index (NDVI)) was used as a simple but powerful measure of vegetation condition. In areas of low-density vegetation, NDVI is generally a strong proxy of vegetation cover fraction, leaf area and biomass. The average seasonal cycle of greenness is inherently predictable and was subtracted from the observations, resulting in greenness anomalies. The monthly greenness anomalies, on the one hand, and anomalies in water storage integrated over different depths,on the other, were used to develop a simple forecast model. A skilful lead time was defined as the forecast period over which rank correlation (ρ) between accessible storage and greenness remained relatively high (ρ>0.60). The results were analysed as a function of climate dryness at each location, defined as the longterm average fraction of months for which potential evapotranspiration exceeds precipitation (see Methods).

We find that larger accessible storage broadly corresponds with slower decay in forecast skill. Vegetation conditions in the majority of global dryland can be forecast 3 months in advance from accurate estimates of current soil water availability.

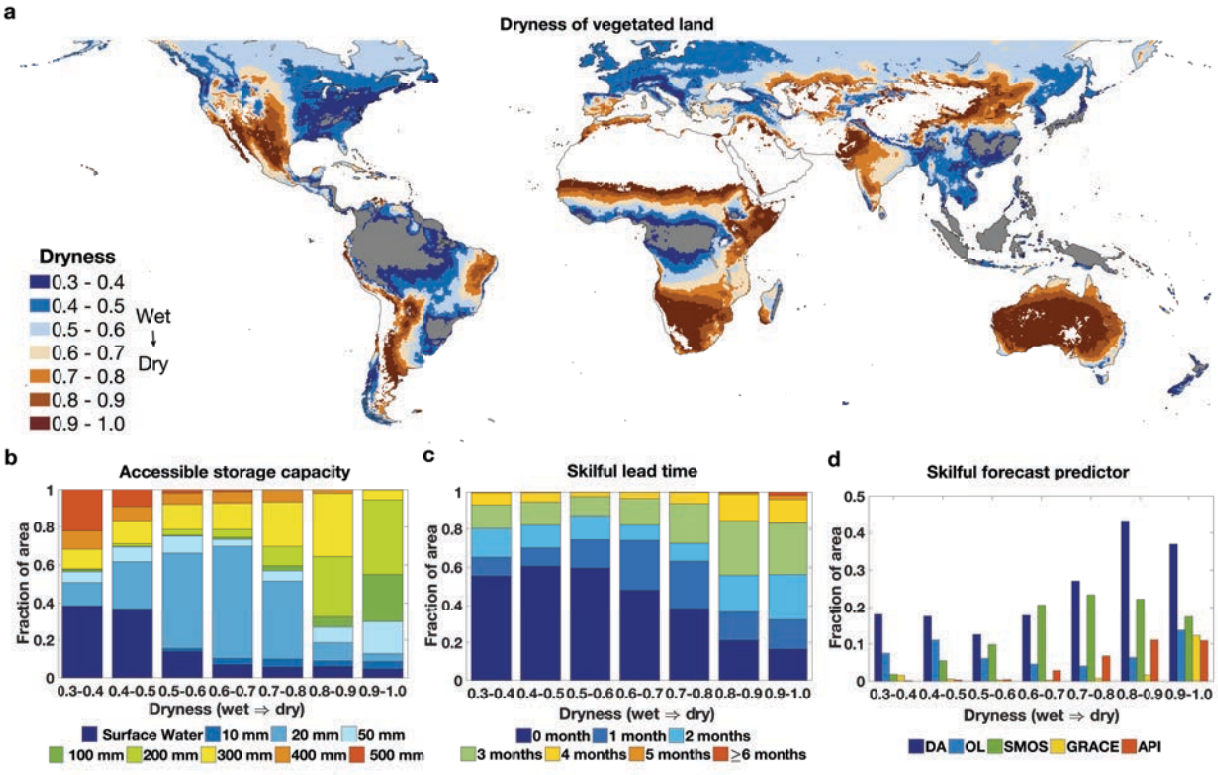

Figure 5-1: Accessible storage and vegetation dynamics prediction skill. Relationship between water availability over different integration depths and vegetation greenness anomalies over humid to arid regions with dryness indices from 0.3 to 1.0. a Distribution of global drylands; areas with minimal vegetation(maximum Normalised Difference Vegetation Index (NDVI) <0.25) and generally high water availability were masked out in white and grey, respectively. b Fraction of area for accessible storage capacity in mm (surface water or below-surface) at different dryness levels. c Fraction of area for the number of months for which skilful (ρ>0.6) forecasts were achieved in different dryness levels. d Fraction of area for which skilful forecasts were possible 3 months in advance using data assimilation (DA), compared to those achieved using only open-loop model results without any assimilation of satellite observations (OL), using satellite-derived near-surface soil moisture (Soil Moisture and Ocean Salinity (SMOS)), using total water storage (Gravity Recovery and Climate Experiment (GRACE)) and using an index calculated from antecedent precipitation only (Antecedent Precipitation Index (API))

5.2 Results

Vegetation in dry climatic zones with dryness value over 0.8 (Fig. 5-1a) generally shows greater accessible storage (>100 mm) and less reliance on surface water than vegetation in more humid zones (Fig. 5-1b). For example,

vegetation in up to 70% of the more humid areas (dryness index 0.4âĂŞ0.6) shows greater response to the shallow soil water with less than 50mm of accessible storage, while more than 65% of dryland vegetation (dryness 0.7âĂŞ1.0) appears to have access to water at >1m below the surface. With increasing dryness, accessible storage is an increasingly strong predictor of future vegetation greenness (Fig. 5-1c). Naturally, forecast skill decayed over time, but skilful forecasts were often still achieved as long as 3 months ahead. In such areas, 80% of the vegetation appeared to have access to deeper soil moisture. Thus, prediction lead time can be broadly interpreted as a measure of vegetation access to deep water stores.

Alternative forecasts were also developed using an antecedent precipitation index and remotely sensed near-surface soil moisture or total water storage, but these typically provided skilful vegetation forecasts for no more than 1 or 2 months (Fig. 5-1d). Skilful forecasts using soil water availability from satellite observations or model simulations could be achieved for no more than 20% of the vegetated arid area (dryness >0.6). Estimates of accessible storage derived through assimilation of satellite observations led to considerably better forecasts; skilful forecasts were provided for a greater fraction of area for all dryness categories. This is the result of the integration of satellite observations of water present near the surface and at greater depth with the process understanding encoded in the ecohydrological model.

Particularly skilful forecasts and long lead times of over 5 months were found for interior Northern Australia, corresponding with dry but dominantly perennial grassland and shrubland showing relatively high accessible storage (c. 200 mm) (Fig. 5-2). Positive spatial correlation between accessible storage and lead time is also evident in other regions. Vegetation condition forecasts in sub-humid and humid regions (dryness <0.5) are generally less robust, particularly towards higher latitudes. This is as would be expected given that temperature and radiation will be equal or stronger drivers of greenness than water availability (Nemani et al., 2003; Wu et al., 2015). Some part of the

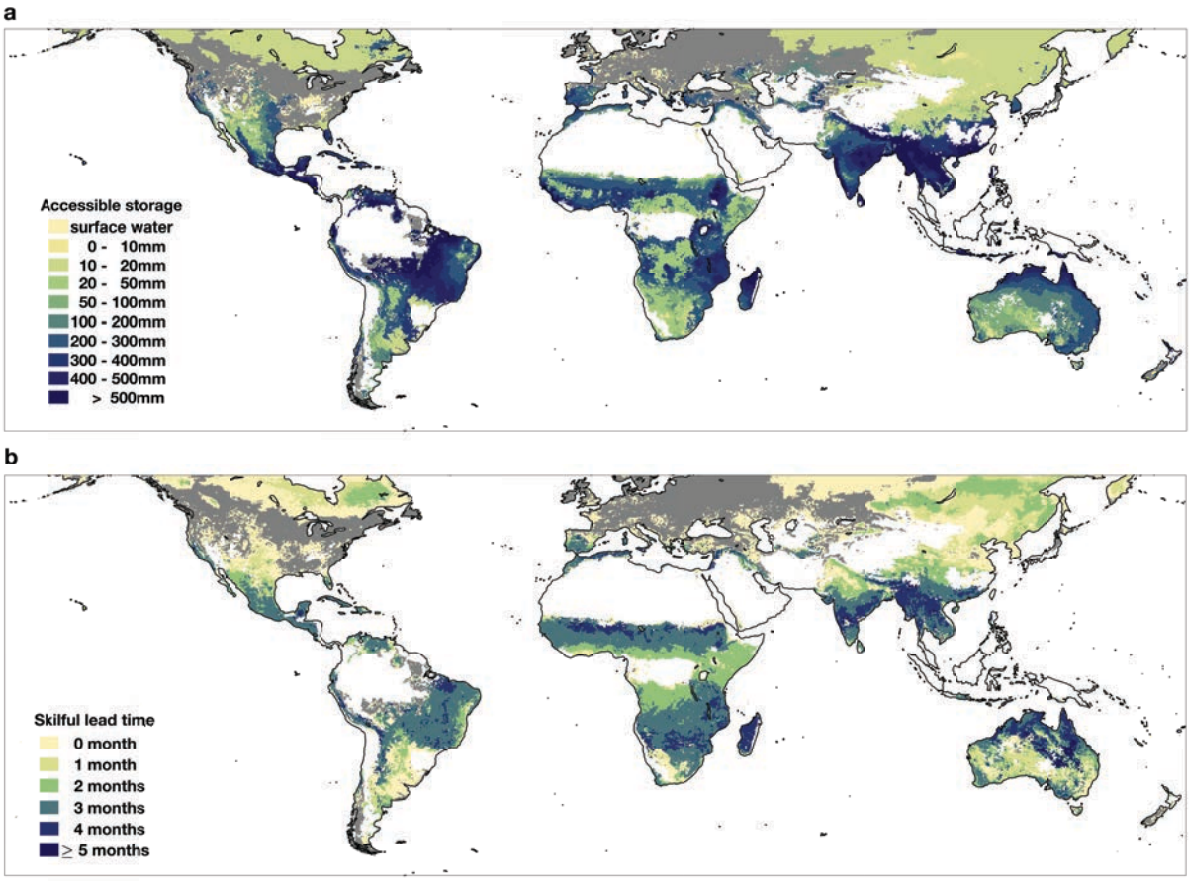

Figure 5-2: Global distribution of (a) maximum accessible storage capacity and (b) skilful forecast lead time. Unvegetated and wet regions were masked as in Figure 1a. Lead time is counted from current month (0) to over 5-months. 0-month lead time implies that skilful greenness predictions can only be made for the current month.

forecast skill can be attributed to the correlation between the average seasonal cycles of water storage and greenness, particularly in monsoon climates. This source of forecast skill can be exploited in the absence of water storage information (see Methods) and can be subtracted from overall skill to highlight regions where water storage information provides an important contribution to forecast skill (Fig. 5-3a). The best performing between the climatology forecast and persistence forecast at each pixel was selected and compared with our result. Significant improvements were found over regions vulnerable to droughts and poorly predictable with seasonal patterns.

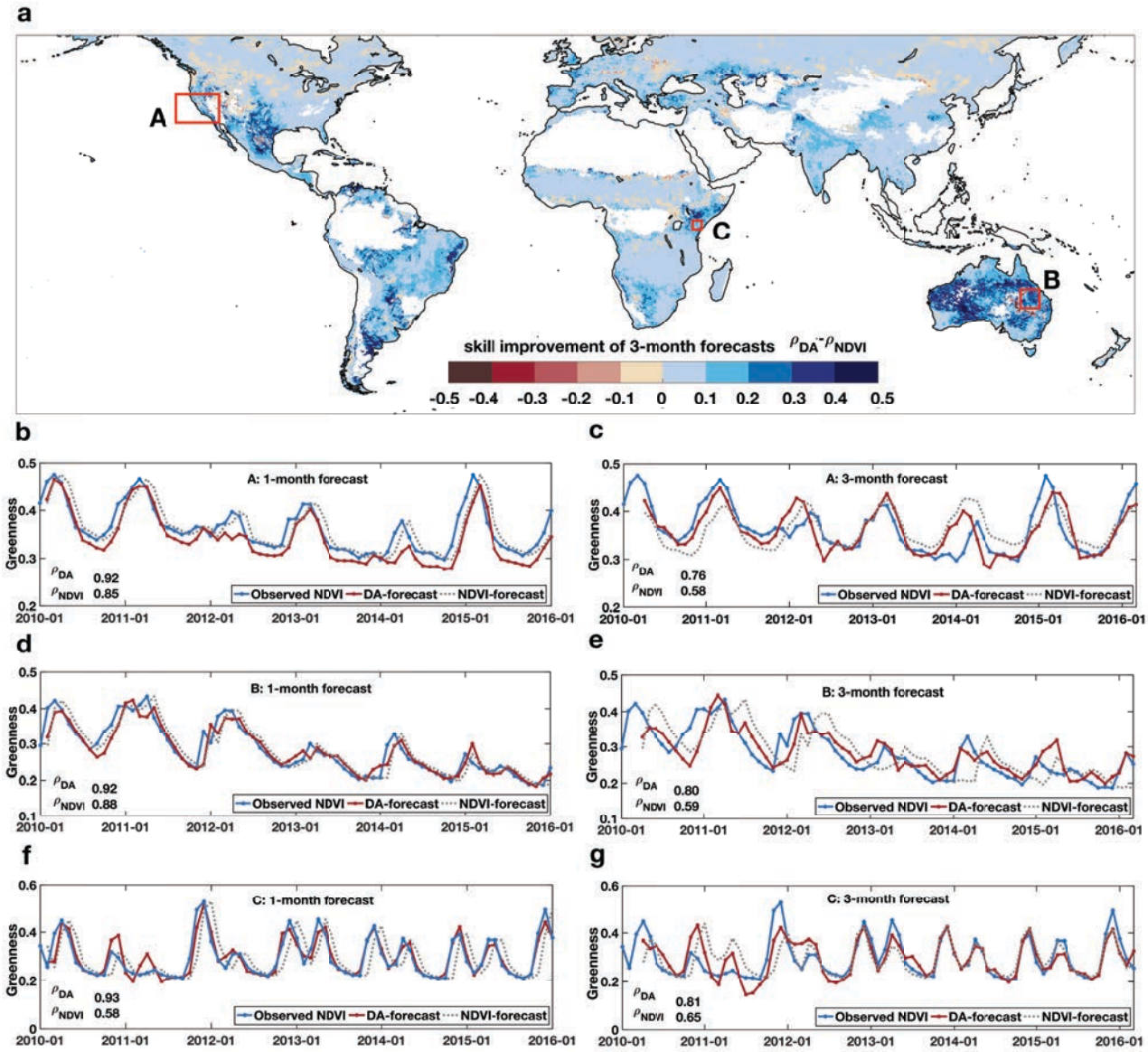

Figure 5-3: The 1-month and 3-month forecasts of vegetation condition. a Difference in correlation (ρ) between 3-month forecasts using accessible storage (DA-forecast, ρ_{DA}) and climatology (NDVI-forecast, ρ_{NDVI}) with greenness observations from 2010 to 2016. (DA: data assimilation, NDVI: Normalised Difference Vegetation Index). bâĂŞg Monthly time series of averaged 1-month and 3-months forecasts of greenness, compared with observed vegetation greenness over regions A, B and C in a

Case studies for southern California, central Queensland and the Horn of Africa illustrate features of the forecasts. Skilful 1-month and 3-month forecasts of vegetation response to drought conditions from 2011 until 2014

in California were made (Fig. 5-3b, c). The developing impacts of a multi-year drought from 2012 onwards in Queensland, Australia, were also forecast 1 month and 3 months ahead (Fig. 5-3d, e). Superior skill to forecast the severe drought in the Horn of Africa from 2011 to 2012 was demonstrated and cannot be achieved with the traditional monitoring forecasts even 1 month ahead (Fig. 5-3f, g). Significant improvements with an increase in correlation of more than 0.2 were achieved with longer lead time compared with NDVI-climatology forecasts. Forecasts using accessible storage showed a slower decay of forecast skill than NDVI-based forecasts by more than 0.1 units and maintained a correlation of 0.8 in 3-month forecasts. A further increase in the historical assimilation period should help to further improve forecast model skill (see Methods).

5.3 Discussion

The interplay between soil water availability and the intensification of drought differs with soil depth and aridity (Schlaepfer et al., 2017). Our study used plant-accessible storage across dryland areas to explore the relationship between water availability and dryland vegetation condition. The accessible storage capacity inferred here is empirically defined and may be less than the total moisture storage that can be accessed by the deepest-rooted individuals within the ecosystem. Rather, our results indicate the soil water store that empirically best predicts vegetation anomalies for the visually dominant ecosystem component as observed by remote sensing. Nonetheless, in semi-arid to arid regions we found spatial patterns that are very similar to previously reported root-zone storage capacity and rooting depths (Schulze et al., 1996; Kleidon, 2004; Wang-Erlandsson et al., 2016).

Our estimates of the accessible storage combine soil water dynamics information captured by multiple satellite sensors through data assimilation. A stronger response of vegetation greenness to water availability was found using

accessible storage, when compared against water availability derived from only satellite observations or the ecohydrological model, and results from previous studies (Andela et al., 2013; Chen et al., 2014; Yang et al., 2014; Bolten and Crow, 2012). Our findings suggest that incorporating current soil water availability, can significantly improve the accuracy of vegetation condition forecasts 3 months in advance for the majority of drylands globally. Such forecasts can help to improve drought early warning system and reduce economic and environmental impacts. This capacity may become even more important in the context of projected increases in the occurrence and severity of drought under climate change in some regions (Dai, 2013; Trenberth et al., 2014; Sheffield and Wood, 2008b).

The assimilation of satellite-observed water dynamics into an ecohydrological model enables the estimation of vegetationaccessible storage, providing insights into dryland ecology as well as providing a basis for seasonal drought impact forecasting. Knowing how vegetation accesses water below the surface illuminates potential vegetation condition in dry environments and their buffering capacity to mitigate against droughts of different duration and intensity. This in turn can inform effective action to prepare and manage for drought.

5.4 Methods

We limited the study region to include only arid to moderately humid vegetated land, defined by a dryness index of >0.3. We defined dryness as the average fraction of months that the mean potential evapotranspiration exceeds mean precipitation. The potential evapotranspiration was calculated using the PenmanMonteith equation (Monteith, 1981) with 30 years of meteorological data (Beck et al., 2017; Weedon et al., 2014). Greenness was derived from the MODIS MOD13C2 NDVI product (https://lpdaac.usgs.gov), which is a monthly composite of cloud-free observations resampled globally to 0.25°

resolution. We regarded areas with maximum NDVI <0.25 through time as unvegetated and excluded them from our analysis. Our study region covered about 50% of total land area and 90% of the vegetated area.

The World-Wide Water (W3) model(van Dijk et al., 2013c) (http://wald.anu.edu.au/) simulates water stores and flows in vegetation, surface water, soil and unconfined groundwater systems. The model was driven by global estimates of daily precipitation (Beck et al., 2017), radiation, air temperature, wind speed, snowfall rate and surface pressure (Weedon et al., 2014). Soil and vegetation water and energy fluxes were simulated independently for deep-rooted vegetation and shallow-rooted vegetation in each hydrological response unit with different aerodynamic control of evaporation and interception capacities. The soil water store was separated into three unsaturated soil layers, namely, top (0–5 cm), shallow (5–100 cm) and deep (1âĂŞ10 m) layer, where shallow-rooted vegetation and deep-rooted vegetation have different degrees of access to moisture in the different soil layers. The unconfined groundwater store was estimated with the mass balance from the groundwater storage, deep drainage from deep soil layer, capillary rise from the groundwater, groundwater evaporation and groundwater discharge. The W3 model also includes the simulation of canopy and biomass change coupling with water balance dynamics. The water in the biomass, surface water, soil and groundwater comprised the total water storage in the W3 model.

Three contrasting satellite water observations with different penetration depths from surface to the total water column were used in this study, namely, surface water extent, near-surface soil moisture and changes in total water storage. The surface water extent was estimated from MODIS 8-day composites using the reflectance dissimilarity between water and dry surfaces in shortwave infrared spectral band18, analogous to the microwave method of estimating water extent using brightness temperature (De Groeve, 2010). The MODIS-derived surface water extent was assimilated into the W3 model through a simple nudging approach with a high gain from the MODIS water fraction

estimations to describe surface water dynamics not reliably simulated by the model. Monthly $3° \times 3°$ GRACE mascon solutions (Watkins et al., 2015) were obtained from the Jet Propulsion Laboratory (http://grace.jpl.nasa.gov). In contrast to GRACE, which has the capability of detecting water storage change accumulated in the total water column, SMOS can only penetrate the land surface for up to 5 cm. The $0.25° \times 0.25°$ retrievals of near-surface soil moisture from the Centre Aval de Traitement des Données SMOS (Kerr et al., 2013) for both ascending and descending orbits were used to derive the daily averaged soil moisture content and to constrain the model simulated top-layer soil moisture (0–5 cm). To resolve the disparity in spatial, vertical and temporal resolution, the GRACE and SMOS data were assimilated into the W3 model using an Ensemble Kalman Smoother with a fixed 1-month window (Tian et al., 2017). A single monthly GRACE observation together with all the daily SMOS observations within a 1-month window were included in the observation vector. The state vector was comprised of all model estimates of daily soil water storage in three layers and groundwater over a month and updated with GRACE and SMOS simultaneously. The observation operator including temporal accumulation components enables direct comparison with the GRACE and SMOS observations. The forecasts of water storage in different layers were adjusted with the Kalman gain matrix (Allen et al., 2003) based on the uncertainties in the W3 model and satellite observations. The model uncertainties were estimated from the sample covariance computed from 100 ensemble members which were generated through the perturbation of meteorological forcings (precipitation, air temperature and radiation in this case). The observation uncertainties were quantified using the spatially and temporally varying uncertainties in the GRACE and SMOS products. GRACE and SMOS observations imparted different constraints on the estimation of water storage at different layers through both model physics and simultaneous adjustment from varianceâĂŞcovariance structure between model states and observations. The smoother approach with a 1-month assimilation window also considered

the temporal correlation between model states to separate water storage change into different depths based on different temporal dynamics. Data assimilation produced daily global $0.25° \times 0.25°$ estimates of water in the near-surface soil, shallow root zone, deep root zone and unconfined groundwater.

The statistical relationships between water storage dynamics and vegetation greenness anomalies were assessed using Spearman's rank correlation (ρ). The lagged ρ between water storage integrated over different depths and greenness anomalies over the subsequent 1 to 12 months was calculated and used to define an optimal integration depth (in mm of equivalent water thickness), interpreted as the vegetation-accessible storage. Given accessible storage as a time-dependent variable, the 98th percentile of the accessible storage over the study period at each grid was calculated as the maximum storage for the soil layer that vegetation growth responds to most strongly. The number of months for which lagged $\rho > 0.6$ was used as an indicator of skilful forecast lead time. The specific value of threshold used was based on maximising skilful forecasts. Nevertheless, the area of skilful forecasts remains stable with changes in threshold values. Alternative predictors tested included an antecedent precipitation index with a constant decay coefficient of 0.9 (Hooke, 1979), the satellite-derived SMOS soil moisture, GRACE total column storage estimates and the water storage estimates from model open-loop run without any data assimilation.

A deterministic forecast of the vegetation greenness anomaly $dV(t)$ in t month's time was obtained from a linear combination of the 'current' greenness anomaly $dV(t = 0)$ and the anomaly in water storage over the determined optimal integration depth z, denoted by $S(z, t = 0)$ as follows:

$$dV(t) = dV(t_0) + \beta_1 S(z_0, t_0) + \beta_2 \tag{5.1}$$

where β_1, β_2 are regression coefficients. Comparison was made with persistence forecasts and climatology forecasts. The persistence forecast simply assumes the next month having the same anomaly as current month,

$dV(t) = dV(t_0)$. Climatology forecasts use the average of previous available observations for month (t) as the forecasts. The study period was limited to 6 years by the available observations and forcing data, starting from the launch of SMOS in 2010 to the end of the forcing data archives at the end of 2015. Independent hindcast evaluation was achieved by splitting the time series into three equal segments; the performance for each time segment was calculated using a forecast model derived from data for the other two time segments. The averaged seasonal cycle excluding the evaluation period was added to the predicted greeness anomalies to obtain absolute greenness. The skill of water storage-derived forecasts was evaluated against the best performance from two NDVI-based forecasts at each pixel.

Chapter 6

Summary and outlook

This research investigated the potential of assimilating satellite water content retrievals to improve the estimation of water availability and vegetation response. It was motivated by the desire to improve drought impacts forecasting for more efficient agriculture planning and reduced economical and environmental damage. For the first time, total water storage change observed from space gravity mission and near-surface soil moisture retrievals from microwave sensor were assimilated jointly into an ecohydrological model. Our efforts of developing the global joint assimilation framework led to significant improvement in the estimation of root-zone soil water and groundwater storage, which cannot be directly observed from space. For example, unmonitored water extraction by human activity such as groundwater withdrawals and irrigation would be detected with our joint assimilation. Accurate estimation of water availability can strengthen the forecasting skill on anticipating vegetation conditions. This chapter presents a summary of the benefits, limitation and further research directions of this study.

6.1 Conclusions

6.1.1 Satellite data assimilation

Data assimilation is a powerful technique to combine model simulations and observations with the consideration of individual uncertainties. The increasing number and accuracy of space-borne sensors provide an unique opportunity to support and improve land surface modeling. Our study on the joint assimilation of satellite water content retrievals with different spatio-temporal scales and different data types contributes to building up the multi-variable and multi-scale data assimilation techniques for terrestrial systems.

In chapter 3, we demonstrated that the ensemble Kalman smoother is a more efficient approach to deal with the assimilation of observational data with different temporal scale than an ensemble Kalman filter. The consideration of temporal correlation ensures accurate separation of water storage with different magnitudes of temporal dynamics. For example, surface soil moisture gains more corrections in daily variations from SMOS observation, while groundwater gains more correction on seasonal variations from GRACE observations. The joint assimilation largely mitigates the drawbacks of single-variable assimilation on erroneous redistribution of water storage. The integration of SMOS data not only helps to better disaggregate the soil water storage from GRACE TWS data, but also helps to improve the spatial resolution.

Having constraints on both total water storage and near-surface soil moisture ensures more accurate estimates of individual water storage compartments. In particular, the joint assimilation of GRACE and SMOS can help in the detection of water loss by human activities, such as groundwater extraction and irrigation. Accurate estimates of surface soil moisture can also mitigate uncertainties in the precipitation forcing, in turn affecting the water and energy balance. The improved estimation of individual water storage offers potential for drought and groundwater monitoring, as well as water cycle reanalysis applications.

6.1.2 Improved estimation of soil water availability

We evaluated the soil moisture estimation for three different layers from different assimilation experiments with in-situ measurements over Australia in Chapter 3. The assimilation of SMOS soil moisture retrievals alone enables more accurate shallow root-zone soil moisture estimation, but barely impacts on deeper soil moisture estimation. The main benefit of the joint assimilation is on improving deep root-zone soil moisture estimation which cannot be directly measured at large scale by either in-situ instruments or satellites.

In Chapter 4, we found that joint assimilation successfully improved root-zone soil moisture estimations globally, in agreement with in-situ measurements, which in turns, improved the estimation of vegetation response to soil water availability. The joint assimilation detected more severe deficit in plant available soil water in eastern Australia and eastern Brazil from 2010 to 2016 than inferred from model open-loop simulations, consistent with the reduced vegetation greenness observed by the MODIS instruments. Vegetation responds differently to soil water availability at different depths because of variable vegetation properties, climate regions and soil properties. Given accurate knowledge of root-zone soil moisture variation, the vegetation greenness and productivity can be better predicted. Our efforts to improve global root-zone soil moisture estimation help to address the lack of studies on quantifying the vegetation response to water availability at large scale. Overall, joint assimilation provided new insights for monitoring and forecasting plant water stress and vegetation vigor.

6.1.3 Advancing drought impacts

We used the global joint assimilation results to infer an apparent vegetation-accessible water storage in Chapter 5 to forecast vegetation conditions. The accessible storage integrated the effect of vertical root distribution, soil properties, aridity and vegetation type. We found that skillful forecasts of vegetation

conditions can be achieved several months in advance for most of the world's drylands. Improved forecasting skill was achieved with the use of water availability information when compared to climatology or persistence forecasts. Our study demonstrates that joint assimilation not only provides an effective tool for monitoring and forecasting global water and vegetation dynamics, but also provides new insights into dryland ecology and drought impact forecasting. Skillful forecasts of drought impacts on vegetation can inform effective action through agricultural planning, drought relief, water management and fire preparedness.

6.2 Limitation and future work

Since the model used in this study is a one-dimensional catchment model without considering lateral water distribution, the assimilation does not include spatial correlation between grid cells. Although surface water routing is not included, the assimilation of coarse-scale GRACE data can mitigate the missing recharge or extraction to large extent. Consideration of spatial correlation may further improve the water balance estimation through lateral redistribution of water storage and worth further investigation.

The study period of the joint assimilation was necessarily limited to 7 years period from 2010 to 2016, due to the availability of reanalysis meteorological forcing dataset and satellite observations. Extension of this period is preferable for a better understanding of the impacts of water stress on ecosystem. The success launch of the GRACE-FO mission provides an opportunity to develop an operational the near-real time data assimilation system together with the continuing SMAP and SMOS missions. Global 10km resolution rainfall observations from GPM also provide new opportunities to improve the spatial resolution of model-data assimilation outputs. Our findings from the joint assimilation of satellite observations with different types and different scales also indicate the potential of using more available observational data

to constrain the land surface model. High-resolution, near-real time global vegetation conditions forecasting is of great potential value in drought early warning and water resource management, especially for less developed countries with inadequate monitoring infrastructure.

Bibliography

Adegoke, J. O. and Carleton, A. M. Relations between soil moisture and satellite vegetation indices in the us corn belt. *Journal of Hydrometeorology*, 3(4):395–405, 2002.

Allen, J., Eknes, M., and Evensen, G. An ensemble kalman filter with a complex marine ecosystem model: hindcasting phytoplankton in the cretan sea. In *Annales Geophysicae*, volume 21, pages 399–411, 2003.

Andela, N., Liu, Y., Van Dijk, A., De Jeu, R., and McVicar, T. Global changes in dryland vegetation dynamics (1988-2008) assessed by satellite remote sensing: comparing a new passive microwave vegetation density record with reflective greenness data. *Biogeosciences*, 10(10), 2013.

Anderson, J. L. and Anderson, S. L. A monte carlo implementation of the nonlinear filtering problem to produce ensemble assimilations and forecasts. *Monthly Weather Review*, 127(12):2741–2758, 1999.

Andreadis, K. M. and Lettenmaier, D. P. Assimilating remotely sensed snow observations into a macroscale hydrology model. *Advances in water resources*, 29(6):872–886, 2006.

Anyamba, A. and Tucker, C. J. Analysis of sahelian vegetation dynamics using noaa-avhrr ndvi data from 1981–2003. *Journal of Arid Environments*, 63(3): 596–614, 2005.

Badeck, F.-W., Bondeau, A., Böttcher, K., Doktor, D., Lucht, W., Schaber, J., and Sitch, S. Responses of spring phenology to climate change. *New Phytologist*, 162(2):295–309, 2004.

Bauer, P., Thorpe, A., and Brunet, G. The quiet revolution of numerical weather prediction. *Nature*, 525(7567):47, 2015.

Beck, H. E., van Dijk, A. I., Levizzani, V., Schellekens, J., Miralles, D. G., Martens, B., and de Roo, A. Mswep: 3-hourly 0.25 global gridded precipitation (1979-2015) by merging gauge, satellite, and reanalysis data. *Hydrology and Earth System Sciences*, 21(1):589, 2017.

Bergström, S., Singh, V., et al. The hbv model. *Computer models of watershed hydrology.*, pages 443–476, 1995.

Bolten, J. and Crow, W. Improved prediction of quasi-global vegetation conditions using remotely-sensed surface soil moisture. *Geophysical Research Letters*, 39(19), 2012.

Breshears, D. D., Cobb, N. S., Rich, P. M., Price, K. P., Allen, C. D., Balice, R. G., Romme, W. H., Kastens, J. H., Floyd, M. L., Belnap, J., et al. Regional vegetation die-off in response to global-change-type drought. *Proceedings of the National Academy of Sciences*, 102(42):15144–15148, 2005.

Brocca, L., Melone, F., Moramarco, T., Wagner, W., Naeimi, V., Bartalis, Z., and Hasenauer, S. Improving runoff prediction through the assimilation of the ascat soil moisture product. *Hydrology and Earth System Sciences*, 14 (10):1881–1893, 2010.

Bruinsma, S., Lemoine, J.-M., Biancale, R., and Valès, N. Cnes/grgs 10-day gravity field models (release 2) and their evaluation. *Advances in Space Research*, 45(4):587–601, 2010. ISSN 02731177. doi: 10.1016/j.asr.2009.10.012.

Brutsaert, W. On a derivable formula for long-wave radiation from clear skies. *Water Resources Research*, 11(5):742–744, 1975.

Bryan, B. A., Crossman, N. D., Nolan, M., Li, J., Navarro, J., and Connor, J. D. Land use efficiency: anticipating future demand for land-sector greenhouse gas emissions abatement and managing trade-offs with agriculture, water, and biodiversity. *Global change biology*, 21(11):4098–4114, 2015.

Canadell, J., Jackson, R., Ehleringer, J., Mooney, H., Sala, O., and Schulze, E.-D. Maximum rooting depth of vegetation types at the global scale. *Oecologia*, 108(4):583–595, 1996.

Cassel, D. and Nielsen, D. Field capacity and available water capacity. *Methods of Soil Analysis: Part 1—Physical and Mineralogical Methods*, (methodsofsoilan1):901–926, 1986.

Chakrabarti, S., Bongiovanni, T., Judge, J., Zotarelli, L., and Bayer, C. Assimilation of smos soil moisture for quantifying drought impacts on crop yield in agricultural regions. *Selected Topics in Applied Earth Observations and Remote Sensing, IEEE Journal of*, 7(9):3867–3879, 2014.

Channan, S., Collins, K., and Emanuel, W. Global mosaics of the standard modis land cover type data. *University of Maryland and the Pacific Northwest National Laboratory, College Park, Maryland, USA*, 30, 2014.

Chanzy, A., Schmugge, T., Calvet, J.-C., Kerr, Y., Van Oevelen, P., Grosjean, O., and Wang, J. Airborne microwave radiometry on a semi-arid area during hapex-sahel. *Journal of Hydrology*, 188:285–309, 1997.

Chen, J. L., Wilson, C. R., Tapley, B. D., Yang, Z. L., and Niu, G. Y. 2005 drought event in the amazon river basin as measured by grace and estimated by climate models. *Journal of Geophysical Research*, 114(B5), 2009. ISSN 0148-0227. doi: 10.1029/2008jb006056.

Chen, T., De Jeu, R., Liu, Y., Van der Werf, G., and Dolman, A. Using satellite based soil moisture to quantify the water driven variability in ndvi: A case study over mainland australia. *Remote Sensing of Environment*, 140: 330–338, 2014.

Clark, M. P., Rupp, D. E., Woods, R. A., Zheng, X., Ibbitt, R. P., Slater, A. G., Schmidt, J., and Uddstrom, M. J. Hydrological data assimilation with the ensemble kalman filter: Use of streamflow observations to update states in a distributed hydrological model. *Advances in water resources*, 31 (10):1309–1324, 2008.

Cohn, S. E., Sivakumaran, N., and Todling, R. A fixed-lag kalman smoother for retrospective data assimilation. *Monthly Weather Review*, 122(12):2838–2867, 1994.

Crausbay, S. D., Ramirez, A. R., Carter, S. L., Cross, M. S., Hall, K. R., Bathke, D. J., Betancourt, J. L., Colt, S., Cravens, A. E., Dalton, M. S., et al. Defining ecological drought for the twenty-first century. *Bulletin of the American Meteorological Society*, 98(12):2543–2550, 2017.

Crow, W. T. and Wood, E. F. The assimilation of remotely sensed soil brightness temperature imagery into a land surface model using ensemble kalman filtering: A case study based on estar measurements during sgp97. *Advances in Water Resources*, 26(2):137–149, 2003.

Crow, W. T., Kustas, W. P., and Prueger, J. H. Monitoring root-zone soil moisture through the assimilation of a thermal remote sensing-based soil moisture proxy into a water balance model. *Remote Sensing of Environment*, 112(4):1268–1281, 2008.

Dai, A. Increasing drought under global warming in observations and models. *Nature Climate Change*, 3(1):52, 2013.

De Groeve, T. Flood monitoring and mapping using passive microwave remote sensing in namibia. *Geomatics, Natural Hazards and Risk*, 1(1):19–35, 2010.

de Jeu, R. A. Retrieval of land surface parameters using passive microwave remote sensing. 2003.

Dee, D. P. Bias and data assimilation. *Quarterly Journal of the Royal Meteorological Society*, 131(613):3323–3343, 2005.

Dente, L., Su, Z., and Wen, J. Validation of smos soil moisture products over the maqu and twente regions. *Sensors*, 12(8):9965–9986, 2012.

Desilets, D. and Zreda, M. Footprint diameter for a cosmic-ray soil moisture probe: Theory and monte carlo simulations. *Water Resources Research*, 49 (6):3566–3575, 2013.

Didan, K. Mod13c2 modis/terra vegetation indices monthly l3 global 0.05 deg cmg v006, nasa eosdis land processes daac, 2015.

D'Odorico, P., Caylor, K., Okin, G. S., and Scanlon, T. M. On soil moisture–vegetation feedbacks and their possible effects on the dynamics of dryland ecosystems. *Journal of Geophysical Research: Biogeosciences*, 112(G4), 2007.

Dorigo, W., Wagner, W., Hohensinn, R., Hahn, S., Paulik, C., Xaver, A., Gruber, A., Drusch, M., Mecklenburg, S., Oevelen, P. v., et al. The international soil moisture network: a data hosting facility for global in situ soil moisture measurements. *Hydrology and Earth System Sciences*, 15(5): 1675–1698, 2011.

Draper, C., Mahfouf, J.-F., Calvet, J.-C., Martin, E., and Wagner, W. Assimilation of ascat near-surface soil moisture into the sim hydrological model over france. *Hydrology and Earth System Sciences*, 15(12):3829–3841, 2011.

Draper, C. S., Walker, J. P., Steinle, P. J., de Jeu, R. A., and Holmes, T. R. An evaluation of amsr–e derived soil moisture over australia. *Remote Sensing of Environment*, 113(4):703–710, 2009.

Draper, C., Reichle, R., De Lannoy, G., and Liu, Q. Assimilation of passive and active microwave soil moisture retrievals. *Geophysical Research Letters*, 39(4), 2012.

Dumedah, G., Walker, J. P., and Merlin, O. Root-zone soil moisture estimation from assimilation of downscaled soil moisture and ocean salinity data. *Advances in Water Resources*, 84:14–22, 2015.

Dunne, K. and Willmott, C. J. Global distribution of plant-extractable water capacity of soil. *International Journal of Climatology: A Journal of the Royal Meteorological Society*, 16(8):841–859, 1996.

Dunne, S. and Entekhabi, D. Land surface state and flux estimation using the ensemble kalman smoother during the southern great plains 1997 field experiment. *Water resources research*, 42(1), 2006.

Dunne, S. C., Entekhabi, D., and Njoku, E. G. Impact of multiresolution active and passive microwave measurements on soil moisture estimation using the ensemble kalman smoother. *IEEE Transactions on Geoscience and Remote Sensing*, 45(4):1016–1028, 2007.

Eicker, A., Schumacher, M., Kusche, J., Döll, P., and Schmied, H. M. Calibration/data assimilation approach for integrating grace data into the watergap global hydrology model (wghm) using an ensemble kalman filter: First results. *Surveys in Geophysics*, 35(6):1285–1309, 2014. ISSN 0169-3298 1573-0956. doi: 10.1007/s10712-014-9309-8.

Evensen, G. The ensemble kalman filter: theoretical formulation and practical implementation. *Ocean Dynamics*, 53(4):343–367, 2003. ISSN 1616-7341 1616-7228. doi: 10.1007/s10236-003-0036-9.

Evensen, G. Sequential data assimilation with a nonlinear quasi-geostrophic model using monte carlo methods to forecast error statistics. *Journal of Geophysical Research: Oceans*, 99(C5):10143–10162, 1994.

Evensen, G. and Van Leeuwen, P. J. An ensemble kalman smoother for nonlinear dynamics. *Monthly Weather Review*, 128(6):1852–1867, 2000.

Famiglietti, J. S. Remote sensing of terrestrial water storage, soil moisture and surface waters. *The state of the planet: frontiers and challenges in geophysics*, pages 197–207, 2004.

Fan, Y., Miguez-Macho, G., Jobbágy, E. G., Jackson, R. B., and Otero-Casal, C. Hydrologic regulation of plant rooting depth. *Proceedings of the National Academy of Sciences*, page 201712381, 2017.

Forman, B. A., Reichle, R., and Rodell, M. Assimilation of terrestrial water storage from grace in a snow-dominated basin. *Water Resources Research*, 48(1), 2012.

Franz, T. E., Zreda, M., Ferre, T., Rosolem, R., Zweck, C., Stillman, S., Zeng, X., and Shuttleworth, W. Measurement depth of the cosmic ray soil moisture probe affected by hydrogen from various sources. *Water Resources Research*, 48(8), 2012.

Frost, A., Ramchurn, A., and Smith, A. The bureau's operational awra landscape (awra-l) model. *Melbourne, Bureau of Meteorology*, 47, 2016.

Gibbs, W. J. Rainfall deciles as drought indicators. 1967.

Girotto, M., De Lannoy, G. J., Reichle, R. H., Rodell, M., Draper, C., Bhanja, S. N., and Mukherjee, A. Benefits and pitfalls of grace data assimilation: A case study of terrestrial water storage depletion in india. *Geophysical Research Letters*, 44(9):4107–4115, 2017.

Gruhier, C., Rosnay, P. d., Hasenauer, S., Holmes, T., Jeu, R. d., Kerr, Y., Mougin, E., Njoku, E., Timouk, F., Wagner, W., et al. Soil moisture active and passive microwave products: intercomparison and evaluation over a sahelian site. *Hydrology and Earth System Sciences*, 14(1):141–156, 2010.

Gu, Y., Brown, J. F., Verdin, J. P., and Wardlow, B. A five-year analysis of modis ndvi and ndwi for grassland drought assessment over the central great plains of the united states. *Geophysical Research Letters*, 34(6), 2007.

Gu, Y., Hunt, E., Wardlow, B., Basara, J. B., Brown, J. F., and Verdin, J. P. Evaluation of modis ndvi and ndwi for vegetation drought monitoring using oklahoma mesonet soil moisture data. *Geophysical Research Letters*, 35(22), 2008.

Guerschman, J. P., Warren, G., Byrne, G., Lymburner, L., Mueller, N., and Van-Dijk, A. Modis-based standing water detection for flood and large reservoir mapping: algorithm development and applications for the australian continent. *Water for a Healthy Country National Research Flagship Report, Canberra*, 2011.

Hansen, M., DeFries, R., Townshend, J., Carroll, M., Dimiceli, C., and Sohlberg, R. Global percent tree cover at a spatial resolution of 500 meters: First results of the modis vegetation continuous fields algorithm. *Earth Interactions*, 7(10):1–15, 2003.

Hawdon, A., McJannet, D., and Wallace, J. Calibration and correction procedures for cosmic-ray neutron soil moisture probes located across australia. *Water Resources Research*, 50(6):5029–5043, 2014.

Holgate, C., De Jeu, R., van Dijk, A., Liu, Y., Renzullo, L., Dharssi, I., Parinussa, R., Van Der Schalie, R., Gevaert, A., Walker, J., et al. Comparison of remotely sensed and modelled soil moisture data sets across australia. *Remote Sensing of Environment*, 186:479–500, 2016.

Hooke, J. M. An analysis of the processes of river bank erosion. *Journal of Hydrology*, 42(1-2):39–62, 1979.

Hou, A. Y., Kakar, R. K., Neeck, S., Azarbarzin, A. A., Kummerow, C. D., Kojima, M., Oki, R., Nakamura, K., and Iguchi, T. The global precipitation measurement mission. *Bulletin of the American Meteorological Society*, 95 (5):701–722, 2014.

Houborg, R., Rodell, M., Li, B., Reichle, R., and Zaitchik, B. F. Drought indicators based on model-assimilated gravity recovery and climate experiment (grace) terrestrial water storage observations. *Water Resources Research*, 48 (7), 2012.

Houser, P. R., Shuttleworth, W. J., Famiglietti, J. S., Gupta, H. V., Syed, K. H., and Goodrich, D. C. Integration of soil moisture remote sensing and hydrologic modeling using data assimilation. *Water Resources Research*, 34 (12):3405–3420, 1998.

Houtekamer, P. L. and Mitchell, H. L. Ensemble kalman filtering. *Quarterly Journal of the Royal Meteorological Society*, 131(613):3269–3289, 2005.

Hu, X., Chen, J., Zhou, Y., Huang, C., and Liao, X. Seasonal water storage change of the yangtze river basin detected by grace. *Science in China Series D*, 49(5):483–491, 2006. ISSN 1006-9313 1862-2801. doi: 10.1007/s11430-006-0483-5.

Huete, A., Didan, K., Miura, T., Rodriguez, E. P., Gao, X., and Ferreira, L. G. Overview of the radiometric and biophysical performance of the modis vegetation indices. *Remote sensing of environment*, 83(1-2):195–213, 2002.

Huete, A. R. A soil-adjusted vegetation index (savi). *Remote sensing of environment*, 25(3):295–309, 1988.

Huffman, G. J., Bolvin, D. T., Nelkin, E. J., Wolff, D. B., Adler, R. F., Gu, G., Hong, Y., Bowman, K. P., and Stocker, E. F. The trmm multisatellite precipitation analysis (tmpa): Quasi-global, multiyear, combined-sensor precipitation estimates at fine scales. *Journal of Hydrometeorology*, 8(1): 38–55, 2007.

Ichii, K., Kawabata, A., and Yamaguchi, Y. Global correlation analysis for ndvi and climatic variables and ndvi trends: 1982-1990. *International journal of remote sensing*, 23(18):3873–3878, 2002.

Jackson, R., Canadell, J., Ehleringer, J. R., Mooney, H., Sala, O., and Schulze, E. A global analysis of root distributions for terrestrial biomes. *Oecologia*, 108(3):389–411, 1996.

Jackson, T. J., Bindlish, R., Cosh, M. H., Zhao, T., Starks, P. J., Bosch, D. D., Seyfried, M., Moran, M. S., Goodrich, D. C., Kerr, Y. H., et al. Validation of soil moisture and ocean salinity (smos) soil moisture over watershed networks in the us. *IEEE Transactions on Geoscience and Remote Sensing*, 50(5): 1530–1543, 2012.

Jacquette, E., Al Bitar, A., Mialon, A., Kerr, Y., Quesney, A., Cabot, F., and Richaume, P. Smos catds level 3 global products over land. In *Remote Sensing*, pages 78240K–78240K. International Society for Optics and Photonics, 2010.

Ji, L. and Peters, A. J. Assessing vegetation response to drought in the northern great plains using vegetation and drought indices. *Remote Sensing of Environment*, 87(1):85–98, 2003.

Jiang, D., Wang, J., Huang, Y., Zhou, K., Ding, X., and Fu, J. The review of grace data applications in terrestrial hydrology monitoring. *Advances in Meteorology*, 2014:1–9, 2014. ISSN 1687-9309 1687-9317. doi: 10.1155/2014/725131.

Jiang, X., Rauscher, S. A., Ringler, T. D., Lawrence, D. M., Williams, A. P., Allen, C. D., Steiner, A. L., Cai, D. M., and McDowell, N. G. Projected

future changes in vegetation in western north america in the twenty-first century. *Journal of Climate*, 26(11):3671–3687, 2013.

Joyce, R. J., Janowiak, J. E., Arkin, P. A., and Xie, P. Cmorph: A method that produces global precipitation estimates from passive microwave and infrared data at high spatial and temporal resolution. *Journal of Hydrometeorology*, 5(3):487–503, 2004.

Kerr, Y., Jacquette, E., Al Bitar, A., Cabot, F., Mialon, A., Richaume, P., Quesney, A., Berthon, L., and Wigneron, J. Catds smos l3 soil moisture retrieval processor: Algorithm theoretical baseline document (atbd). *CESBIO: Toulouse, France*, 2013.

Kerr, Y. H., Waldteufel, P., Wigneron, J.-P., Martinuzzi, J.-M., Font, J., and Berger, M. Soil moisture retrieval from space: The soil moisture and ocean salinity (smos) mission. *Geoscience and Remote Sensing, IEEE Transactions on*, 39(8):1729–1735, 2001.

Kerr, Y. H., Waldteufel, P., Wigneron, J.-P., Delwart, S., Cabot, F., Boutin, J., Escorihuela, M.-J., Font, J., Reul, N., Gruhier, C., et al. The smos mission: New tool for monitoring key elements ofthe global water cycle. *Proceedings of the IEEE*, 98(5):666–687, 2010.

Kerr, Y. H., Waldteufel, P., Richaume, P., Wigneron, J. P., Ferrazzoli, P., Mahmoodi, A., Al Bitar, A., Cabot, F., Gruhier, C., Juglea, S. E., et al. The smos soil moisture retrieval algorithm. *Geoscience and Remote Sensing, IEEE Transactions on*, 50(5):1384–1403, 2012.

Kerr, Y., Vergely, J., Waldteufel, P., Richaume, P., Anterrieu, E., and Moreno, R. Catds smos l3 processor: Algorithm theoretical baseline document for the soil moisture retrieval (atbd). *CNES-CESBIO, Toulouse, France, CATDS-ATBD-SM-L3, V1*, 1, 2008.

Keyantash, J. and Dracup, J. A. The quantification of drought: an evaluation of drought indices. *Bulletin of the American Meteorological Society*, 83(8): 1167–1180, 2002.

Khaki, M., Ait-El-Fquih, B., Hoteit, I., Forootan, E., Awange, J., and Kuhn, M. A two-update ensemble kalman filter for land hydrological data assimilation with an uncertain constraint. *Journal of Hydrology*, 555:447–462, 2017.

Kleidon, A. Global datasets of rooting zone depth inferred from inverse methods. *Journal of Climate*, 17(13):2714–2722, 2004.

Kogan, F. Application of vegetation index and brightness temperature for drought detection. *Advances in space research*, 15(11):91–100, 1995.

Koster, R. D., Guo, Z., Yang, R., Dirmeyer, P. A., Mitchell, K., and Puma, M. J. On the nature of soil moisture in land surface models. *Journal of Climate*, 22(16):4322–4335, 2009.

Koster, R. D., Mahanama, S. P., Livneh, B., Lettenmaier, D. P., and Reichle, R. H. Skill in streamflow forecasts derived from large-scale estimates of soil moisture and snow. *Nature Geoscience*, 3(9):613, 2010.

Kurtenbach, E., Mayer-Gürr, T., and Eicker, A. Deriving daily snapshots of the earth's gravity field from grace l1b data using kalman filtering. *Geophysical Research Letters*, 36(17), 2009.

Laio, F., Porporato, A., Ridolfi, L., and Rodriguez-Iturbe, I. Plants in water-controlled ecosystems: active role in hydrologic processes and response to water stress: Ii. probabilistic soil moisture dynamics. *Advances in Water Resources*, 24(7):707–723, 2001.

Landerer, F. and Swenson, S. Accuracy of scaled grace terrestrial water storage estimates. *Water Resources Research*, 48(4), 2012. ISSN 1944-7973.

Leblanc, M. J., Tregoning, P., Ramillien, G., Tweed, S. O., and Fakes, A. Basin-scale, integrated observations of the early 21st century multiyear drought in southeast australia. *Water resources research*, 45(4), 2009.

Leenaars, J. G., Claessens, L., Heuvelink, G. B., Hengl, T., González, M. R., van Bussel, L. G., Guilpart, N., Yang, H., and Cassman, K. G. Mapping rootable depth and root zone plant-available water holding capacity of the soil of sub-saharan africa. *Geoderma*, 324:18–36, 2018.

Leroux, D. J., Kerr, Y. H., Richaume, P., and Fieuzal, R. Spatial distribution and possible sources of smos errors at the global scale. *Remote Sensing of Environment*, 133:240–250, 2013.

Leroux, D. J., Kerr, Y. H., Al Bitar, A., Bindlish, R., Jackson, T. J., Berthelot, B., and Portet, G. Comparison between smos, vua, ascat, and ecmwf soil moisture products over four watersheds in us. *IEEE Transactions on Geoscience and Remote Sensing*, 52(3):1562–1571, 2014.

Li, B., Rodell, M., Zaitchik, B. F., Reichle, R. H., Koster, R. D., and van Dam, T. M. Assimilation of grace terrestrial water storage into a land surface model: Evaluation and potential value for drought monitoring in western and central europe. *Journal of Hydrology*, 446:103–115, 2012. ISSN 0022-1694.

Li, Y., Ryu, D., Western, A. W., and Wang, Q. J. Assimilation of stream discharge for flood forecasting: The benefits of accounting for routing time lags. *Water Resources Research*, 49(4):1887–1900, 2013. ISSN 00431397. doi: 10.1002/wrcr.20169.

Lievens, H., Tomer, S. K., Al Bitar, A., De Lannoy, G., Drusch, M., Dumedah, G., Franssen, H.-J. H., Kerr, Y., Martens, B., Pan, M., et al. Smos soil moisture assimilation for improved hydrologic simulation in the murray darling basin, australia. *Remote Sensing of Environment*, 168:146–162, 2015.

Lievens, H., Reichle, R. H., Liu, Q., De Lannoy, G., Dunbar, R. S., Kim, S., Das, N. N., Cosh, M., Walker, J. P., and Wagner, W. Joint sentinel-1 and smap data assimilation to improve soil moisture estimates. *Geophysical Research Letters*, 2017.

Liu, Q., Reichle, R. H., Bindlish, R., Cosh, M. H., Crow, W. T., de Jeu, R., De Lannoy, G. J. M., Huffman, G. J., and Jackson, T. J. The contributions of precipitation and soil moisture observations to the skill of soil moisture estimates in a land data assimilation system. *Journal of Hydrometeorology*, 12(5):750–765, 2011. ISSN 1525-755X 1525-7541. doi: 10.1175/jhm-d-10-05000.1.

Liu, W. and Kogan, F. Monitoring regional drought using the vegetation condition index. *International Journal of Remote Sensing*, 17(14):2761–2782, 1996.

Liu, Y., Weerts, A. H., Clark, M., Hendricks Franssen, H. J., Kumar, S., Moradkhani, H., Seo, D. J., Schwanenberg, D., Smith, P., van Dijk, A. I. J. M., van Velzen, N., He, M., Lee, H., Noh, S. J., Rakovec, O., and Restrepo, P. Advancing data assimilation in operational hydrologic forecasting: progresses, challenges, and emerging opportunities. *Hydrology and Earth System Sciences*, 16(10):3863–3887, 2012a. ISSN 1607-7938. doi: 10.5194/hess-16-3863-2012.

Liu, Y. Y., Dorigo, W. A., Parinussa, R., de Jeu, R. A., Wagner, W., McCabe, M. F., Evans, J., and Van Dijk, A. Trend-preserving blending of passive and active microwave soil moisture retrievals. *Remote Sensing of Environment*, 123:280–297, 2012b.

Long, D., Chen, X., Scanlon, B. R., Wada, Y., Hong, Y., Singh, V. P., Chen, Y., Wang, C., Han, Z., and Yang, W. Have grace satellites overestimated groundwater depletion in the northwest india aquifer? *Scientific reports*, 6, 2016.

Martens, B., Miralles, D., Lievens, H., Fernández-Prieto, D., and Verhoest, N. Improving terrestrial evaporation estimates over continental australia through assimilation of smos soil moisture. *International Journal of Applied Earth Observation and Geoinformation*, 2015.

McKee, T. B., Doesken, N. J., Kleist, J., et al. The relationship of drought frequency and duration to time scales. In *Proceedings of the 8th Conference on Applied Climatology*, volume 17, pages 179–183. American Meteorological Society Boston, MA, 1993.

Monteith, J. Evaporation and surface temperature. *Quarterly Journal of the Royal Meteorological Society*, 107(451):1–27, 1981.

Moody, E. G., King, M. D., Platnick, S., Schaaf, C. B., and Gao, F. Spatially complete global spectral surface albedos: Value-added datasets derived from terra modis land products. *Geoscience and Remote Sensing, IEEE Transactions on*, 43(1):144–158, 2005.

Narasimhan, B. and Srinivasan, R. Development and evaluation of soil moisture deficit index (smdi) and evapotranspiration deficit index (etdi) for agricultural drought monitoring. *Agricultural and Forest Meteorology*, 133(1-4): 69–88, 2005.

Narayan, U., Lakshmi, V., and Njoku, E. G. Retrieval of soil moisture from passive and active l/s band sensor (pals) observations during the soil moisture experiment in 2002 (smex02). *Remote Sensing of Environment*, 92(4): 483–496, 2004.

Nemani, R. R., Keeling, C. D., Hashimoto, H., Jolly, W. M., Piper, S. C., Tucker, C. J., Myneni, R. B., and Running, S. W. Climate-driven increases in global terrestrial net primary production from 1982 to 1999. *science*, 300 (5625):1560–1563, 2003.

Ni, F., Cavazos, T., Hughes, M. K., Comrie, A. C., and Funkhouser, G. Cool-season precipitation in the southwestern usa since ad 1000: comparison of linear and nonlinear techniques for reconstruction. *International Journal of Climatology: A Journal of the Royal Meteorological Society*, 22(13):1645–1662, 2002.

Oliva, R., Daganzo, E., Kerr, Y. H., Mecklenburg, S., Nieto, S., Richaume, P., and Gruhier, C. Smos radio frequency interference scenario: Status and actions taken to improve the rfi environment in the 1400–1427-mhz passive band. *IEEE Transactions on Geoscience and Remote Sensing*, 50(5):1427–1439, 2012.

Palmer, W. C. Keeping track of crop moisture conditions, nationwide: The new crop moisture index. 1968.

Peña-Arancibia, J., Van Dijk, A., Mulligan, M., and Bruijnzeel, L. A. The role of climatic and terrain attributes in estimating baseflow recession in tropical catchments. *Hydrology and Earth System Sciences*, 14(11):2193–2205, 2010.

Pettorelli, N., Vik, J. O., Mysterud, A., Gaillard, J.-M., Tucker, C. J., and Stenseth, N. C. Using the satellite-derived ndvi to assess ecological responses to environmental change. *Trends in ecology & evolution*, 20(9):503–510, 2005.

Pinori, S., Crapolicchio, R., and Mecklenburg, S. Preparing the esa-smos (soil moisture and ocean salinity) mission-overview of the user data products and data distribution strategy. In *Microwave Radiometry and Remote Sensing of the Environment, 2008. MICRORAD 2008*, pages 1–4. IEEE, 2008.

Porporato, A., Daly, E., and Rodriguez-Iturbe, I. Soil water balance and ecosystem response to climate change. *The American Naturalist*, 164(5): 625–632, 2004.

Pozzi, W., Sheffield, J., Stefanski, R., Cripe, D., Pulwarty, R., Vogt, J. V., Heim Jr, R. R., Brewer, M. J., Svoboda, M., Westerhoff, R., et al. Toward global drought early warning capability: Expanding international cooperation for the development of a framework for monitoring and forecasting. *Bulletin of the American Meteorological Society*, 94(6):776–785, 2013.

Ramillien, G., Famiglietti, J. S., and Wahr, J. Detection of continental hydrology and glaciology signals from grace: A review. *Surveys in Geophysics*, 29(4-5):361–374, 2008. ISSN 0169-3298 1573-0956. doi: 10.1007/s10712-008-9048-9.

Reichle, R. H. and Koster, R. D. Bias reduction in short records of satellite soil moisture. *Geophysical Research Letters*, 31(19), 2004. ISSN 0094-8276. doi: 10.1029/2004gl020938.

Reichle, R. H. and Koster, R. D. Global assimilation of satellite surface soil moisture retrievals into the nasa catchment land surface model. *Geophysical Research Letters*, 32(2), 2005.

Reichle, R. H., McLaughlin, D. B., and Entekhabi, D. Hydrologic data assimilation with the ensemble kalman filter. *Monthly Weather Review*, 130(1): 103–114, 2002.

Renzullo, L. J., van Dijk, A. I. J. M., Perraud, J. M., Collins, D., Henderson, B., Jin, H., Smith, A. B., and McJannet, D. L. Continental satellite soil moisture data assimilation improves root-zone moisture analysis for water resources assessment. *Journal of Hydrology*, 519:2747–2762, 2014. ISSN 00221694. doi: 10.1016/j.jhydrol.2014.08.008.

Reyer, C. P., Leuzinger, S., Rammig, A., Wolf, A., Bartholomeus, R. P., Bonfante, A., De Lorenzi, F., Dury, M., Gloning, P., Jaoudé, R. A., et al. A plant's perspective of extremes: terrestrial plant responses to changing climatic variability. *Global change biology*, 19(1):75–89, 2013.

Reynolds, J. F., Smith, D. M. S., Lambin, E. F., Turner, B., Mortimore, M., Batterbury, S. P., Downing, T. E., Dowlatabadi, H., Fernández, R. J., Herrick, J. E., et al. Global desertification: building a science for dryland development. *science*, 316(5826):847–851, 2007.

Robinson, A. R. and Lermusiaux, P. F. Overview of data assimilation. *Harvard reports in physical/interdisciplinary ocean science*, 62:1–13, 2000.

Rodell, M. and Famiglietti, J. The potential for satellite-based monitoring of groundwater storage changes using grace: the high plains aquifer, central us. *Journal of Hydrology*, 263(1):245–256, 2002. ISSN 0022-1694. URL http://ac.els-cdn.com/S0022169402000604/1-s2.0-S0022169402000604-main.pdf?_tid=c8cd21cc-02c4-11e5-a2f0-00000aab0f02&acdnat=1432548171_4fac1c26b276d09c45e7fb4e5b3c94d9.

Rodell, M. and Houser, P. Updating a land surface model with modis-derived snow cover. *Journal of Hydrometeorology*, 5(6):1064–1075, 2004.

Rodell, M., Famiglietti, J., Wiese, D., Reager, J., Beaudoing, H., Landerer, F., and Lo, M.-H. Emerging trends in global freshwater availability. *Nature*, page 1, 2018.

Rodell, M., Velicogna, I., and Famiglietti, J. S. Satellite-based estimates of groundwater depletion in india. *Nature*, 460(7258):999, 2009.

Sabater, J. M., Jarlan, L., Calvet, J.-C., Bouyssel, F., and De Rosnay, P. From near-surface to root-zone soil moisture using different assimilation techniques. *Journal of Hydrometeorology*, 8(2):194–206, 2007.

Saji, N., Goswami, B., Vinayachandran, P., and Yamagata, T. A dipole mode in the tropical indian ocean. *Nature*, 401(6751):360, 1999.

Santos, W. J. R., Silva, B. M., Oliveira, G. C., Volpato, M. M. L., Lima, J. M., Curi, N., and Marques, J. J. Soil moisture in the root zone and its relation to plant vigor assessed by remote sensing at management scale. *Geoderma*, 221:91–95, 2014.

Schlaepfer, D. R., Bradford, J. B., Lauenroth, W. K., Munson, S. M., Tietjen, B., Hall, S. A., Wilson, S. D., Duniway, M. C., Jia, G., Pyke, D. A., et al. Climate change reduces extent of temperate drylands and intensifies drought in deep soils. *Nature communications*, 8:14196, 2017.

Schmugge, T. and Jackson, T. Mapping surface soil moisture with microwave radiometers. *Meteorology and Atmospheric Physics*, 54(1-4):213–223, 1994.

Schulze, E.-D., Mooney, H., Sala, O., Jobbagy, E., Buchmann, N., Bauer, G., Canadell, J., Jackson, R., Loreti, J., Oesterheld, M., et al. Rooting depth, water availability, and vegetation cover along an aridity gradient in patagonia. *Oecologia*, 108(3):503–511, 1996.

Schumacher, M., Forootan, E., van Dijk, A., Schmied, H. M., Crosbie, R., Kusche, J., and Döll, P. Improving drought simulations within the murray-darling basin by combined calibration/assimilation of grace data into the

watergap global hydrology model. *Remote Sensing of Environment*, 204: 212–228, 2018.

Schumacher, M., Kusche, J., and Döll, P. A systematic impact assessment of grace error correlation on data assimilation in hydrological models. *Journal of Geodesy*, pages 1–23, 2016.

Seneviratne, S. I., Corti, T., Davin, E. L., Hirschi, M., Jaeger, E. B., Lehner, I., Orlowsky, B., and Teuling, A. J. Investigating soil moisture–climate interactions in a changing climate: A review. *Earth-Science Reviews*, 99 (3-4):125–161, 2010.

Sheffield, J. and Wood, E. F. Global trends and variability in soil moisture and drought characteristics, 1950–2000, from observation-driven simulations of the terrestrial hydrologic cycle. *Journal of Climate*, 21(3):432–458, 2008a.

Sheffield, J. and Wood, E. F. Projected changes in drought occurrence under future global warming from multi-model, multi-scenario, ipcc ar4 simulations. *Climate dynamics*, 31(1):79–105, 2008b.

Sheffield, J., Goteti, G., Wen, F., and Wood, E. F. A simulated soil moisture based drought analysis for the united states. *Journal of Geophysical Research: Atmospheres*, 109(D24), 2004.

Shokri, A., Walker, J. P., van Dijk, A. I., and Pauwels, V. R. Performance of different ensemble kalman filter structures to assimilate grace terrestrial water storage estimates into a high-resolution hydrological model: A synthetic study. *Water Resources Research*, 54(11):8931–8951, 2018.

Singh, J., Milchunas, D., and Lauenroth, W. Soil water dynamics and vegetation patterns in a semiarid grassland. *Plant ecology*, 134(1):77–89, 1998.

Smith, A., Walker, J., Western, A., Young, R., Ellett, K., Pipunic, R., Grayson, R., Siriwardena, L., Chiew, F., and Richter, H. The murrumbidgee soil moisture monitoring network data set. *Water Resources Research*, 48(7), 2012.

Snyder, K. and Tartowski, S. Multi-scale temporal variation in water availability: implications for vegetation dynamics in arid and semi-arid ecosystems. *Journal of Arid Environments*, 65(2):219–234, 2006.

Sun, C., Walker, J. P., and Houser, P. R. A methodology for snow data assimilation in a land surface model. *Journal of Geophysical Research: Atmospheres*, 109(D8), 2004.

Swenson, S. and Wahr, J. Post-processing removal of correlated errors in grace data. *Geophysical Research Letters*, 33(8), 2006.

Syed, T. H., Famiglietti, J. S., Rodell, M., Chen, J., and Wilson, C. R. Analysis of terrestrial water storage changes from grace and gldas. *Water Resources Research*, 44(2), 2008.

Tangdamrongsub, N., Steele-Dunne, S. C., Gunter, B. C., Ditmar, P. G., and Weerts, A. H. Data assimilation of grace terrestrial water storage estimates into a regional hydrological model of the rhine river basin. *Hydrology and Earth System Sciences*, 19(4):2079–2100, 2015. ISSN 1607-7938. doi: 10.5194/hess-19-2079-2015.

Tangdamrongsub, N., Shin-Chan, H., Decker, M., Yeo, I.-Y., and Kim, H. On the use of the grace normal equation of inter-satellite tracking data for estimation of soil moisture and groundwater in australia. *Hydrology and Earth System Sciences*, 22(3):1811, 2018.

Tapley, B. D., Bettadpur, S., Watkins, M., and Reigber, C. The gravity recovery and climate experiment: Mission overview and early results. *Geophysical Research Letters*, 31(9), 2004.

Thomas, B. F., Famiglietti, J. S., Landerer, F. W., Wiese, D. N., Molotch, N. P., and Argus, D. F. Grace groundwater drought index: Evaluation of california central valley groundwater drought. *Remote Sensing of Environment*, 198:384–392, 2017.

Tian, S., Tregoning, P., Renzullo, L. J., van Dijk, A. I., Walker, J. P., Pauwels, V., and Allgeyer, S. Improved water balance component estimates through joint assimilation of grace water storage and smos soil moisture retrievals. *Water Resources Research*, 53(3):1820–1840, 2017.

Tian, S., Van Dijk, A. I., Tregoning, P., and Renzullo, L. J. Forecasting dryland vegetation condition months in advance through satellite data assimilation. *Nature communications*, 10(1):469, 2019.

Tokumoto, I., Heilman, J. L., Schwinning, S., McInnes, K. J., Litvak, M. E., Morgan, C. L., and Kamps, R. H. Small-scale variability in water storage and plant available water in shallow, rocky soils. *Plant and soil*, 385(1-2):193–204, 2014.

Trenberth, K. E., Dai, A., Van Der Schrier, G., Jones, P. D., Barichivich, J., Briffa, K. R., and Sheffield, J. Global warming and changes in drought. *Nature Climate Change*, 4(1):17, 2014.

Turner, M., Walker, J., and Oke, P. Ensemble member generation for sequential data assimilation. *Remote Sensing of Environment*, 112(4):1421–1433, 2008. ISSN 00344257. doi: 10.1016/j.rse.2007.02.042.

van Dijk, A. I. J. M., Renzullo, L. J., and Rodell, M. Use of gravity recovery and climate experiment terrestrial water storage retrievals to evaluate model estimates by the australian water resources assessment system.

Water Resources Research, 47(11):n/a–n/a, 2011. ISSN 00431397. doi: 10.1029/2011wr010714.

van Dijk, A. I. J. M., Renzullo, L. J., Wada, Y., and Tregoning, P. A global water cycle reanalysis (2003–2012) merging satellite gravimetry and altimetry observations with a hydrological multi-model ensemble. *Hydrology and Earth System Sciences*, 18(8):2955–2973, August 2014a.

van Dijk, A. Awra technical report 3, landscape model (version 0.5) technical description. Technical report, WIRADA/CSIRO Water for a Healthy Country Flagship, Canberra, 2010a.

van Dijk, A. Climate and terrain factors explaining streamflow response and recession in australian catchments. *Hydrology and Earth System Sciences*, 14(1):159–169, 2010b.

Van Dijk, A. and Renzullo, L. J. Water resource monitoring systems and the role of satellite observations. *Hydrology and Earth System Sciences*, 15(1): 39–55, 2011.

Van Dijk, A., Renzullo, L. J., and Rodell, M. Use of gravity recovery and climate experiment terrestrial water storage retrievals to evaluate model estimates by the australian water resources assessment system. *Water Resources Research*, 47(11), 2011.

van Dijk, A. I. J. M., Peña-Arancibia, J. L., Wood, E. F., Sheffield, J., and Beck, H. E. Global analysis of seasonal streamflow predictability using an ensemble prediction system and observations from 6192 small catchments worldwide. *Water Resources Research*, 49(5):2729–2746, 2013a. ISSN 00431397. doi: 10.1002/wrcr.20251.

van Dijk, A. I., Beck, H. E., Crosbie, R. S., de Jeu, R. A., Liu, Y. Y., Podger, G. M., Timbal, B., and Viney, N. R. The millennium drought in southeast australia (2001–2009): Natural and human causes and implications for water resources, ecosystems, economy, and society. *Water Resources Research*, 49 (2):1040–1057, 2013b.

van Dijk, A. I., Peña-Arancibia, J. L., Wood, E. F., Sheffield, J., and Beck, H. E. Global analysis of seasonal streamflow predictability using an ensemble prediction system and observations from 6192 small catchments worldwide. *Water Resources Research*, 49(5):2729–2746, 2013c.

van Dijk, A. I., Renzullo, L. J., Wada, Y., and Tregoning, P. A global water cycle reanalysis (2003–2012) merging satellite gravimetry and altimetry observations with a hydrological multi-model ensemble. *Hydrology and Earth System Sciences*, 18(8):2955–2973, 2014b.

Van Dijk, A. I., Brakenridge, G. R., Kettner, A. J., Beck, H. E., De Groeve, T., and Schellekens, J. River gauging at global scale using optical and passive microwave remote sensing. *Water Resources Research*, 52(8):6404–6418, 2016.

Wahr, J. and Zhong, S. Computations of the viscoelastic response of a 3-d compressible earth to surface loading: an application to glacial isostatic adjustment in antarctica and canada. *Geophysical Journal International*, 192(2):557–572, 2012.

Wahr, J., Molenaar, M., and Bryan, F. Time variability of the earth's gravity field: Hydrological and oceanic effects and their possible detection using grace. *Journal of Geophysical Research: Solid Earth*, 103(B12):30205–30229, 1998.

Walker, J. P. and Houser, P. R. A methodology for initializing soil moisture in a global climate model: Assimilation of near-surface soil moisture observations. *Journal of Geophysical Research: Atmospheres*, 106(D11):11761–11774, 2001a. ISSN 01480227. doi: 10.1029/2001jd900149.

Walker, J. P. and Houser, P. R. Hydrologic data assimilation. *Advances in water science methodologies. Londres: Taylor & Francis, ed*, 1:25–48, 2005.

Walker, J. P. and Houser, P. R. A methodology for initializing soil moisture in a global climate model: Assimilation of near-surface soil moisture observations. *Journal of Geophysical Research: Atmospheres*, 106(D11):11761–11774, 2001b.

Walker, J. P., Willgoose, G. R., and Kalma, J. D. One-dimensional soil moisture profile retrieval by assimilation of near-surface observations: a comparison of retrieval algorithms. *Advances in Water Resources*, 24(6):631–650, 2001.

Wang, J., Price, K., and Rich, P. Spatial patterns of ndvi in response to precipitation and temperature in the central great plains. *International journal of remote sensing*, 22(18):3827–3844, 2001.

Wang, X., Xie, H., Guan, H., and Zhou, X. Different responses of modis-derived ndvi to root-zone soil moisture in semi-arid and humid regions. *Journal of hydrology*, 340(1-2):12–24, 2007.

Wang-Erlandsson, L., Bastiaanssen, W. G., Gao, H., Jägermeyr, J., Senay, G. B., Van Dijk, A. I., Guerschman, J. P., Keys, P. W., Gordon, L. J., and Savenije, H. H. Global root zone storage capacity from satellite-based evaporation. *Hydrology and Earth System Sciences*, 20(4):1459–1481, 2016.

Wardlow, B. D., Egbert, S. L., and Kastens, J. H. Analysis of time-series modis 250 m vegetation index data for crop classification in the us central great plains. *Remote Sensing of Environment*, 108(3):290–310, 2007.

Watkins, M. M., Wiese, D. N., Yuan, D.-N., Boening, C., and Landerer, F. W. Improved methods for observing earth's time variable mass distribution with grace using spherical cap mascons. *Journal of Geophysical Research: Solid Earth*, 120(4):2648–2671, 2015.

Weedon, G. P., Balsamo, G., Bellouin, N., Gomes, S., Best, M. J., and Viterbo, P. The wfdei meteorological forcing data set: Watch forcing data methodology applied to era-interim reanalysis data. *Water Resources Research*, 50 (9):7505–7514, 2014.

Wu, D., Zhao, X., Liang, S., Zhou, T., Huang, K., Tang, B., and Zhao, W. Time-lag effects of global vegetation responses to climate change. *Global change biology*, 21(9):3520–3531, 2015.

Xie, Z., Huete, A., Ma, X., Restrepo-Coupe, N., Devadas, R., Clarke, K., and Lewis, M. Landsat and grace observations of arid wetland dynamics in a dryland river system under multi-decadal hydroclimatic extremes. *Journal of Hydrology*, 543:818–831, 2016a.

Xie, Z., Huete, A., Restrepo-Coupe, N., Ma, X., Devadas, R., and Caprarelli, G. Spatial partitioning and temporal evolution of australia's total water storage under extreme hydroclimatic impacts. *Remote sensing of environment*, 183:43–52, 2016b.

Xu, X., Tolson, B. A., Li, J., Staebler, R. M., Seglenieks, F., Haghnegahdar, A., and Davison, B. Assimilation of smos soil moisture over the great lakes basin. *Remote Sensing of Environment*, 169:163–175, 2015.

Yang, Y., Long, D., Guan, H., Scanlon, B. R., Simmons, C. T., Jiang, L., and Xu, X. Grace satellite observed hydrological controls on interannual and seasonal variability in surface greenness over mainland australia. *Journal of Geophysical Research: Biogeosciences*, 119(12):2245–2260, 2014.

Yang, Y., Donohue, R. J., and McVicar, T. R. Global estimation of effective plant rooting depth: Implications for hydrological modeling. *Water Resources Research*, 52(10):8260–8276, 2016.

Ye, N., Walker, J., Guerschman, J., Ryu, D., and Gurney, R. Standing water effect on soil moisture retrieval from l-band passive microwave observations. *Remote Sensing of Environment*, 169:232–242, 2015.

Yebra, M., Chuvieco, E., and Riaño, D. Estimation of live fuel moisture content from modis images for fire risk assessment. *Agricultural and forest meteorology*, 148(4):523–536, 2008.

Yeh, P. J. F., Swenson, S. C., Famiglietti, J. S., and Rodell, M. Remote sensing of groundwater storage changes in illinois using the gravity recovery and climate experiment (grace). *Water Resources Research*, 42(12):n/a–n/a, 2006. ISSN 00431397. doi: 10.1029/2006wr005374.

Zaitchik, B. F., Rodell, M., and Reichle, R. H. Assimilation of grace terrestrial water storage data into a land surface model: Results for the mississippi river basin. *Journal of Hydrometeorology*, 9(3):535–548, 2008. ISSN 1525-755X 1525-7541. doi: 10.1175/2007jhm951.1.

Zhang, Y., Viney, N., Frost, A., Oke, A., Brooks, M., Chen, Y., and Campbell, N. Collation of australian modeller's streamflow dataset for 780 unregulated australian catchments. *Water for a Healthy Country National Research Flagship, 115pp. Catchment Management*, 2013.

Appendix

The following information are the supplementary materials included in the publication in Chapter 3.

The catchment boundaries and coincident model grid cells for streamflow evaluation are shown in Figure S1. Table S1 provides the locations of OzNet, OzFlux and CosmOz network and their corresponding model grids in the evaluation, as well as the number of observations. Table S2 and Table S3 provide the correlation of model estimated top-layer (0-10cm) and root-zone soil water storage (0-30 cm and 0-90 cm) with *in situ* observations at each grid cell (corresponding to Figure 6). Table S4 summarises the evaluation results of streamflow and evapotranspiration estimates against in-situ measurements.

Figure S1

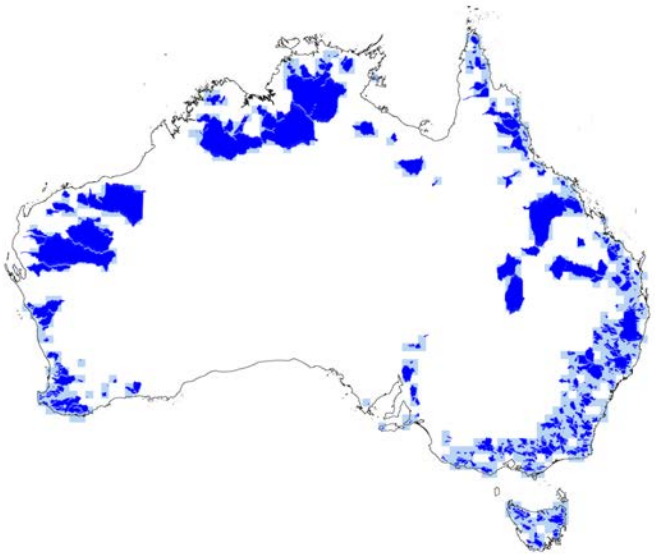

Figure 6-1: Catchment boundaries and coincident model grid cells for streamflow evaluation

Table S1

Table 6.1: Locations of aggregated surface soil moisture in-situ observations

Sites	Network	No. Obs	Latitude	Longitude
Alice Springs Mulga	OzFlux	1213	-22.25	133.25
A1, A2, A3, A4, A5	Oznet	1043	-35.25	148.25
Arcturus Emerald	OzFlux	903	-23.75	148.25
Baldry	CosmOz	1007	-32.75	148.75
Daintree	OzFlux	726	-16.25	145.25
Daly Pasture, Daly Uncleared, Daly Regrowth	OzFlux	1461	-14.25	131.25
Daly	CosmOz	938	-14.25	131.25
Dry river	OzFlux	1305	-15.25	132.25
Gingin	OzFlux	667	-31.25	115.75
Gnangara	CosmOz	667	-31.25	115.75
Great Western Woodlands	OzFlux	355	-30.25	120.75
Griffith	CosmOz	539	-34.25	146.25
Howard Spring	OzFlux	1438	-12.25	131.25
K1, K2, K3, K4, K5, K7, K10, K13	Oznet	1376	-35.25	147.75
K6, K8, K11, K12, K14	Oznet	490	-35.25	147.25
M1	Oznet	480	-36.25	148.75
M2	Oznet	484	-35.25	149.25
M3	Oznet	481	-34.75	148.25
M4	Oznet	482	-33.75	147.25
M5	Oznet	335	-34.75	143.75
M6	Oznet	481	-34.75	144.75
M7	Oznet	481	-34.25	146.25
Red Dirt Melon Farm	OzFlux	619	-14.75	132.25
Riggs Creek	OzFlux	890	-36.75	145.75
Robson	CosmOz	1161	-17.25	145.75
Sturt Plains	OzFlux	1385	-17.25	133.25
Tea Tree East	OzFlux	532	-22.25	133.75
Tullochgorum	CosmOz	1113	-41.75	147.75
Tumbarumba	OzFlux	365	-35.75	148.25
Tumbarumba	CosmOz	899	-35.75	148.25
Wallaby Creek	OzFlux	1008	-37.25	145.25
Weany	CosmOz	1126	-19.75	146.75
Whroo	OzFlux	759	-36.75	145.25
Y10, Y12, Y13	Oznet	1390	-35.25	146.25
Y11	Oznet	830	-35.25	145.75
Y1, Y6	Oznet	806	-34.75	145.75
Y2, Y3, Y4, Y5, Y7, Y8, Y9	Oznet	1435	-34.75	146.25
Yanco	CosmOz	1005	-35.25	146.25

Table S2

Table 6.2: Correlation of model-estimated surface soil relative wetness compared with in-situ data

Site	Open-loop	EnKF-SMOS	EnKS-SMOS	EnKS-GRACE	Joint
A1,A2,A3,A4,A5	0.40	0.47	0.50	0.63	0.51
Alice Springs Mulga	0.66	0.76	0.77	0.67	0.72
Arcturus Emerald	0.53	0.67	0.66	0.57	0.65
Baldry	0.68	0.85	0.86	0.74	0.86
Daintree	0.57	0.67	0.60	0.55	0.61
Daly	0.78	0.81	0.81	0.74	0.77
Daly(CosmOz)	0.85	0.85	0.85	0.80	0.82
Dry River	0.78	0.78	0.77	0.71	0.74
Gingin	0.64	0.64	0.70	0.70	0.68
Gnangara	0.70	0.71	0.75	0.75	0.73
Great Western Woodlands	0.45	0.53	0.55	0.46	0.56
Griffith	0.46	0.60	0.62	0.49	0.59
Howard Springs	0.81	0.80	0.81	0.79	0.80
K1,K2,K3,K4,K5,K7,K10,K13	0.69	0.80	0.83	0.69	0.77
K6,K8,K11,K12,K14	0.70	0.77	0.79	0.71	0.77
M1	0.58	0.67	0.65	0.63	0.67
M2	0.65	0.83	0.80	0.74	0.76
M3	0.62	0.65	0.70	0.49	0.63
M4	0.69	0.78	0.81	0.72	0.80
M5	0.66	0.64	0.78	0.62	0.76
M6	0.43	0.74	0.70	0.72	0.69
M7	0.47	0.68	0.70	0.57	0.71
RDM Farm	0.72	0.71	0.72	0.68	0.69
Riggs Creek	0.52	0.70	0.70	0.63	0.69
Robson	0.76	0.77	0.76	0.78	0.77
Sturt Plains	0.61	0.73	0.74	0.73	0.72
Tea Tree East	0.41	0.54	0.53	0.43	0.49
Tumbarumba	0.65	0.74	0.71	0.81	0.72
Tullochgorum	0.67	0.84	0.87	0.84	0.85
Tumbarumba (CosmOz)	0.63	0.59	0.55	0.65	0.52
Wallaby Creek	0.59	0.63	0.65	0.50	0.65
Weany	0.82	0.83	0.84	0.80	0.83
Whroo	0.50	0.58	0.65	0.64	0.65
Y1,Y6	0.50	0.63	0.64	0.77	0.61
Y10,Y12,Y13	0.60	0.78	0.80	0.63	0.76
Y11	0.54	0.77	0.80	0.59	0.77
Y2,Y3Y4Y5Y7Y8Y9	0.67	0.82	0.84	0.74	0.80
Yanco	0.72	0.71	0.76	0.70	0.79
Average	0.61	0.70	0.72	0.65	0.70

Table S3

Table 6.3: Correlation of model-estimated root-zone soil water storage compared with in-situ data

Compared with Oznet data (0-30 cm)					
Site	Open-loop	EnKF-SMOS	EnKS-SMOS	EnKS-GRACE	Joint
A1,A2,A3,A4,A5	0.55	0.77	0.76	0.77	0.77
K1,K2,K3,K4,K5,K7,K10,K13	0.70	0.79	0.81	0.79	0.83
K6,K8,K11,K12,K14	0.63	0.74	0.70	0.76	0.72
M1	0.47	0.78	0.75	0.73	0.77
M4	0.43	0.79	0.77	0.77	0.80
M7	0.50	0.74	0.74	0.75	0.74
Y10,Y12,Y13	0.67	0.65	0.68	0.63	0.64
Y1,Y6	0.23	0.10	0.11	0.30	0.18
Y2,Y3,Y4,Y5,Y7,Y8,Y9	0.45	0.55	0.59	0.59	0.62
average	0.51	0.66	0.66	0.68	0.67
Compared with Oznet data (30-90 cm)					
Site	Open-loop	EnKF-SMOS	EnKS-SMOS	EnKS-GRACE	Joint
A1,A2,A3,A4,A5	0.76	0.42	0.38	0.78	0.66
K1,K2,K3,K4,K5,K7,K10,K13	0.79	0.75	0.79	0.68	0.80
K6,K8,K11,K12,K14	0.10	0.34	0.41	0.06	0.21
M1	-0.21	0.22	0.06	0.08	0.27
M4	0.83	0.72	0.66	0.86	0.78
M7	0.78	0.85	0.83	0.75	0.77
Y10,Y12,Y13	0.58	0.63	0.71	0.65	0.66
Y1,Y6	0.48	0.68	0.56	0.50	0.59
Y2,Y3,Y4,Y5,Y7,Y8,Y9	0.41	0.43	0.41	0.40	0.53
average	0.50	0.56	0.54	0.52	0.58
Compared with Oznet data (0-90 cm)					
Site	Open-loop	EnKF-SMOS	EnKS-SMOS	EnKS-GRACE	Joint
A1,A2,A3,A4,A5	0.78	0.59	0.62	0.87	0.77
K1,K2,K3,K4,K5,K7,K10,K13	0.81	0.83	0.86	0.77	0.86
K6,K8,K11,K12,K14	0.50	0.63	0.67	0.40	0.54
M1	0.05	0.49	0.36	0.34	0.52
M4	0.62	0.66	0.78	0.83	0.80
M7	0.63	0.85	0.86	0.86	0.81
Y10,Y12,Y13	0.67	0.70	0.77	0.71	0.72
Y1,Y6	0.48	0.68	0.56	0.50	0.59
Y2,Y3,Y4,Y5,Y7,Y8,Y9	0.47	0.51	0.52	0.47	0.60
average	0.56	0.66	0.67	0.64	0.69
average	0.56	0.66	0.67	0.64	0.69

Table S4

Table 6.4: Evaluation of streamflow and evapotranspiration estimates with in-situ measurements for open-loop model simulations and different data assimilation experiments

	Open-loop	EnKF-SMOS	EnKS-SMOS	EnKS-GRACE	EnKS-Joint
Mean r_{ET}	0.78	0.83	0.80	0.77	0.79
Max $r^a_{ET} - r^o_{ET}$	n/a	0.44	0.12	0	0.06
$r^a_{ET} > r^o_{ET}$ (%)	n/a	63	56	0	44
$r^a_{ET} = r^o_{ET}$ (%)	n/a	19	13	44	38
Mean r_Q	0.81	0.84	0.84	0.86	0.85
Max $r^a_Q - r^o_Q$	n/a	0.22	0.19	0.22	0.17
$r^a_Q > r^o_Q$ (%)	n/a	64	64	71	70
$r^a_Q = r^o_Q$ (%)	n/a	5	7	7	7

r_Q: correlation or root mean square error of streamflow;
r_{ET}: correlation or root mean square error of evapotranspiration;
$r^a - r^o$: correlation improvement against open-loop model simulations.